

UNIVERSITÉ DU QUÉBEC

MÉMOIRE PRÉSENTÉ À  
L'UNIVERSITÉ DU QUÉBEC À TROIS-RIVIÈRES

COMME EXIGENCE PARTIELLE  
DE LA MAÎTRISE EN PHYSIQUE

PAR  
JULIAN MICHELSEN

HYDROGEN ADSORPTION ON METAL DOPED NANO CARBONS

DÉCEMBRE 2007

Université du Québec à Trois-Rivières

Service de la bibliothèque

Avertissement

L'auteur de ce mémoire ou de cette thèse a autorisé l'Université du Québec à Trois-Rivières à diffuser, à des fins non lucratives, une copie de son mémoire ou de sa thèse.

Cette diffusion n'entraîne pas une renonciation de la part de l'auteur à ses droits de propriété intellectuelle, incluant le droit d'auteur, sur ce mémoire ou cette thèse. Notamment, la reproduction ou la publication de la totalité ou d'une partie importante de ce mémoire ou de cette thèse requiert son autorisation.



## Acknowledgements

First I would like to thank my director, Prof. Richard Chahine for inviting me to do my masters at the IRH and making this thesis possible, also giving me great personal support especially when I arrived in Canada. I also thank my principal Dr. Walter Schütz for sending me to the IRH and his financial support and interest in hydrogen storage. Furthermore, I would like to thank Dr. Lyubov Lafi for helping me with the essential chemical processes and Daniel Cossement who assisted me during all the time I worked at the IRH. I'd also like to thank Prof. Pierre Bénard for his great help concerning theoretical problems and all the students at the IRH who helped me to find my way through the UQTR.

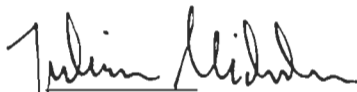
This thesis originated out of a collaboration between the Institut de recherche sur l'hydrogène (IRH) in Trois-Rivières, Canada and FutureCarbon GmbH in Bayreuth, Germany. The development of the doping procedures used within this thesis as well as the improvement of some characterization methods like the gravimetric and volumetric method were performed at the IRH in Canada between September 2005 and May 2006. The investigation of the samples produced was continued at FutureCarbon GmbH in Germany from June 2006 to October 2007.

## Summary

Hydrogen storage is the main technological barrier of a viable hydrogen economy. In the last decades, different hydrogen storage technologies have been developed and evaluated, however, none of them has shown a high potential for a practical application due to disadvantages like poor volumetric/gravimetric storage capacities, too high or too low hydrogen binding energies or inappropriate ad/absorption or desorption rates. Recent research has pointed out an opportunity for the development of a new hydrogen storage material whose storage effect is based on the interaction between a carbon carrier material and a metal deposited on its surface. Simulations show a possible hydrogen uptake of around 8wt % for titanium doped single-walled nanotubes. Others have shown an increase of the hydrogen storage capacity of carbon materials by doping them with noble metals like palladium and platinum.

In this master thesis the focus lies on the synthesis and characterization of such metal doped nano-carbons. The metals used for the doping process are titanium, palladium and platinum. Different methods like chemical vapor deposition (CVD) and wet-chemical doping are used to obtain a metal coating on the selected materials. The quality of the metal coverage is analyzed via X-ray diffraction (XRD) and/or X-ray photoelectron spectroscopy (XPS). The hydrogen adsorption capacity of the synthesized samples, is investigated by volumetric and gravimetric adsorption measurement methods that were partly developed within this thesis. An additional task was to modify an existing Sieverts apparatus in order to allow the determination of adsorption isotherms at temperatures lower than 77 K. Therefore, a liquid helium cooling system was developed and installed.

As adsorption measurements and imaging techniques on the samples produced show, the titanium decorated on the surface of the carbon samples tends to oxidize and thus preventing an adsorption of great amounts of hydrogen. Another difficulty turned out to be the adjustment of the thickness of the metal layer.

  
Étudiant

  
Directeur de recherche

# Introduction

Le développement d'une économie de l'hydrogène repose sur la mise au point d'un mode de stockage efficace et sûr ainsi que d'un système de production à faible coût, ce qui représente un des grands enjeux actuels. Les systèmes actuels de stockage de l'hydrogène ne sont pas encore en mesure de concurrencer ceux de stockage traditionnels pétrole et/ou gaz, en particulier dans le secteur automobile où la sécurité, l'économie et la fiabilité d'un système de stockage ainsi que son poids et son prix jouent un rôle important. L'économie de l'hydrogène étant actuellement considérée comme une alternative possible à l'économie du pétrole, un apaisement considérable pour l'environnement et une voie vers une indépendance par rapport au pétrole, des recherches particulièrement intensives ont lieu en ce qui concerne le stockage de l'hydrogène. Les technologies de stockage utilisées dans le domaine de l'automobile pour la mise au point des prototypes tels que le stockage à haute pression ou sous forme liquide à 20 K dans des réservoirs isolés thermiquement posent des problèmes pratiques d'utilisation et de commercialisation. On ne peut atteindre que des densités de stockage volumiques et gravimétriques très basses. Actuellement, des programmes de recherche se consacrent à la validation de plusieurs technologies alternatives en ce qui concerne le stockage de l'hydrogène. Parmi ces technologies on compte, en premier lieu, celles utilisant les soit disant hydrures complexes et hydrures chimiques, un hydrure étant un composé chimique où l'hydrogène a un lien chimique avec d'autres éléments. Par exemple en ce qui concerne les hydrures métalliques, on a déjà pu atteindre des densités volumiques de stockage très élevées, supérieures à celle de l'hydrogène liquide. L'inconvénient de cette technologie de stockage est que

la dissociation de l'hydrogène, c'est-à-dire son extraction de l'hydruire nécessite beaucoup d'énergie parce que la liaison chimique est relativement stable (énergie de liaison d'environ 80 kJ/mol). En outre, en raison de leur poids élevé, les hydrures métalliques présentent en général une densité gravimétrique de stockage relativement faible. Une autre technologie est en voie de développement; il s'agit de l'adsorption de l'hydrogène à la surface des matériaux (Sorption). Pendant cette adsorption, les molécules d'hydrogène sont liées physiquement par les forces de Van-der-Waals. Les surfaces spécifiques B.E.T de tels matériaux, par exemple les charbons actifs d'un niveau élevé d'activation, atteignent jusqu'à 3000  $m^2/g$ . La quantité d'hydrogène lié augmente lorsque la température baisse et lorsque la pression croît; des températures et des pressions autour de 77 K et de 30 bar constituent de bonnes conditions pour l'adsorption physique de l'hydrogène. En comparaison avec les hydrures complexes et les hydrures chimiques, une simple énergie de liaison physique d'environ 4 kJ/mol [1] entraîne une désorption de l'hydrogène, c'est-à-dire un détachement du substrat des molécules absorbées – une légère augmentation de la température ou une baisse de la pression peut enclencher ce processus. Dans ce cas, il est nécessaire de maintenir la température à une valeur aussi basse que possible afin d'éviter une désorption de l'hydrogène. La solution idéale en ce qui concerne le stockage de l'hydrogène, par exemple pour une utilisation à bord des voitures, devrait maintenir l'extraction de l'hydrogène dans une gamme de température située entre 40 °C et 80 °C. Ces températures pourraient être atteintes grâce à la chaleur dégagée par les cellules de combustible se trouvant dans la voiture. L'énergie de liaison de l'hydrogène nécessaire dans ce cas est d'environ 10 kJ/mol. Les dernières considérations théoriques montrent que pour certains métaux carbonés, par exemple le titane doté de nanotubes de carbone



monofeuillets « SWNT » il est possible d'obtenir des capacités de stockage très élevées pouvant atteindre 8 wt% [2, 3, 4, 5, 6] cela avec des énergies de liaison très modérées. On pourrait alors lier 4 molécules d'hydrogène par atome de titane en procédant de la manière suivante : dissocier la première molécule  $H_2$  et lier les 3 autres. Un effet semblable en ce qui concerne d'autres métaux pourrait être démontré [7, 8, 9, 10]. La possibilité d'adapter l'énergie de liaison dans les matériaux ad/absorbant de l'hydrogène se trouve dans le dopage des matériaux de support tels que le carbone avec les métaux [11, 12, 13, 14]. Dans le présent mémoire, différents systèmes de métaux carbonés sont synthétisés et analysés par rapport à leur capacité. Cette analyse se concentre sur les métaux suivants : la platine, le palladium et en plus particulièrement le titane. Comme matériaux de support, il a été utilisé : le charbon actif IRH 40 fabriqué à l'IRH, les nanomatériaux de carbone de la société FutureCarbon GmbH comme le « Multi-Walled Carbon Nanotubes CNT-MW » ainsi que les « Platelet-Nanofibers CNF-PL ».

## Synthèse des échantillons

Cette partie du document décrit les différents procédés de revêtement des matériaux carbonés utilisés.

### Dopage du titane par procédé dépôt physique et chimique en phase vapeur

Le dépôt en phase vapeur est une des possibilités de revêtement d'un corps solide par un métal [15, 16, 17, 18]. Le substrat devant recevoir le revêtement est placé dans un réacteur contenant des vapeurs métalliques. Ici, le matériau qui doit être dopé est introduit dans un réacteur dont l'atmosphère contient un métal. De cette façon, le métal est déposé sur l'échantillon grâce à des réactions physiques et/ou chimiques. Les tests ont été faits avec du charbon hautement actif comme porteur et du titane comme matériau de dopage. Un gaz, l'hydrogène ou l'argon est injecté à l'aide d'un régulateur d'écoulement sur une petite quantité de tétrachlorure de titane ( $\text{TiCl}_4$ ) dans un tube de verre en quartz dans lequel on a placé une petite quantité de charbon actif et chauffé par un four. Grâce à la faible pression exercée par la vapeur dégagée par le tétrachlorure de titane en contact avec la température ambiante, une certaine quantité du matériau constitutif du dépôt se libère dans le gaz et réagit physiquement ou chimiquement avec le charbon actif. A la sortie du four se trouve un bocal d'eau qui reçoit les gaz échappés afin de protéger l'environnement. Le PH de cette eau peut être analysé afin de se rendre compte de la présence ou non des acides. La figure 1 représente le schéma de principe du dispositif expérimental. Plusieurs expériences ont été menées avec ce dispositif afin de réaliser des

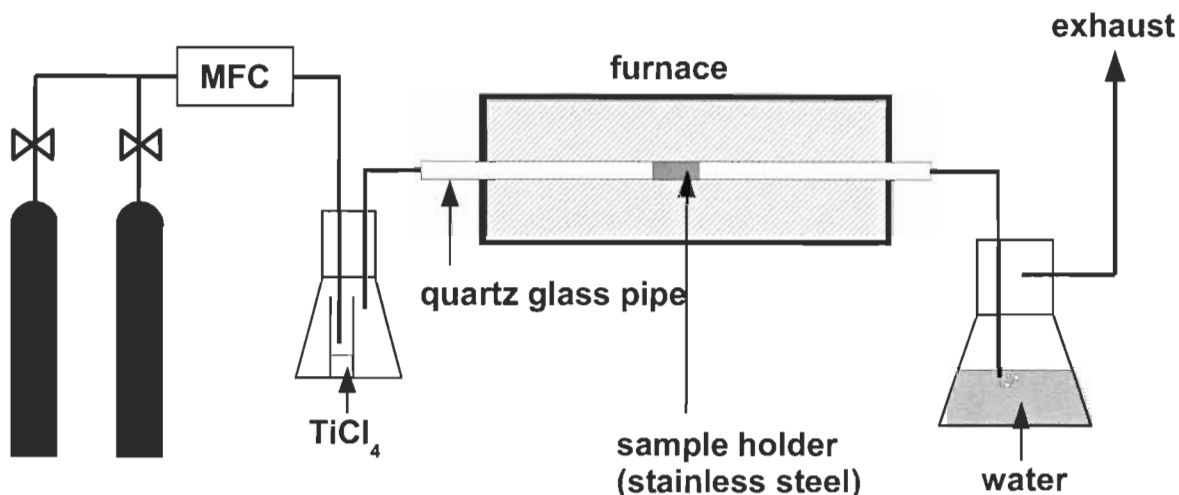


Figure 1 : Dépôt en phase vapeur – Schéma du dispositif expérimental.

revêtement du charbon actif avec du titane. Avec cette méthode, deux approches ont été considérées :

- Une réaction directe du  $\text{TiCl}_4$  avec de l'hydrogène qui libère du titane pur ainsi que du  $\text{HCl}$ . Le  $\text{TiCl}_4$  dissolu dans le gaz réagit avec l'hydrogène dans le four avant d'entrer en contact avec l'échantillon de charbon actif de telle manière que le titane alors libéré puisse se déposer directement sur la surface de l'échantillon du charbon actif à revêtir. Ce processus est défini comme dépôt physique en phase vapeur.
- Une adsorption du  $\text{TiCl}_4$  à la surface du charbon actif avec à la fin une oxydation du  $\text{TiCl}_4$  par de l'eau avec la formation de  $\text{HCl}$  et de  $\text{TiO}_2$  solide. Au cours d'une autre phase de ce processus, ce dernier peut être réduit à du titane pur avec de l'hydrogène sous la formation d'eau. Ce processus est défini comme dépôt chimique en phase vapeur.

Le montage d'essai a été mis au point à l'Institut de Recherche sur l'Hydrogène (IRH) et a été reconsidéré en fonction des exigences qui se présentaient. Une série de test a été pratiquée en utilisant les deux approches citées plus haut. Comme substrat à revêtir, on a été utilisé le charbon actif du type IRH 40 à cause de ses bonnes qualités d'adsorption.

### **Dopage au titane par le processus chimique humide**

D'autres expériences sur le dopage au titane des substrats à base de carbone ont été réalisées en utilisant un procédé spécial, le processus chimique humide. Par ce procédé, l'isopropoxyde de titane agit comme métal d'apport en libérant du titane lorsque du THF est ajouté. Le titane ainsi libéré peut se déposer sur les surfaces d'un substrat. Le substrat à revêtir, le propoxyde de titane et du tétrahydrofurane sont placés dans une ampoule fermée hermétiquement. L'ensemble du dispositif expérimental est baigné dans de l'huile qu'on peut chauffer. Le mélange contenu dans l'ampoule peut être agité à l'aide d'un agitateur magnétique. Après une période de réaction d'environ deux jours, le propoxyde de titane libère du titane qui par la suite se dépose sur la surface du substrat. La figure 2 illustre le dispositif expérimental concernant le procédé chimique humide. À l'aide de cette méthode de revêtement, plusieurs matériaux ont été dopés; le charbon actif « IRH40 » produit par l'IRH ainsi que les nanofibres fabriquées par FutureCarbon GmbH, Multi-Walled Carbon-Nanotubes « CNT-MW » et Carbon Nanofibers Type Platelet « CNF-PL » en font partie. Pour éviter tout contact avec l'oxygène atmosphérique le traitement des échantillons s'est fait dans une boîte à gants.

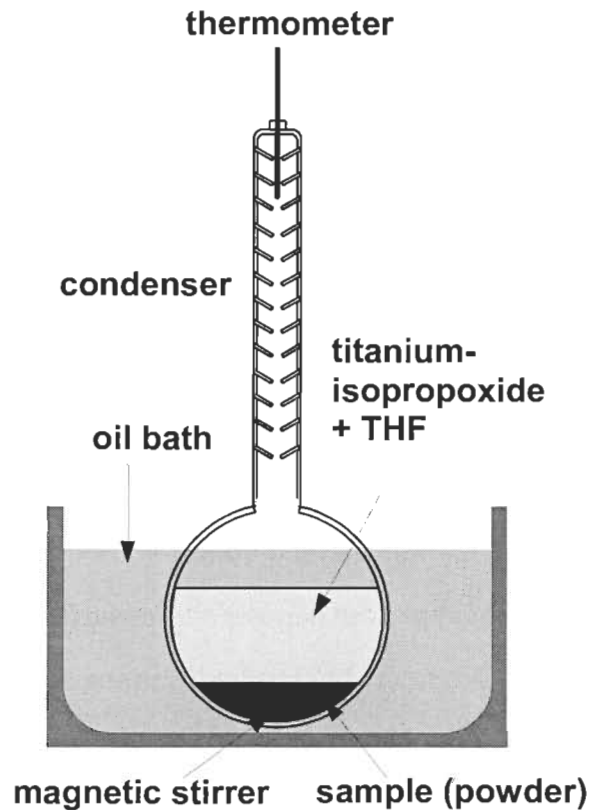


Figure 2 : Processus chimique humide – Schéma du dispositif expérimental

### Dopage au platine/palladium par le processus chimique humide

Avec cette méthode, le revêtement est produit par une décomposition thermique d'un précurseur métallifère placé dans une solution [19]. L'induction se fait à des fréquences micro-ondes. Dans cette méthode, la solution contenue dans le précurseur ainsi que le matériau de carbone à revêtir sont chauffés à l'aide des fréquences micro-ondes. En raison de la conductivité électrique élevée du matériau carboné, une surchauffe partielle à sa surface est obtenue, ce qui entraîne une décomposition et donc une séparation locale du métal. Les tests ont été effectués à l'entreprise FutureCarbon GmbH en Allemagne. La

figure 3 montre le dispositif expérimental développé chez FutureCarbon GmbH.

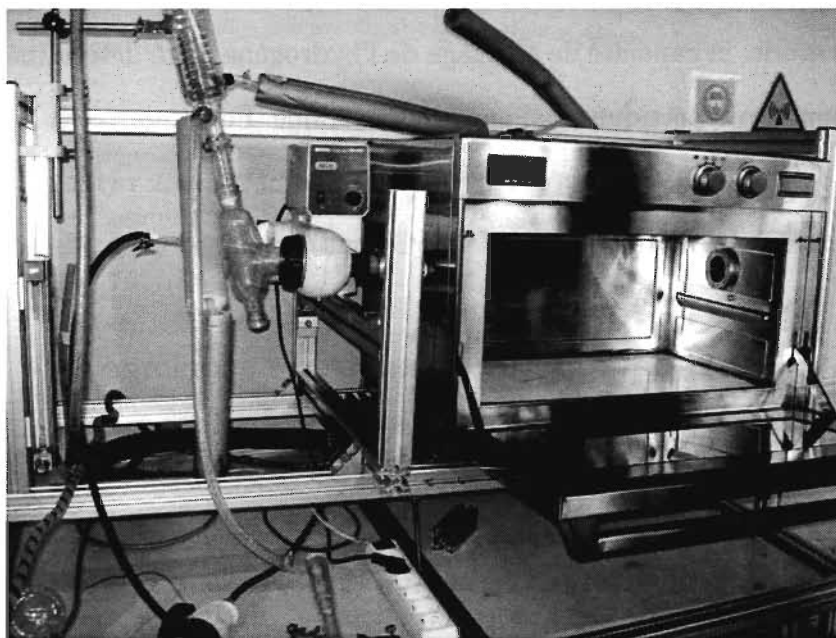


Figure 3 : Dispositif expérimental pour le revêtement des matériaux carbonés par micro-ondes.

## Caractérisation des échantillons synthétisés.

Dans cette étude, la capacité de stockage de l'hydrogène a été déterminée par des méthodes de mesures volumétrique ainsi que gravimétrique. Pour prouver la présence des dépôts métalliques sur les matériaux à revêtir, la diffractométrie aux rayons X (XRD) ainsi que la spectrométrie de photoélectrons X (XPS) ont également été utilisées.

### Mesure volumétrique de la capacité de stockage.

Cette méthode de mesure permet de déterminer la quantité d'hydrogène adsorbée par un échantillon à partir de la différence de pression entre deux volumes connus et reliés entre eux [26, 27]. Le dispositif expérimental (figure 4) se compose essentiellement d'une cellule détectrice contenant l'échantillon à tester et d'une cellule de référence, toutes deux sont séparées l'une de l'autre par une valve (valve principale). Au début de la mesure, on fait le vide dans les deux cellules et on ferme la valve les reliant. Une certaine quantité de gaz hydrogène est d'abord injectée dans la cellule de référence par la valve d'alimentation. Le nombre de molécules d'hydrogène contenu dans la cellule de référence peut être calculé grâce à la pression existante dans cette cellule et le volume connu au moyen de l'équation générale des gaz. Après la fermeture de la valve d'alimentation, la valve principale est ouverte afin que l'hydrogène se répande dans la cellule de mesure, une certaine quantité de gaz d'hydrogène est alors adsorbée par l'échantillon se trouvant dans la cellule. Cette quantité d'hydrogène adsorbée peut être calculée à partir des éléments suivants : baisse de pression causée par l'hydrogène répandue dans la cellule et les volumes connus des deux cellules. Afin de déterminer la capacité de stockage d'hydrogène par

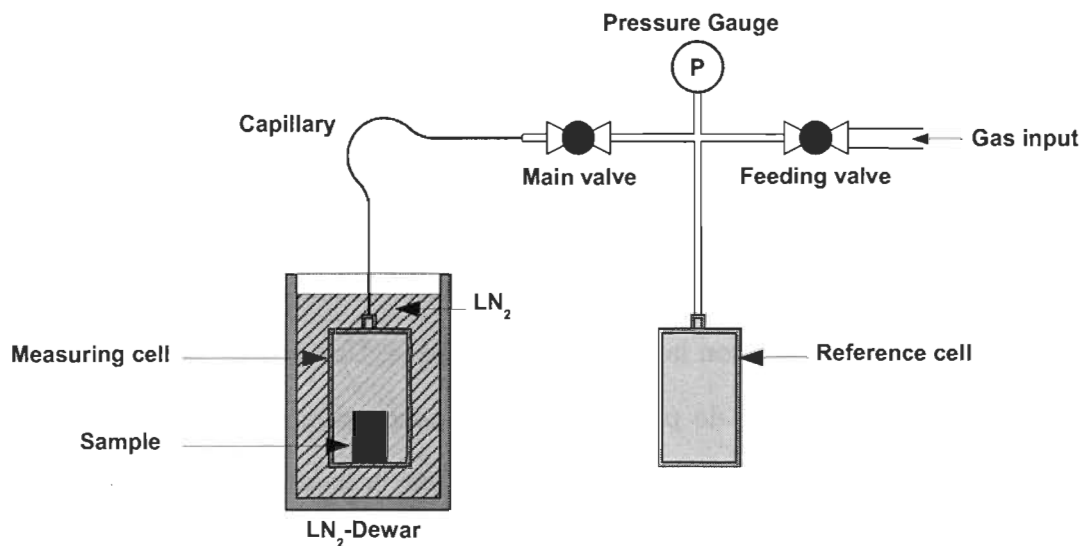


Figure 4 : Montage typique d'un appareillage de mesure volumétrique composé de volumes à mesurer et de volumes de référence séparés l'un de l'autre par la valve principale.

la méthode de mesure volumétrique, deux systèmes de mesure automatiques différents étaient disponibles à l'Institut de Recherche sur l'Hydrogène (IRH), en l'occurrence des systèmes de mesure suivants : « Autosorb-1 » de l'entreprise « QUANTACHROME » et « ASAP 2020 » de l'entreprise « MICROMERITICS ». Les deux systèmes permettant de faire des mesures dans la gamme de température allant de 77 K à 295 K avec des pressions pouvant atteindre 1 bar. Pour permettre également des mesures avec une température de 77 K et des pressions pouvant atteindre 40 bar, un système de mesure volumétrique de l'entreprise FutureCarbon GmbH a été mise au point.



## Mesures gravimétriques de la capacité de stockage

Une autre manière de déterminer la quantité d'hydrogène adsorbée par un échantillon, c'est la méthode de mesure gravimétrique [26, 28, 29]. Dans cette méthode le poids de l'échantillon à tester, celui-ci se trouvant dans une cellule de mesure fermée, est mesuré par une balance de précision. Avant de commencer la mesure, on fait le vide dans la cellule de mesure et ensuite on la remplit d'hydrogène. Une augmentation de poids est alors constatée sur la balance de précision due à l'adsorption d'hydrogène par l'échantillon. Cependant, l'augmentation de poids indiquée par la balance de précision ne correspond pas à la quantité totale adsorbée car la mesure est influencée par des effets de flottabilité qui doivent être additionnés par la suite pour déterminer la vraie quantité d'hydrogène absorbée. Les paramètres de flottabilité peuvent être déterminés par une mesure à l'hélium en raison de son adsorption négligeable sur l'échantillon. Les effets de flottabilité peuvent ainsi être calculés directement. La figure 5 illustre un schéma de principe du dispositif mesure gravimétrique. Pour pouvoir effectuer des mesures de capacité gravimétriques l'IRH a mis au point un système qui permet des mesures à la température ambiante et sous une pression maximale de 100 bar. Les échantillons à mesurer avaient une masse de l'ordre de 100 mg, la résolution de la balance à fléau utilisée dans cet appareillage de mesure Type « CahnD410 » était de 10  $\mu g$ . En comparaison avec ceux utilisés pour les mesures volumétriques, ce dispositif a permis d'atteindre une résolution très élevée même sous haute pression.

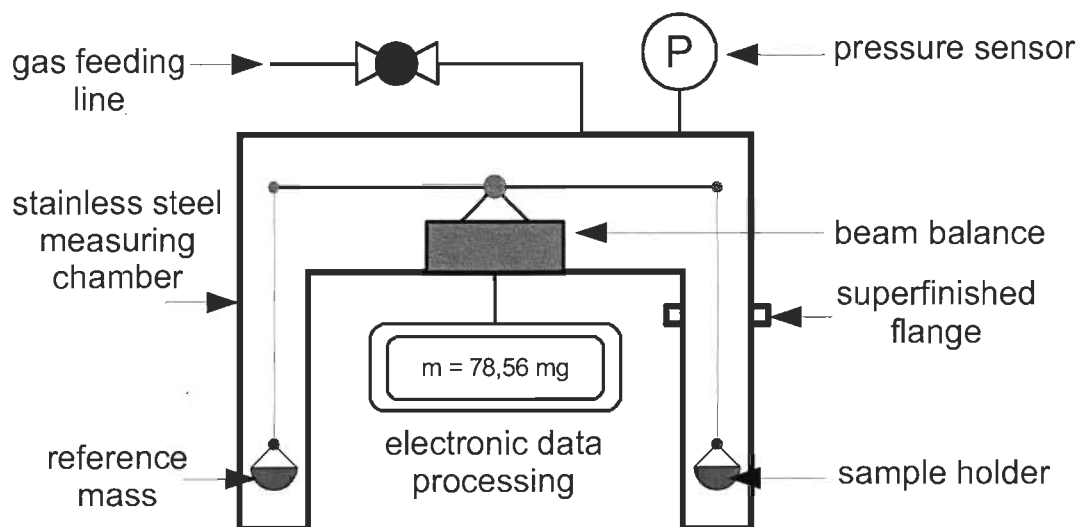


Figure 5 : Schéma d'un système gravimétrique. La mesure de la capacité de stockage d'un échantillon sous une certaine pression se fait avec une balance à fléau. Cependant, les effets de portance doivent être pris en considération.

## Diffraction par rayons X (XRD)

Dans la recherche des matériaux, la diffraction par rayons X est une procédure fréquemment utilisée pour l'analyse des microstructures [22, 23], c'est-à-dire pour obtenir des informations sur la constitution des métaux cristallins. Une structure cristalline est caractérisée par la répartition périodique de ses atomes dans l'espace. Les longueurs de période sont généralement de l'ordre de l'angstrom. Cette méthode d'analyse a été utilisée pour l'étude des caractéristiques des dopages sur des métaux carbonés. L'objectif était de tenter de réaliser des revêtements par applications d'une couche aussi homogène que possible (dans le cas le plus favorable une couche monoatomique) sur les substrats. Toutefois, il convient de noter qu'une telle couche monoatomique ne peut pas être analysée en utilisant une telle technique en raison de sa faible interaction avec les rayons

X. L'apparition d'un pic dans le diagramme du diffractogramme révèle l'existence d'une couche multimoléculaire.

## **Spectrométrie de photoélectrons induit par rayons X (XPS)**

La XPS est basé sur l'effet photoélectrique extérieur, par lequel des photoélectrons sont libérés de l'échantillon sous l'effet de rayonnements électromagnétiques [24, 25]. La détermination de l'énergie cinétique de ces électrons (spectroscopie) permet de tirer des conclusions sur la composition chimique et la constitution électronique de l'échantillon analysé. Le XPS compte aujourd'hui parmi les méthodes les plus utilisées dans la physique des solides ainsi que dans d'autres domaines voisins comme la physique des surfaces et la science des matériaux pour l'analyse de la structure électronique d'un matériau donné. Cette méthode de caractérisation permet une analyse de surface d'un échantillon afin de déterminer le type de matériaux se trouvant sur sa surface ainsi que de leur état de liaison. Contrairement à la méthode déjà présentée – diffractométrie de rayon X – des couches monoatomiques peuvent aussi être détectées.

## Résultats

Dans cette section les résultats des différentes méthodes de caractérisation sont présentés, évalués et commentés.

### Diffraction par rayons X – Résultats

Les échantillons traités par le procédé de dépôt chimique en phase vapeur ou par le processus chimique humide ont d'une manière générale été soumis à une diffraction par rayons X (XRD) afin de mettre en évidence d'éventuelles couches multimoléculaires et de déterminer leur composition. La figure 6 illustre un diffractogramme de rayons X typique. L'analyse montre un échantillon de charbon actif qui a subi un revêtement par

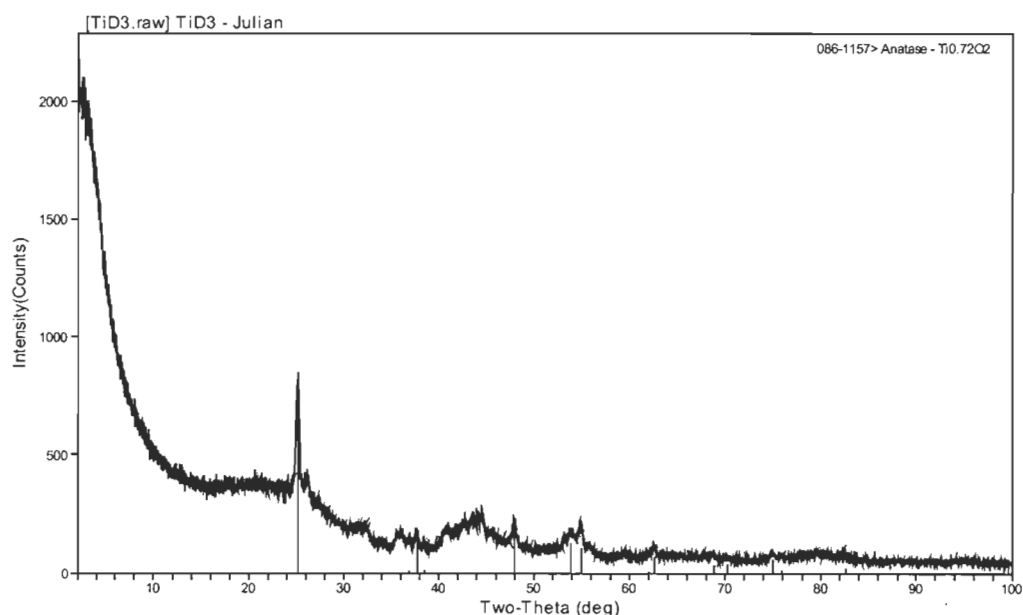


Figure 6 : Diffractogramme de rayons X de l'échantillon « TiD3 ». Le  $\text{TiO}_2$  peut être clairement identifié.

le procédé dépôt chimique en phase vapeur. Ici le  $\text{TiCl}_4$  a d'abord été adsorbé puis réduit en  $\text{TiO}_2$ , ce dernier a ensuite été exposé à l'hydrogène pour ainsi obtenir du titane pur sur la surface de l'échantillon. Dans le diffractogramme, la présence de dioxyde de titane ( $\text{TiO}_2$ ) qui apparaît dans des agglomérats dont le diamètre est au minimum équivalent à celui de 100 molécules est clairement visible. Il y a 2 interprétations possibles en ce qui concerne la présence de  $\text{TiO}_2$  :

- Le revêtement du charbon actif avec le titane s'est d'abord déroulé avec succès. Après le processus de revêtement le titane se trouvant sur l'échantillon s'est oxydé dans la boîte à gants à cause de la grande réactivité de l'échantillon.
- La réduction de  $\text{TiO}_2$  à partir d'hydrogène dans le four de verre en quartz n'a pas réussi parce que la température n'était pas suffisamment élevée ou pour d'autres raisons.

## **Spectrométrie de photoélectrons induits par rayons X – Résultats**

Comme méthode de caractérisation, la spectrométrie de photoélectrons induits par rayons X a seulement été utilisée pour analyser quelques couches atomiques à la surface des échantillons. La figure 7 illustre un spectrogramme typique qui prouve la présence des éléments C,  $\text{O}_2$  ainsi que Ti à la surface de l'échantillon. Grâce à de telles analyses l'état de liaison du revêtement sur l'échantillon a pu être analysé en particulier.

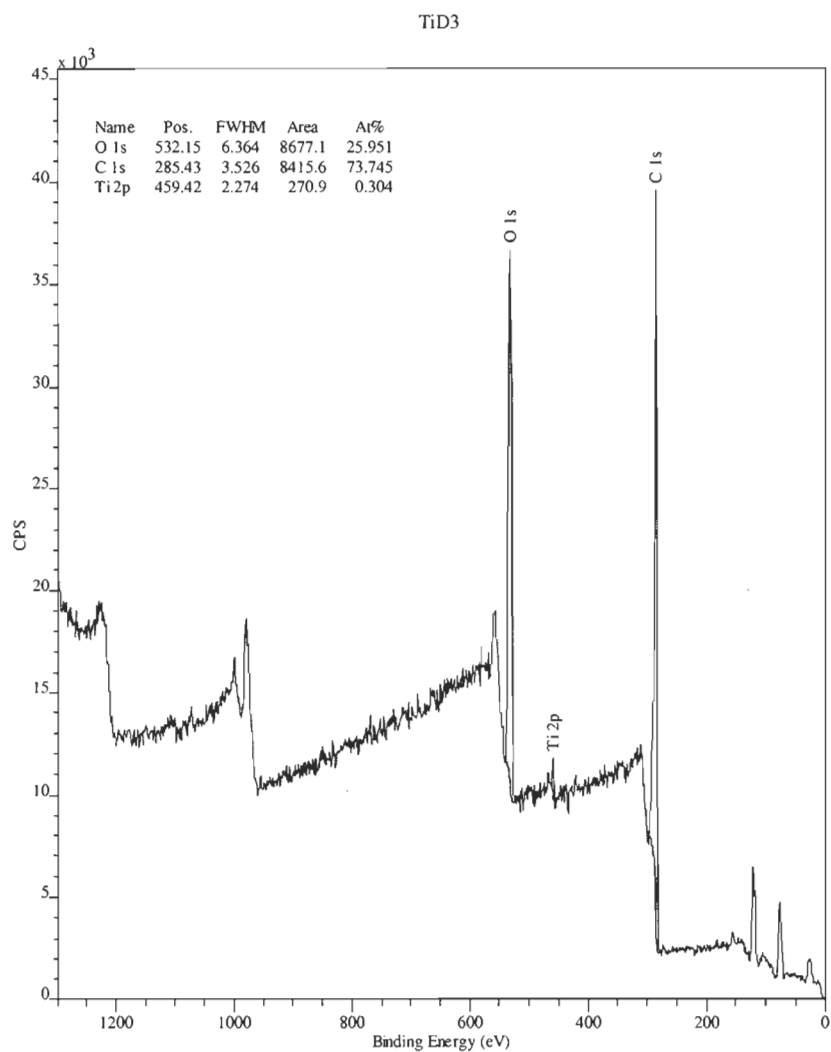


Figure 7 : XPS spectrogramme de l'échantillon « TiD3 »

## Capacité d'adsorption – Résultats

L'influence sur la capacité de stockage de l'hydrogène d'un matériau de stockage à base de carbone et revêtu de métal, ne peut finalement être caractérisée qu'avec une mesure de capacité directe et ainsi être comparée à des matériaux qui n'ont pas subi de revête-

ment. Au cours de cette étude, un vaste spectre de mesures à différentes températures et pressions a pu être réalisé grâce aux méthodes de mesure volumétriques et gravimétriques décrites plus haut. La figure 8 illustre les résultats des mesures gravimétriques à température ambiante et des pressions allant jusqu'à 40 bar. On ne distingue pas de différence

Hydrogen Adsorption on Pd/Pt-doped Materials at 295K

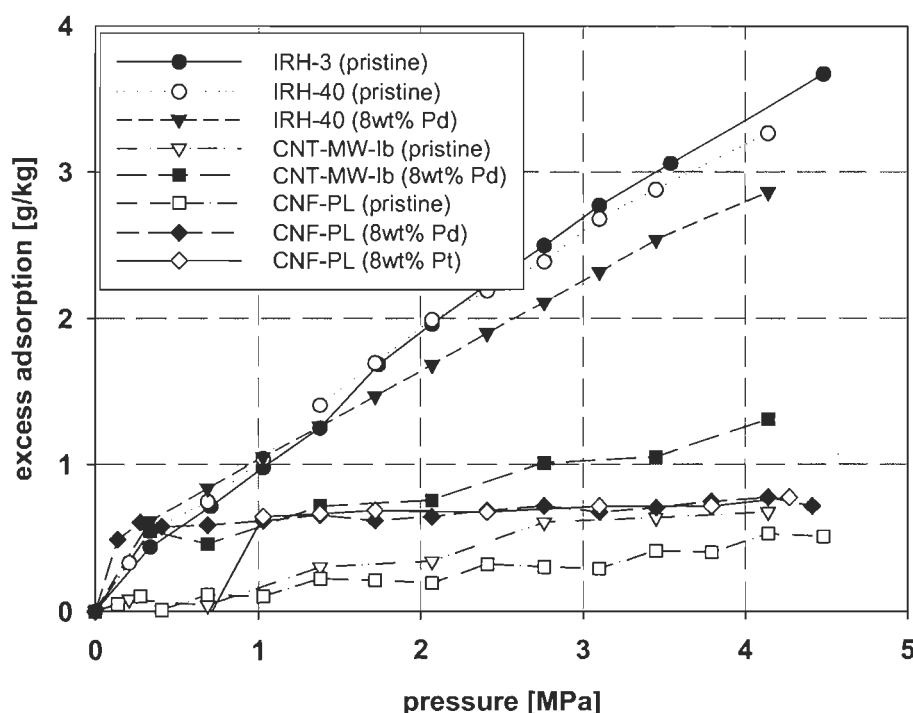


Figure 8 : Mesures de capacité d'hydrogène des échantillons de Pd et de Pt dopés, à température ambiante et à des pressions allant jusqu'à 40 bar, en comparaison à des matériaux sans revêtement.

entre le charbon actif « IRH40 » revêtu et celui non revêtu. Par contre, on peut à peine distinguer une différence en ce qui concerne les nanomatériaux « CNT-MW » et « CNF-PL ». Ils montrent, après revêtement, une capacité de stockage un peu plus élevée. La

quantité d'hydrogène stockée en plus par les nanomatériaux ayant subi un revêtement peut s'expliquer par la formation d'un hydrure métallique.

La figure 9 compare du charbon actif « IRH40 » sans revêtement et du charbon actif avec une couche de titane à une température de 77 K et des pressions allant jusqu'à 1 bar. Une capacité de stockage nettement plus faible du charbon actif revêtu de titane est visible. Durant les analyses XRD précédentes, il a été prouvé que l'oxydation de la couche de titane sur l'échantillon le rendait passif. Le  $\text{TiO}_2$  n'étant pas en mesure de lier

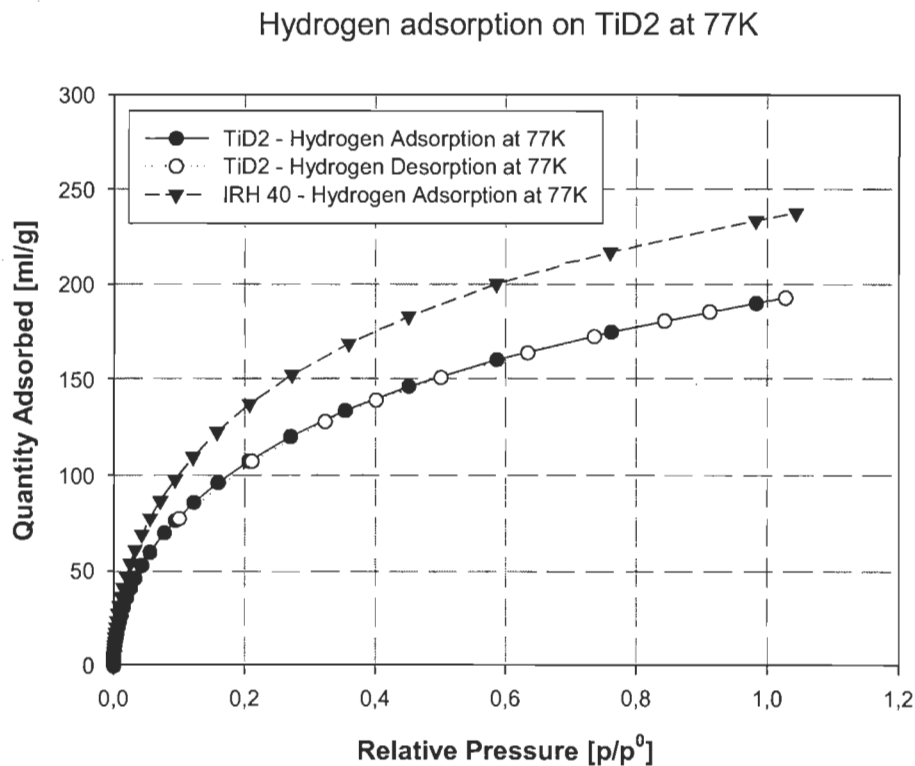


Figure 9 : Mesure de capacité d'hydrogène volumétrique de l'échantillon « TiD2 » à une température de 77 K et des à des pressions allant jusqu'à 1 bar.

de l'hydrogène, il agit comme surcharge qui lors des mesures d'adsorption apparaît sous



forme de faibles capacités de stockage. La figure 10 illustre la prise de vue, à l'aide d'un microscope électronique à balayage, d'un échantillon de charbon actif dont la couche-Ti a été oxydée jusqu'à obtenir du  $\text{TiO}_2$ . Sur cette figure, l'épaisseur très élevée de la couche est également très visible.

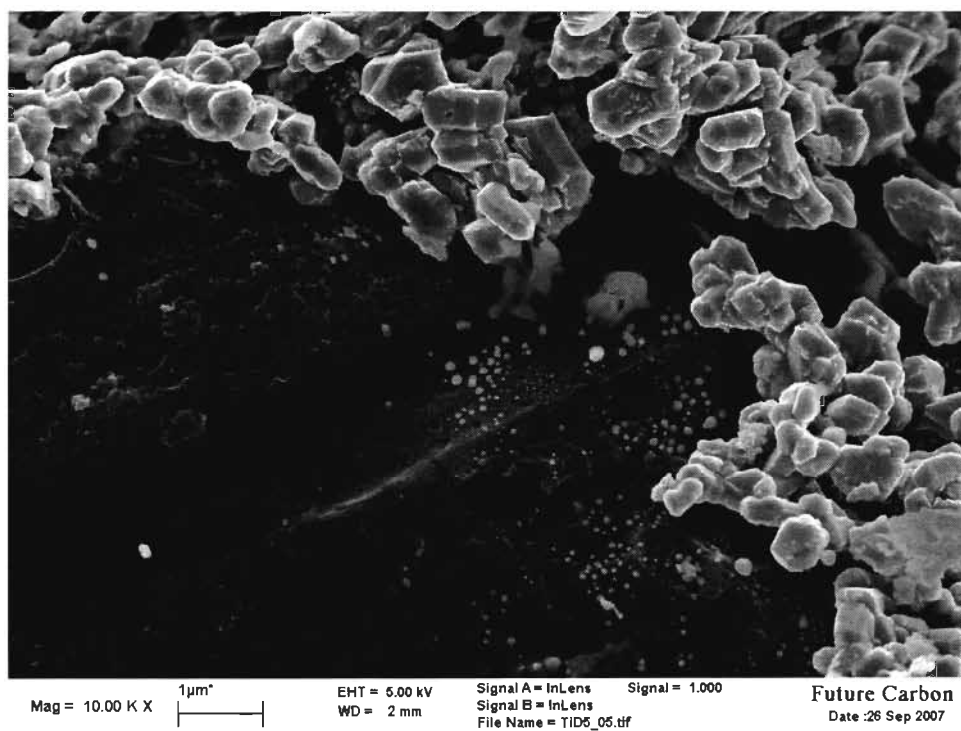


Figure 10 : Prise de vue d'une couche -Ti oxydée sur charbon actif à partir d'un microscope électronique à balayage.

## Résumé.

En conclusion on peut résumer :

- Les processus visant le revêtement des échantillons carbonés avec des métaux se sont déroulés pour la plus grande partie avec succès. Dans tous les cas, ces métaux ont pu être déposés sur les échantillons. Un affinage de certains paramètres a permis de jouer sur l'épaisseur des couches, assez élevée au début et cela en particulier pour le procédé dépôt physique. Finalement, ce sont les méthodes chimiques humides qui se sont avérées comme étant les méthodes les mieux contrôlables lors d'un processus de revêtement.
- Le plus grand problème a été l'oxydation de la couche de titane. Même en stockant les échantillons dans une boîte à gants, le titane s'est oxydé avec le reste d'oxygène s'y trouvant. Une réduction du  $\text{TiO}_2$  à un Ti brut n'a pas pu se faire.
- Les échantillons revêtus de métaux précieux Pt et Pd ont montré une capacité de stockage un peu plus élevée qui peut toutefois s'expliquer par la formation d'un hydrure métallique.

D'autres travaux pourraient viser une amélioration de la méthode de revêtement chimique humide. En ce qui concerne d'autres recherches avec des échantillons revêtus de Ti, une atmosphère absolument interne est indispensable. Dans le meilleur des cas, la synthèse et la caractérisation devraient être effectuées dans une boîte à gants de sorte que le transport des échantillons synthétisés puisse être supprimé.

# Contents

<b>1</b>	<b>Introduction</b>	<b>1</b>
1.1	Hydrogen storage problems . . . . .	1
1.2	Focus of the thesis . . . . .	2
<b>2</b>	<b>Sample Synthesis - Metal doping of carbon materials</b>	<b>4</b>
2.1	Titanium doping via physical and chemical vapor deposition . . . . .	5
2.1.1	Adsorption capacity of $\text{TiCl}_4$ by activated carbon IRH40 . . . . .	6
2.1.2	Ti coating via physical adsorption of $\text{TiCl}_4$ (PVD) . . . . .	8
2.1.3	Ti coating via oxidization of adsorbed $\text{TiCl}_4$ (PVD) . . . . .	11
2.1.4	Ti coating via oxidization of adsorbed $\text{TiCl}_4$ at increased temperatures (PVD) . . . . .	13
2.1.5	Ti coating via direct reaction of $\text{TiCl}_4$ with $\text{H}_2$ (CVD) . . . . .	15
2.1.6	Ti coating via external loading of the sample with $\text{TiCl}_4$ (PVD) .	16
2.1.7	Ti coating via direct injection of $\text{TiCl}_4$ (PVD) . . . . .	18
2.2	Titanium doping via wet chemical processes . . . . .	20
2.2.1	Amount of chemicals used . . . . .	21

2.2.2	Ti doping of multi-walled carbon nanotubes . . . . .	24
2.2.3	Ti doping of carbon nanofibers . . . . .	26
2.2.4	Ti doping of high surface area activated carbon . . . . .	27
2.3	Palladium/platinum doping via Colloidal Microwave Processing (CMP) .	29
<b>3</b>	<b>Sample Characterization</b>	<b>31</b>
3.1	Solid state analytics . . . . .	31
3.1.1	X-ray crystallography (XRD) . . . . .	31
3.1.2	X-ray Photoelectron Spectroscopy (XPS) . . . . .	32
3.2	Hydrogen adsorption measurements . . . . .	34
3.2.1	Volumetric method (Sieverts apparatus) . . . . .	34
3.2.2	Common problems presented the volumetric method . . . . .	40
	Temperature gradient . . . . .	40
	Identification of the systems volume . . . . .	41
3.2.3	Gravimetric method . . . . .	43
<b>4</b>	<b>Results</b>	<b>48</b>
4.1	Results of nano-carbons used for doping processes . . . . .	50
4.2	Results of Ti decorated nano-carbons . . . . .	52
4.3	Results of Pd/Pt decorated nano-carbons . . . . .	57
<b>5</b>	<b>Adsorption measurements at temperatures from 30 K to 77 K</b>	<b>60</b>
<b>6</b>	<b>Conclusion</b>	<b>70</b>

Appendix	73
A XRD results	73
B XPS results	84
C Hydrogen adsorption measurements	93

# List of Figures

2.1	Adsorption of $\text{TiCl}_4$ by activated carbon IRH40. . . . .	8
2.2	Schematic of the systems setup for the first set of experiments. . . . .	9
2.3	Physical setup of PVD/CVD process. The arrangement of the components is varied due to specific needs of the different experiments. . . . .	10
2.4	Schematic of the systems setup for the second set of experiments. . . . .	12
2.5	Schematic of the systems setup for the third set of experiments. . . . .	14
2.6	Schematic of the systems setup for the fourth set of experiments. . . . .	16
2.7	Sketch of the setup of the $\text{TiCl}_4$ loading process. A stainless steel container which contains the activated carbon sample inside a sealable container with a septum. The $\text{TiCl}_4$ is injected through a syringe and may adsorb on the activated carbon through evaporation. . . . .	17
2.8	Sketch of the setup of the $\text{TiCl}_4$ loading process. A stainless steel container which contains the activated carbon sample inside a sealable container with a septum. The $\text{TiCl}_4$ is injected directly on the activated carbon through a syringe and is adsorbed immediately. . . . .	18

2.9	Typical setup of the wet chemical process showing the flask containing the liquid solution and the carbonaceous sample with the condenser mounted on the top. A thermometer allows the observation of the temperature provided by a heating plate which heats the oil bath the flask is located in. The sketch does not show the aluminum foil wrapped around the setup to prevent radiation contacting the chemical solution. . . . .	20
2.10	Model of a tetra-hydrofuran molecule. Red : oxygen, black : carbon, blue : hydrogen . . . . .	24
2.11	SEM/TEM image of multi-walled carbon nanotubes MWNT-Ib produced by FutureCarbon. . . . .	25
2.12	SEM/TEM image of carbon nanofibers CNF-PL produced by FutureCarbon.	26
2.13	Colloidal Microwave Processing (CMP) experimental setup. . . . .	29
3.1	Typical setup of a volumetric measurement system (Sieverts apparatus) showing two volumes (measuring volume and reference volume) separated by the main valve. Through gas expansion from the reference volume into the measuring volume, the hydrogen adsorption capacity of a sample located in the measuring cell can be determined through the pressure drop caused by the gas expansion. . . . .	35
3.2	Volumetric test bed at FutureCarbon GmbH in Bayreuth, Germany. The test bed is designed for the measurement of adsorption isotherms of samples with a mass up to 10 g at temperatures ranging from 77 K to 500 K and pressures up to 100 bar. . . . .	36

3.3	Photo of the beam balance type <i>Cahn D410</i> used for the gravimetric experiments . . . . .	44
3.4	Sketch of a gravimetric measurement system. The hydrogen adsorption at a certain pressure can be determined through the mass measured by the balance minus the buoyancy of the sample caused by the surrounding hydrogen gas. . . . .	45
3.5	Gravimetric setup at the IRH allowing measurements at pressures up to 100 bar. . . . .	46
4.1	(TiD3) Formation of $TiO_2$ on the surface of activated carbon. . . . .	53
4.2	(TiD5) Formation of different metals on the surface of the activated carbon sample. . . . .	54
4.3	(TiD6) Formation of nano-scaled $TiO_2$ on the surface of the activated carbon sample. . . . .	55
4.4	(TiL1) Formation of $TiO_2$ on the surface of multi-walled nanotubes. . . .	56
4.5	(TiL3) Formation of $TiO_2$ on the surface of activated carbon particles. An SE-detector was used for the imaging process to highlight the metal content.	57
A.1	XRD spectrum of activated carbon IRH40 doped with 8wt% <i>Pd</i> showing the peaks related to <i>Pd</i> . . . . .	74
A.2	XRD spectrum of carbon nanotubes CNT-MW 'as synthesized' showing the peaks related to <i>Co</i> . . . . .	75
A.3	XRD spectrum of carbon nanofibers CNF-PL 'as synthesized' showing the peaks related to <i>C</i> . . . . .	75



A.4	XRD spectrum of carbon nanofibers CNF-PL 'as synthesized' showing the peaks related to $Fe_3C$ . . . . .	76
A.5	XRD spectrum of carbon nanofibers CNF-PL doped with 8wt% $Pd$ showing the peaks related to $C$ . . . . .	76
A.6	XRD spectrum of TiD2 showing the peaks related to $TiO_2$ . . . . .	77
A.7	XRD spectrum of TiD3 showing the peaks related to $TiO_2$ . . . . .	77
A.8	XRD spectrum of TiD3 showing the peaks related to $TiH_2$ . . . . .	78
A.9	XRD spectrum of TiD5 showing the peaks related to $NiFe$ . . . . .	78
A.10	XRD spectrum of TiD5 showing the peaks related to $CrFe$ . . . . .	79
A.11	XRD spectrum of TiD5 showing the peaks related to $TiO_2$ . . . . .	79
A.12	XRD spectrum of TiL1 showing the peaks related to $TiO_2$ . . . . .	80
A.13	XRD spectrum of TiL1 showing the peaks related to $TiC_8$ . . . . .	80
A.14	XRD spectrum of TiL1 showing the peaks related to $TiC$ . . . . .	81
A.15	XRD spectrum of TiL1 showing the peaks related to $Ti$ . . . . .	81
A.16	XRD spectrum of TiL2 showing the peaks related to $Ti$ . . . . .	82
A.17	XRD spectrum of TiL2 showing the peaks related to $Ti_2O_3$ . . . . .	82
A.18	XRD spectrum of TiL2 showing the peaks related to $TiO_2$ . . . . .	83
B.1	XPS spectrum of TiD3 showing 3 emission lines for titanium, oxygen and carbon. . . . .	85
B.2	XPS spectrum of TiD3 with focus on emission line Ti 2s. . . . .	86
B.3	XPS spectrum of TiD3 with focus on emission line O 1s. . . . .	87
B.4	XPS spectrum of TiD3 with focus on emission line Ti 2p. . . . .	88

B.5	XPS spectrum of TiD3 with focus on emission line C 1s. . . . .	89
B.6	XPS spectrum of TiD4 showing 2 emission lines for oxygen and carbon. .	90
B.7	XPS spectrum of TiD4 with focus on emission line O 1s. . . . .	91
B.8	XPS spectrum of TiD4 with focus on emission line C 1s. . . . .	92
C.1	Hydrogen adsorption measurements performed with the gravimetric measurement system at a temperature of 295 K and pressures up to 4 MPa. Samples shown are Pd and Pt covered carbon materials in comparison with their undoped pristine materials. . . . .	94
C.2	Hydrogen adsorption measurements performed with the gravimetric measurement system at a temperature of 295 K and pressures up to 4 MPa. Samples shown are Ti covered carbon materials in comparison with their undoped pristine materials. . . . .	95
C.3	Hydrogen adsorption measurements performed with the volumetric measurement system at a temperature of 77 K and pressures up to 1 bar. Sample shown is the activated carbon IRH40. . . . .	96
C.4	Hydrogen adsorption measurements performed with the volumetric measurement system at a temperature of 295 K and pressures up to 1 bar. Sample shown is the activated carbon IRH40. . . . .	97
C.5	Hydrogen adsorption measurements performed with the volumetric measurement system at a temperature of 77 K and pressures up to 1 bar. Sample shown is the Ti covered sample TiD2 in comparison with its pristine material IRH40. . . . .	98

C.6	Hydrogen adsorption measurements performed with the volumetric measurement system at a temperature of 295 K and pressures up to 1 bar. Sample shown is the Ti covered sample TiD2 in comparison with its pristine material IRH40. . . . .	99
C.7	Hydrogen adsorption measurements performed with the volumetric measurement system at a temperature of 77 K and pressures up to 1 bar. Sample shown is the Ti covered sample TiL1 in comparison with its pristine material CNT-MW. . . . .	100
C.8	Hydrogen adsorption measurements performed with the volumetric measurement system at a temperature of 77 K and pressures up to 1 bar. Sample shown is the Ti covered sample TiL3 in comparison with its pristine material IRH40. . . . .	101

# List of Tables

2.1	Explanation to the Dubinin-Raduskevitch relation . . . . .	6
2.2	Properties of Titanium iso-propoxide . . . . .	22
2.3	Properties of tetra-hydrofuran . . . . .	23
2.4	Properties of multi-walled carbon nanotubes MWNT-Ib produced by FutureCarbon . . . . .	24
2.5	Properties of carbon nanofibers CNF-PL produced by FutureCarbon. . .	26
4.1	List of pristine materials, their pretreatments and analysis. . . . .	48
4.2	List of metal doped samples, their pretreatments and analysis. . . . .	49

# Chapter 1

## Introduction

### 1.1 Hydrogen storage problems

The development of a functional and economical hydrogen storage system is a key issue for a working hydrogen economy. Unlike gasoline, hydrogen is gaseous at room temperature and diffuses through tank hulls due to its small molecular size which complicates its efficient storage. Commonly used storage technologies like high pressure tanks or liquid hydrogen storage systems are quite well developed but still show unacceptable characteristics in energy density, economy and complexity for practical applications. Beside the storage of hydrogen in gaseous or liquid states, another possibility is to let the hydrogen interact with a solid material in order to bind to the surface or its molecular grid.

In the last decades, a lot of research has been aimed at the development of an adequate material for this type of hydrogen storage. However, a suitable material has not been found yet. One of the major characteristics of such a material is its sorption enthalpy.

Whereas this sorption enthalpy is very low for physisorption on activated carbon or single-walled carbon nanotubes [1] (around  $4 \frac{\text{kJ}}{\text{mol}}$ ), resulting in a weak bonding of the hydrogen molecules to the adsorbents surface; the sorption enthalpy is quite high for metal hydrides (classic materials around  $80 \frac{\text{kJ}}{\text{mol}}$ ) resulting in a very strong bonding of the hydrogen to the metal. Consequently, in the case of physisorption, very low temperatures and high pressures are necessary to obtain an acceptable amount of hydrogen stored, whereas in the case of chemisorption on metal hydrides energy is required to break the strong bonding between the metal and the hydrogen in order to release it. Experts came to the conclusion that a useful material for hydrogen storage should have a sorption enthalpy around  $12 - 20 \frac{\text{kJ}}{\text{mol}}$ . Metal doped nano-carbons are a promising candidate for filling the gap between physisorption and classical chemisorption on metal hydrides.

## 1.2 Focus of the thesis

In this master thesis the focus lies on carbon materials doped with metals like titanium, palladium and platinum. Recent research has shown that for titanium covered single-walled nanotubes a hydrogen storage capacity of about 8wt% can be reached [2 - 6]. These studies have shown that each single Ti atom coated on a single-walled nanotube binds up to four hydrogen molecules. The first  $\text{H}_2$  adsorption should be dissociative with no energy barrier while the other three adsorptions should be molecular with significantly elongated H-H bonds. A similar effect was predicted for other metals [7 - 10]. Others have demonstrated that the hydrogen storage capacity of nano-carbons can be improved by hydrogen spillover [11, 12] from a supported catalyst [13, 14]. The goal of this thesis

is to successfully demonstrate the practical feasibility of the theoretical research done so far. For this purpose, different carbon materials like carbon nanofibers, multi-walled carbon nanotubes and high surface area activated carbon were coated/doped with metals by different coating technologies like physical/chemical vapor deposition (PVD/CVD) [15 - 18], colloidal microwave processing (CMP) [19] and other wet chemical coating mechanisms to be able to compare a large amount of materials and their potential applicability for coating processes. The synthesized materials were further characterized via spectral analysis like X-ray photoelectron spectroscopy (XPS) and X-ray diffraction (XRD) to check the quality of the metal coating on the surface. Finally, the hydrogen adsorption capacity of the samples produced was determined by volumetric and gravimetric measurement techniques and compared with pristine materials.

## Chapter 2

# Sample Synthesis - Metal doping of carbon materials

This chapter describes the different doping techniques used in this thesis. According to the sample type and the kind of metal used for the doping, different processes seem to be adequate. These are in detail:

1. Physical/Chemical vapor deposition where particularly high surface area activated carbon is used as a support for the metal dopant.
2. A wet chemical approach where the coating process is performed in a liquid solution at temperatures around 80 °C .
3. Colloidal microwave processing (CMP) that allows the coating of nanofibers in a liquid solution through a metal containing precursor which is selectively heated by microwaves.



The first two processes were developed and set up at the IRH, the CMP has been developed at the University of Bayreuth in Germany and set up at FutureCarbon GmbH. The following sections explain these three processes and the experiments linked with them.

## 2.1 Titanium doping via physical and chemical vapor deposition

The idea of this coating technique is to deposit metal on the surface of a carbon sample located inside a quartz glass furnace, with the help of a carrier gas carrying an evaporated, metal containing chemical. In the case of titanium as a dopant, liquid titanium tetrachloride ( $\text{TiCl}_4$ ) is used as a source of metal. To classify the process it is necessary to distinguish between two different doping procedures :

1. By inducing a chemical reaction between one of the carrier gases (e.g. hydrogen) and the evaporated  $\text{TiCl}_4$ , pure titanium is produced that may be deposited on the samples surface. The process is usually carried out at temperatures above 600 °C. This technique is classified as chemical vapor deposition (CVD).
2.  $\text{TiCl}_4$  is evaporated and carried to the sample with the help of a carrier gas where it is physically adsorbed (physisorbed) on the samples surface through weak Van-der-Waals forces. As a consequence, this process requires a large samples surface area in order to guarantee the adsorption of high amounts of  $\text{TiCl}_4$ . The only carbon material that meets those requirements is high surface area activated carbon with a BET surface area ranging around  $2000 \frac{\text{m}^2}{\text{g}}$  and above. In further processes, the

adsorbed  $\text{TiCl}_4$  can be chemically treated in order to release the titanium and to get rid of the chloride. This technique is classified as physical vapor deposition (PVD).

For the following set of experiments the super activated carbon type IRH40 was used which is a in-house product of the IRH and, due to its high surface area, is suitable for this coating process. The activated carbon IRH40 has a BET-surface area of  $2300 \frac{\text{m}^2}{\text{g}}$  and a density of  $0,39 \frac{\text{g}}{\text{cm}^3}$ .

### 2.1.1 Adsorption capacity of $\text{TiCl}_4$ by activated carbon IRH40

To determine the amount of  $\text{TiCl}_4$  adsorbed on the surface of the activated carbon the classical Dubini-Raduskevitch relation can be used [20] :

$$W_e = W_0 \cdot d_L \cdot e^{-\frac{k}{\beta^2} \cdot R^2 \cdot T^2 \cdot \ln^2\left(\frac{P}{P^0}\right)} \quad (2.1)$$

Table 2.1 shows an explanation of the variables used in the formula 2.1. Relation 2.1 can

<i>Symbol</i>	<i>Description</i>	<i>Value</i>	<i>Unit</i>
$W_e$	adsorption capacity of IRH40		$g_{\text{TiCl}_4}/g_{\text{AC}}$
$W_0$	microporous volume of IRH40	0,77	$\frac{\text{ml}}{\text{g}}$
$d_L$	liquid density of $\text{TiCl}_4$	1,726	ml
$k$	carbon structural factor		
$\beta$	affinity coefficient of $\text{TiCl}_4$ to carbon		
$R$	gas constant	8,314	$\frac{\text{J}}{\text{mol} \cdot \text{K}}$
$T$	temperature		K
$P$	$\text{TiCl}_4$ pressure		
$P^0$	vapor pressure of $\text{TiCl}_4$ at 20 °C	9,956	mmHg

Table 2.1 : Explanation to the Dubinin-Raduskevitch relation

be replaced by the following equation [21] :

$$W_e = W_0 \cdot d_L \cdot e^{-\frac{B}{P_e^{1,8}} \cdot R^2 \cdot T^2 \cdot \ln^2\left(\frac{P}{P_0}\right)} \quad (2.2)$$

where B represents a relative carbon structural constant and  $P_e$  the molecular polarizability, which is determined with the refractive index  $n_D$  (Lorentz formula) :

$$P_e = \left( \frac{n_D^2 - 1}{n_D^2 + 2} \right) \cdot \frac{M_w}{d_L} = 38,10 \quad (2.3)$$

where  $n_D$  is the refractive index of  $\text{TiCl}_4$  (1,61) and  $M_w$  its molecular weight (189,68g). The relative structural constant of IRH40 is determined using equation 2.3 and the adsorption data of  $N_2$  at 77 K. The molecular polarizability of liquid  $N_2$  is 4,54 ( $n_D = 1,205$ ) and the factor B calculated from the relation is  $6,08 \cdot 10^{-7}$ . Figure 2.1 represents the adsorption of  $\text{TiCl}_4$  by IRH40 as a function of the relative pressure. The ratio of Ti in  $\text{TiCl}_4$  is about 25wt%, as a consequence it is possible to assess the partial gas pressure of  $\text{TiCl}_4$  when knowing the relative pressure needed to reach a certain amount of Ti to be deposited in the microporous structure of the activated carbon.

With further chemical treatments the titanium now present on the samples surface can be separated from the Cl whereas the latter one can be removed to achieve a pure titanium coating.

The following subsections explain the different sets of experiments performed whereas every set is finally represented by one sample which is then further analyzed and discussed.

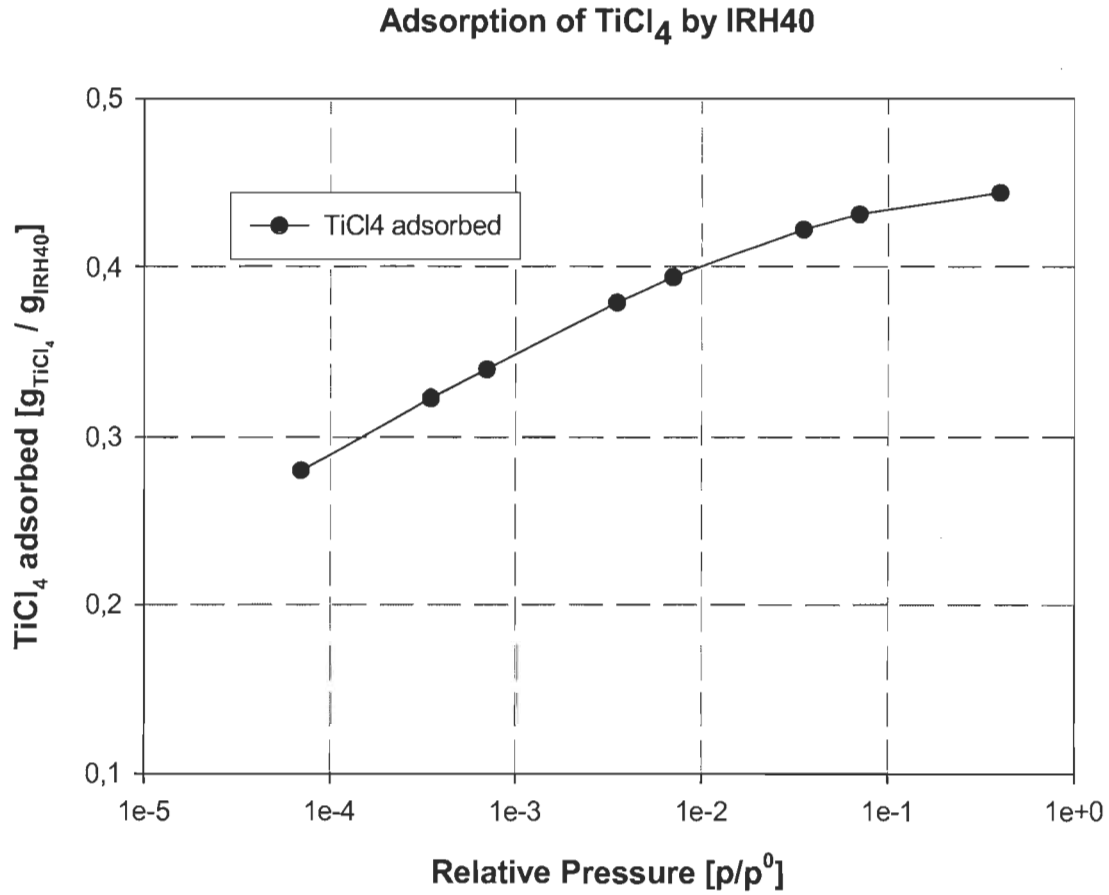


Figure 2.1 : Adsorption of  $\text{TiCl}_4$  by activated carbon IRH40.

### 2.1.2 Ti coating via physical adsorption of $\text{TiCl}_4$ (PVD)

The idea behind the first set of experiments made, was to evaporate a certain amount of  $\text{TiCl}_4$  with the help of argon as a carrier gas and to let it than adsorb on a small amount (2,5g) of activated carbon. As a next step hydrogen gas is lead over the sample at around 500 °C in order to form HCl and pure Ti, whereas the HCl can be washed out in further processes. Figure 2.2 shows the schematic process for this first set of experiments. Figure

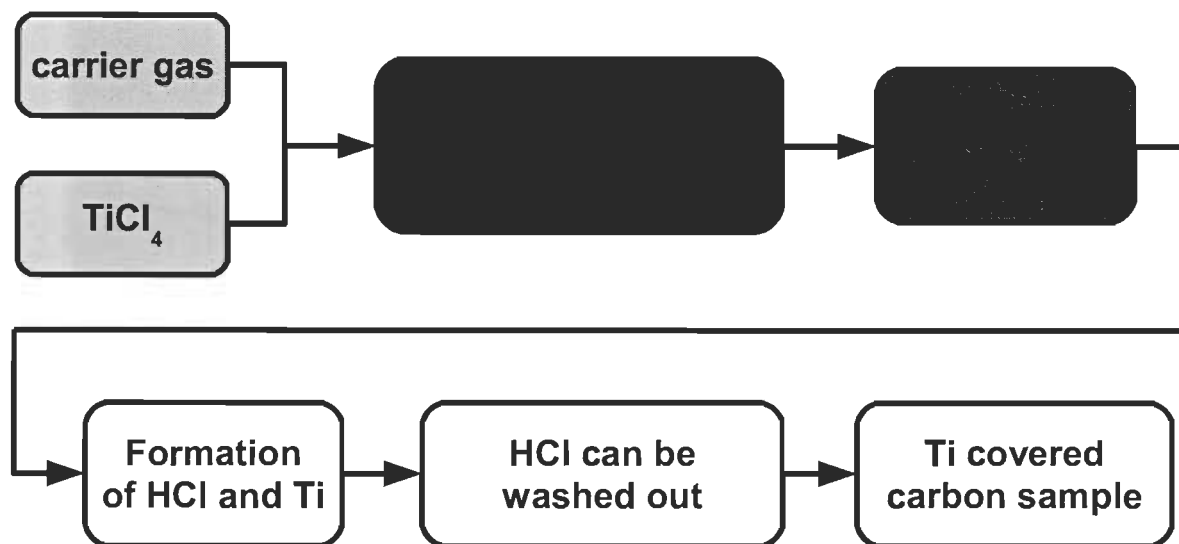


Figure 2.2 : Schematic of the systems setup for the first set of experiments.

2.3 shows the physical setup of the components used. A hydrogen and an argon gas bottle are connected via a Matheson glass tube rotameter type 610A with a maximum hydrogen flow rate of  $240STP \frac{ml}{min}$  to a quartz glass furnace type Lindberg Heavy-Duty 54031-A allowing a maximum temperature of 1100 °C. The TiCl<sub>4</sub> is put in a small glass container inside an Erlenmeyer flask that is positioned in the gas flow between the gas supply and the tubular furnace. A small glass tube which leads the carrier gas inside the flask is located approximately 1cm above the liquid level of the TiCl<sub>4</sub>. Through the low vapor pressure of the TiCl<sub>4</sub>, the carrier gas is able to transport evaporated TiCl<sub>4</sub> molecules to the sample being located in a stainless steel container inside the furnace, a fraction of the TiCl<sub>4</sub> molecules is thereby physisorbed by the sample. The exhaust gas is lead to a second Erlenmeyer flask that is filled with water, where the remaining TiCl<sub>4</sub> molecules in the gas may react with the water under the formation of HCl and TiO<sub>2</sub> which condenses

as a white powder. After this procedure the process gas is switched to hydrogen in order to induce a reaction with the  $\text{TiCl}_4$  located on the sample to form pure Ti and HCl. The arrangement of the components shown in figure 2.3 is varied due to the specific needs of the different experiments. The experiments were carried out by the following steps :

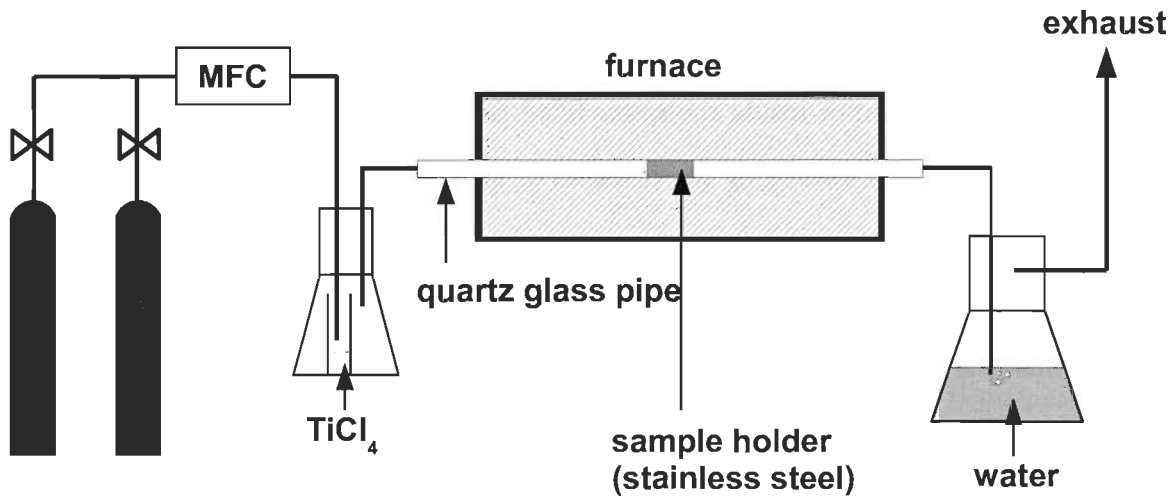


Figure 2.3 : Physical setup of PVD/CVD process. The arrangement of the components is varied due to specific needs of the different experiments.

1. heat sample under argon at  $500\text{ }^{\circ}\text{C} > 4\text{ h}$ ,
2. 2,5 g of high surface area activated carbon is put in the sample holder which is then placed in the quartz glass tube of the furnace,
3.  $600\text{ }\mu\text{l}$  of  $\text{TiCl}_4$  are evaporated under an argon flow  $(0,1\frac{\text{l}}{\text{min}})$ . This operation lasts about 12 h,
4. the gas supply is switched to hydrogen  $(0,5\frac{\text{l}}{\text{min}})$ ,

5. the temperature of the furnace is set to 500 °C (ramp  $3\frac{K}{min}$ ) and kept at this level for 4 h,
6. the temperature is decreased to ambient conditions (ramp  $3\frac{K}{min}$ ) and the furnace is purged with argon.

During the evaporation process of the  $TiCl_4$  and the heat up procedure of the furnace, the formation of white vapor inside the water filled Erlenmeyer flask was sighted. This vapor turned out to be HCl formed by the reaction of  $TiCl_4$  with water. A big amount of  $TiCl_4$  did not adsorb on the sample but was directly lead into the water filled Erlenmeyer flask where it reacted to HCl and  $TiO_2$ . During the heat up process of the furnace additional  $TiCl_4$  was desorbed and able to react with the water. A pH-value of 2 was determined using litmus paper at the end of the experiment. As a consequence the amount of  $TiCl_4$  being present on the samples surface to possibly react with the hydrogen is believed to be very low.

The sample representing this set of experiments is named **TiD1**.

### 2.1.3 Ti coating via oxidization of adsorbed $TiCl_4$ (PVD)

It turns out from the first set of experiments that the biggest problem was the  $TiCl_4$  desorbing of the surface of the sample when the furnace was heated up. The approach of the second experiment was to let the  $TiCl_4$  react with water when it is still adsorbed on the sample to form solid  $TiO_2$  which will not desorb when the temperature is increased.



The only new task is to somehow chemically process the  $\text{TiO}_2$  to obtain pure Ti. Therefore the sample was treated with hydrogen at high temperatures. Figure 2.4 shows the schematic of the setup for the second set of experiments. The experiments were carried

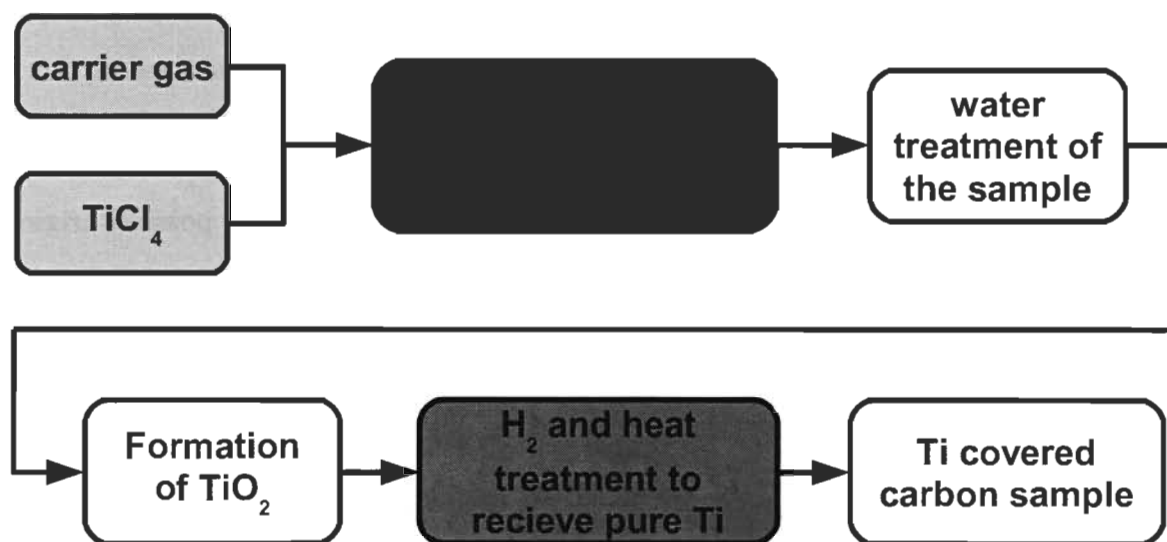


Figure 2.4 : Schematic of the systems setup for the second set of experiments.

out by the following steps :

1. heat sample under argon at  $500\text{ }^{\circ}\text{C} > 2\text{ h}$ ,
2. 1,6 g of high surface area activated carbon is put in the sample holder that is then placed in the quartz glass tube of the furnace (the amount of activated carbon used was decreased in comparison with the first set of experiments to reduce the amount of  $\text{TiCl}_4$  needed and to decrease the reaction time),
3. approx.  $400\text{ }\mu\text{l}$  of  $\text{TiCl}_4$  are evaporated under an argon flow ( $0,1\frac{\text{l}}{\text{min}}$ ). This operation takes approx. 12 h,



4. a small amount (approx. 5 ml) of water is put at the entrance of the furnace and evaporated under an argon flow ( $0,1 \frac{l}{min}$ ) for at least 8 h,
5. the gas supply is switched to hydrogen ( $0,5 \frac{l}{min}$ ),
6. the temperature of the furnace is set to 650 °C (ramp  $3 \frac{K}{min}$ ) and kept at this level for 4 hours,
7. heat under argon at 500 °C for about 16 h to evaporate any water possibly originated by the hydrogen treatment,
8. the temperature is decreased to ambient conditions (ramp  $3 \frac{K}{min}$ ) and the furnace is purged with argon.

As in the first set of experiments the formation of HCL in the Erlenmeyer flask was detected as a consequence of  $TiCl_4$  reacting with the water. The processed samples appeared to be more greyish than the initial carbon material. One sample was refilled and prepared for the XRD measurement in an argon filled glove box, nevertheless small quantities of  $O_2$  may have entered the sample holder while it was located in the glove-box. The sample representing this set of experiments is named **TiD2**.

#### **2.1.4 Ti coating via oxidization of adsorbed $TiCl_4$ at increased temperatures (PVD)**

The focus of the third set of experiments was to better reduce the  $TiO_2$  and to avoid the formation of new  $TiO_2$  after the treatment. These problems were solved by increasing the temperature during the  $H_2$  treatment of the sample and by letting the sample cool down

to ambient temperature under a  $H_2$  atmosphere. The latter action aims the formation of titanium hydride ( $TiH_2$ ) whereas the hydrogen bonded to the Ti might prohibit the reaction of  $O_2$  with the Ti. Figure 2.5 shows the schematic of the setup of the third set of experiments. The experiments were carried out by the following steps :

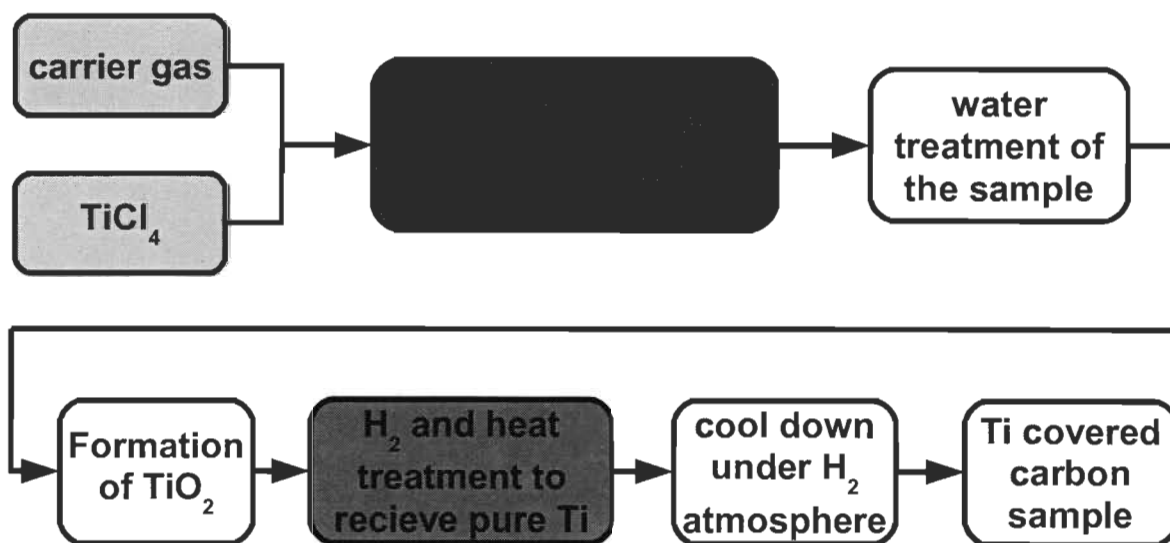


Figure 2.5 : Schematic of the systems setup for the third set of experiments.

1. heat sample under argon at  $500\text{ }^{\circ}\text{C} > 2\text{ h}$ ,
2. approx. 1,6 g of high surface area activated carbon is put in the sample holder which is then placed in the quartz glass tube of the furnace,
3. approx.  $500\text{ }\mu\text{l}$  of  $TiCl_4$  are evaporated under an argon flow  $(0,1\frac{l}{min})$ . This operation takes approx. 12 h,
4. a small amount (approx. 5 ml) of water is put at the entrance of the furnace and evaporated under an argon flow  $(0,1\frac{l}{min})$  for at least 8 h,

5. heat treatment under argon at 500 °C for about 3 h to evaporate any possibly condensed water,
6. the gas supply is switched to hydrogen ( $0,5 \frac{l}{min}$ ),
7. the temperature of the furnace is set to 800 °C (ramp  $3 \frac{K}{min}$ ) and kept at this level for 4 hours,
8. the temperature is decreased to ambient conditions (ramp  $3 \frac{K}{min}$ ), the hydrogen flow is kept.

The sample representing this set of experiments is named **TiD3**.

### **2.1.5 Ti coating via direct reaction of $TiCl_4$ with $H_2$ (CVD)**

The approach of the fourth set of experiments is different from the former ones.  $TiCl_4$  is evaporated directly under a  $H_2$  flow in order to let it react together in the hot zone of the furnace where arising Ti might be directly deposited on the surface of the carbon sample. This attempt allows to dope the sample with Ti without producing any  $TiO_2$  intentionally. Figure 2.6 shows the schematic of the setup of the fourth set of experiments. The experiments were carried out by the following steps :

1. heat sample under argon at 500 °C >2 h,
2. approx. 1,6 g of high surface area activated carbon is put in the sample holder which is then placed in the quartz glass tube of the furnace,
3. approx. 200  $\mu l$  of  $TiCl_4$  are evaporated under a hydrogen flow ( $0,1 \frac{l}{min}$ ) at a temperature of 950 °C This operation takes approx. 5 h,

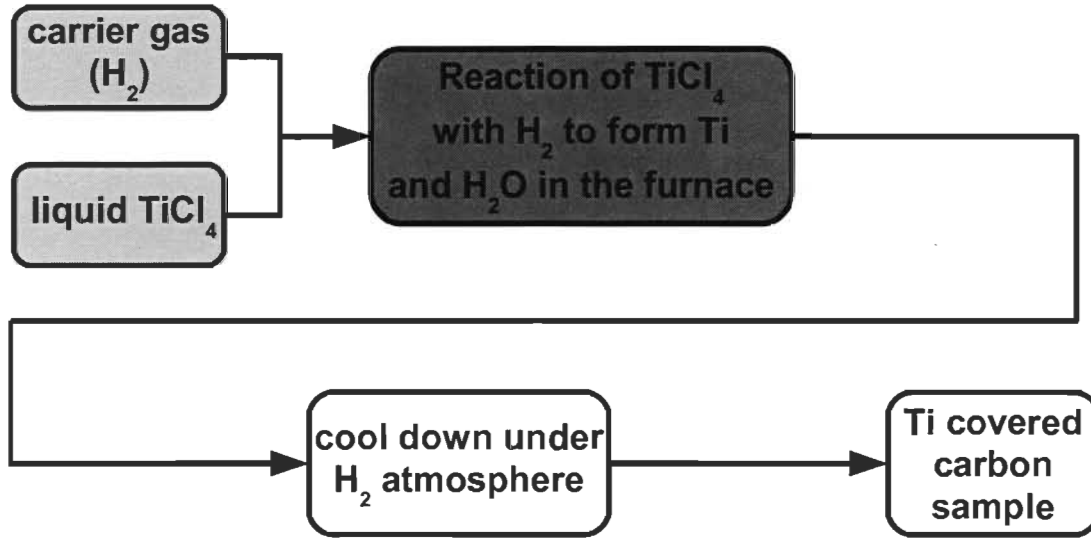


Figure 2.6 : Schematic of the systems setup for the fourth set of experiments.

4. the temperature is decreased to ambient conditions (ramp  $3 \frac{K}{min}$ ), the hydrogen is kept flowing.

The sample representing this set of experiments is named **TiD4**.

### 2.1.6 Ti coating via external loading of the sample with $TiCl_4$ (PVD)

The fifth set of experiments aimed at an external (out of the furnace) loading (adsorption) of the sample with  $TiCl_4$ . For that purpose, a small sealable container with a septum at the top was provided, to be able to load the activated carbon sample inside that container with  $TiCl_4$ . The sample was located inside a stainless steel container which is used for the subsequent heat treatment in the quartz glass furnace. Figure 2.7 shows a sketch of the setup for the external  $TiCl_4$  loading process. The idea behind this setup was to let

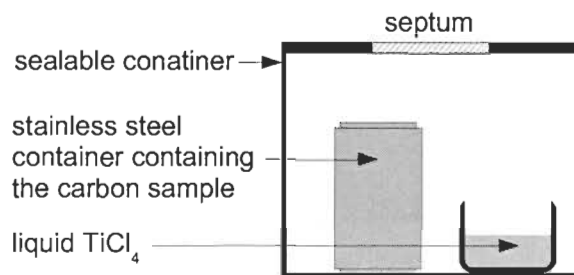


Figure 2.7 : Sketch of the setup of the  $\text{TiCl}_4$  loading process. A stainless steel container which contains the activated carbon sample inside a sealable container with a septum. The  $\text{TiCl}_4$  is injected through a syringe and may adsorb on the activated carbon through evaporation.

the  $\text{TiCl}_4$  adsorb on the activated carbons surface through evaporation. After saturation occurs, the sample was treated with water to let the  $\text{TiCl}_4$  react to  $\text{HCl}$  and  $\text{TiO}_2$ . The experiments were carried out by the following steps :

1. Preparation of the sealable and the stainless steel container containing 1g of activated carbon.
2. Injection of 1,5 *ml*  $\text{TiCl}_4$  in the sealable container at room temperature.
3. Adsorption of  $\text{TiCl}_4$  on the activated carbon for 24 h.
4. Injection of  $\text{H}_2\text{O}$  directly on the activated carbon in the stainless steel container (exothermal reaction).
5. Filtering and purifying of the activated carbon with distilled water outside of the sealable container.
6. Heat treatment under Argon at 500 °C >4 h.

7. Reduction of the  $\text{TiO}_2$  to pure Ti through  $\text{H}_2$  treatment at  $950\text{ }^\circ\text{C}$   $>4\text{ h}$  (This step was repeated 3 times).

The sample representing this set of experiments is named **TiD5**.

### 2.1.7 Ti coating via direct injection of $\text{TiCl}_4$ (PVD)

The approach for the 6<sup>th</sup> set of experiments was quite similar to the 5<sup>th</sup>. The major difference is that the  $\text{TiCl}_4$  was injected directly on the activated carbon and adsorbed immediately. Figure 2.8 shows a sketch of the setup for the external  $\text{TiCl}_4$  loading process. The experiments were carried out by the following steps :

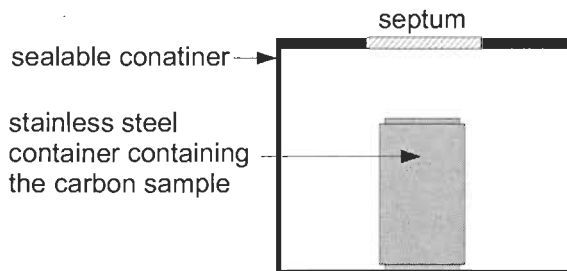


Figure 2.8 : Sketch of the setup of the  $\text{TiCl}_4$  loading process. A stainless steel container which contains the activated carbon sample inside a sealable container with a septum. The  $\text{TiCl}_4$  is injected directly on the activated carbon through a syringe and is adsorbed immediately.

1. Preparation of the sealable and the stainless steel container containing 1 g of activated carbon.
2. Injection of 1,5 ml  $\text{TiCl}_4$  in the sealable container at room temperature directly on the activated carbon.

3. Adsorption of  $\text{TiCl}_4$  on the activated carbon for 1h.
4. Injection of  $\text{H}_2\text{O}$  directly on the activated carbon in the stainless steel container (exothermal reaction).
5. Filtering and purifying of the activated carbon with distilled water outside of the sealable container.
6. Heat treatment under Argon at  $500\text{ }^\circ\text{C}$  >4 h.
7. Reduction of the  $\text{TiO}_2$  to pure Ti through  $\text{H}_2$  treatment at  $950\text{ }^\circ\text{C}$  >4 h (This step was repeated 3 times).

The sample representing this set of experiments is named **TiD6**.

## 2.2 Titanium doping via wet chemical processes

Another approach to cover carbonaceous samples with metals is the use of a liquid, metal containing solution as a donor. Titanium iso-propoxide is mixed together with tetrahydrofuran (THF) whereas both react and pure titanium is released which is deposited on the surface of the sample present in the liquid solution. To avoid the formation of  $\text{TiO}_2$  this process is carried out in a closed system. Additionally, THF is light sensitive, so the system has to be insulated from light sources by the use of aluminum foil. Figure 2.9 shows the setup of the process. A typical synthesis is carried out by the following

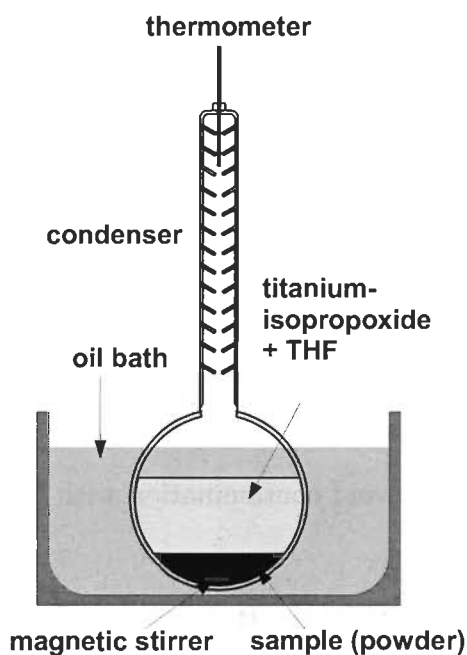


Figure 2.9 : Typical setup of the wet chemical process showing the flask containing the liquid solution and the carbonaceous sample with the condenser mounted on the top. A thermometer allows the observation of the temperature provided by a heating plate which heats the oil bath the flask is located in. The sketch does not show the aluminum foil wrapped around the setup to prevent radiation contacting the chemical solution.



steps :

1. 25 ml titanium iso-propoxide and 100 ml THF is put in a 5 liter flask together with about 1,5 g of a carbonaceous powdered sample.
2. A magnetic stirrer is put in the flask.
3. A condenser with a temperature sensor on the top is mounted on top of the flask and the system is hermetically sealed with sealing agent.
4. The bottom of the glass flask is put in an oil bath on top of the heating plate. To avoid chemical reactions caused by incidence of light, the system is also optically insulated by aluminum foil.
5. The temperature of the heating plate is set to about 80 °C and the magnetic stirrer is activated.
6. The system remains in that state for 3 days.
7. The process is finished, the sample can be refilled and prepared for the heat treatment in a glove box to avoid contamination with  $O_2$ .

### 2.2.1 Amount of chemicals used

1g carbon sample equals  $\frac{1}{12}mol$  carbon atoms. For a sufficient titanium surface coverage an amount of 1 titanium atom for 3 carbon atoms seems to be adequate. The amount of titanium iso-propoxide necessary for 1g carbon sample can be calculated from its molecular weight (See table 2.2)

<i>Titanium iso-propoxide</i>	
Density [ $\rho$ ]	$0,97 \frac{g}{cm^3}$
Molecular weight [M]	$284,26 \frac{g}{mol}$
CAS number	546-68-9
Purity	97vol.%

Table 2.2 : Properties of Titanium iso-propoxide

$$\begin{aligned}
\frac{1}{12} mol \text{ (C-atoms)} \cdot \frac{1}{3} &\Rightarrow \frac{1}{36} mol \text{ (Ti.iso-prop.)} \\
m_{Ti.iso-prop.} = M_{Ti.iso-prop.} \cdot \frac{1}{36} &= 284,26 \frac{g}{mol} \cdot \frac{1}{36} \approx 7,9g \\
V_{Ti.iso-prop.} = \frac{m}{\rho} &= \frac{7,9g}{0,97 \frac{g}{cm^3}} = 8,14cm^3
\end{aligned} \tag{2.5}$$

However, the purity of the titanium iso-propoxide used is just 97% :

$$\Rightarrow 8,14ml \cdot \frac{100}{97} = 8,4ml \text{ (Ti.iso-prop.)} \tag{2.6}$$

A safety factor of 3 was chosen to guarantee a sufficient amount of titanium in the liquid solution, consequently the final amount of titanium iso-propoxide used for 1 g of carbon sample is :

$$8,4ml \cdot 3 \approx 25ml \text{ } V_{Ti.iso-prop.} \text{ per 1 g carbon} \tag{2.7}$$

Every titanium iso-propoxide molecule requires 4 tetra-hydrofuran (THF) molecules to react with, in order to release the titanium molecule. Properties of tetra-hydrofuran are given in table 2.3. Equation 2.8 shows the calculation of the mass of THF required to satisfy every titanium-iso-propoxide molecule with 4 THF molecules. The calculation

includes a safety factor of 2.

$$\begin{aligned}
M_{Ti.iso-prop.} &= 284,26g \\
M_{THF} &= 72,11g \\
M_{THF,required} &= 4 \cdot 2 \cdot 72,11g = 576,88g \cong 2 \cdot M_{Ti.iso-prop.} \\
\Rightarrow m_{THF,required} &\cong 2 \cdot m_{Ti.iso-prop.}
\end{aligned} \tag{2.8}$$

According to the different densities of both substances, the volume of THF required is calculated by :

$$\begin{aligned}
\rho &= \frac{m}{V} \\
m_{THF,required} &\cong 2 \cdot m_{Ti.iso-prop.} \\
V_{THF,required} &= \frac{2 \cdot \rho_{THF} \cdot V_{Ti.iso-prop.}}{\rho_{THF}} \\
V_{THF,required} &= \frac{2 \cdot 0,889 \frac{g}{cm^3} \cdot 25ml}{0,97 \frac{g}{cm^3}} \approx 46ml
\end{aligned} \tag{2.9}$$

Figure 2.10 shows a model of a tetra-hydrofuran molecule.

<i>tetra-hydrofuran</i>	
Density $[\rho]$	$0,889 \frac{g}{cm^3}$
Molecular weight $[M]$	$72,11 \frac{g}{mol}$
CAS number	109-99-9

Table 2.3 : Properties of tetra-hydrofuran

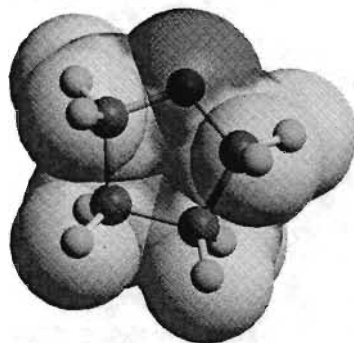


Figure 2.10 : Model of a tetrahydrofuran molecule. Red : oxygen, black : carbon, blue : hydrogen

### 2.2.2 Ti doping of multi-walled carbon nanotubes

For the first set of experiments, non purified (as synthesized) multi-walled nanotubes (MWNT) quality Ib produced by FutureCarbon were used as a titanium acceptor. Table 2.4 shows some relevant properties and figure 2.11 a SEM/TEM image of this material.

The experiments were carried out by the following steps :

<i>MWNT – Ib</i>	
Dimensions [ $d$ ]	$15nm$
BET-surface [M]	$\approx 200 \frac{m^2}{g}$
Purity	$> 98\%$

Table 2.4 : Properties of multi-walled carbon nanotubes MWNT-Ib produced by FutureCarbon

1. Heat treatment of the nanotubes at 300 °C under vacuum for over 12 h in order to remove any water, oxygen or other substances from the surface.
2. 12,5 ml titanium iso-propoxide and 90 ml THF is put in a 5 liter flask together with about 0,5 g of powdered multi-walled nanotubes CNT-MW.

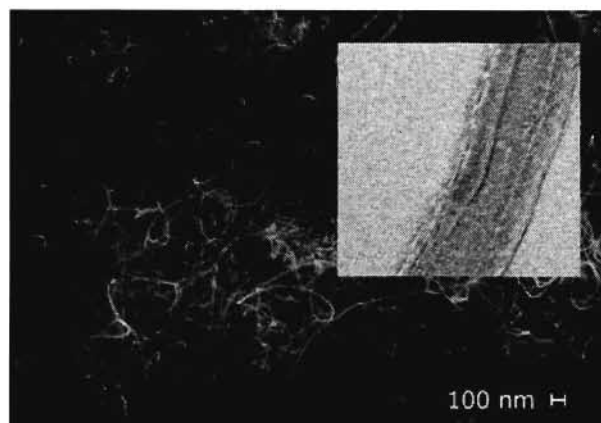


Figure 2.11 : SEM/TEM image of multi-walled carbon nanotubes MWNT-Ib produced by FutureCarbon.

3. A magnetic stirrer is put in the flask.
4. A condenser with a temperature sensor on the top is mounted on top of the flask and the system is hermetically sealed with sealing agent.
5. The bottom of the glass flask is put in the oil bath on top of a heating plate. To avoid chemical reactions caused by incidence of light, the system is also optically insulated with aluminum foil.
6. The temperature of the heating plate is set to around 80 °C and the magnetic stirrer is activated.
7. The system remains in that state for 3 days.
8. The process is finished, the sample is refilled and prepared for the heat treatment in a glove-box to avoid contamination with  $O_2$ .

The sample representing this set of experiments is named **TiL1**.

### 2.2.3 Ti doping of carbon nanofibers

For the second set of experiments, non purified (as synthesized) carbon nanofibers CNF platelet structure produced by FutureCarbon were used as a titanium acceptor. Table 2.5 shows some properties and figure 2.12 a SEM/TEM image of this material. The

<i>CNF – PL</i>	
Dimensions [ <i>d</i> ]	150nm
BET-surface [M]	$\approx 120 \frac{m^2}{g}$
Purity	> 95%

Table 2.5 : Properties of carbon nanofibers CNF-PL produced by FutureCarbon.

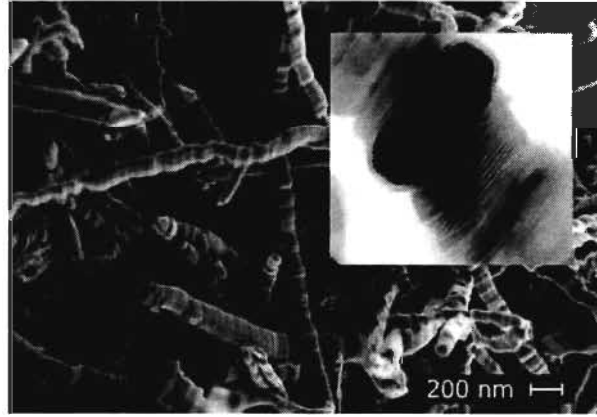


Figure 2.12 : SEM/TEM image of carbon nanofibers CNF-PL produced by FutureCarbon.

experiments were carried out by the following steps :

1. Heat treatment of the nanotubes at 300 °C under vacuum for over 12 h in order to remove any water, oxygen or other substances from the surface.

2. 17 ml titanium iso-propoxide and 38 ml THF is put in a 5 liter flask together with about 1 g of powdered nanofibers CNF-PL.
3. A magnetic stirrer and boiling stones are put in the flask.
4. A condenser with a temperature sensor on the top is mounted on top of the flask and the system is hermetically sealed.
5. The bottom of the glass flask is put in the oil bath on top of the heating plate. To avoid chemical reactions caused by incidence of light, the system is also optically insulated with aluminum foil.
6. The temperature of the heating plate is set at about 80 °C and the magnetic stirrer is activated.
7. The system remains in that state for 3 days.
8. The process is finished, the sample is refilled and prepared for the heat treatment in a glove box to avoid contamination with  $O_2$

The sample representing this set of experiments is named **TiL2**.

#### **2.2.4 Ti doping of high surface area activated carbon**

For the third set of experiments, activated carbon type IRH40 produced from the Institut de Recherche sur l'Hydrogène (IRH) was used as a titanium acceptor. The experiments were carried out by the following steps :

1. Heat treatment of the activated carbon at 300 °C under vacuum for over 12 h in order to remove any water, oxygen or other substances from the surface.
2. 26 ml titanium iso-propoxide and 155 ml THF is put in a 5 liter flask together with about 1,46 g of powdered IRH40.
3. A magnetic stirrer and boiling stones are put in the flask.
4. A condenser with a temperature sensor is mounted on top of the flask. The system is hermetically sealed.
5. The bottom of the glass flask is put in the oil bath on top of the heating plate. To avoid chemical reactions caused by incidence of light, the system is also optically insulated with aluminum foil.
6. The temperature of the heating plate is set at about 80 °C and the magnetic stirrer is activated.
7. The system remains in that state for 3 days.
8. The process is finished; the sample is refilled and prepared for the heat treatment in a glove box to avoid contamination with  $O_2$ .

The sample representing this set of experiments is named **TiL3**.



## 2.3 Palladium/platinum doping via Colloidal Microwave Processing (CMP)

For the synthesis of Pd/Pt doped nano-carbons, a microwave supported coating technique called Colloidal Microwave Processing (CMP) was used [19]. Figure 2.13 shows the physical setup as it was used for the doping process.

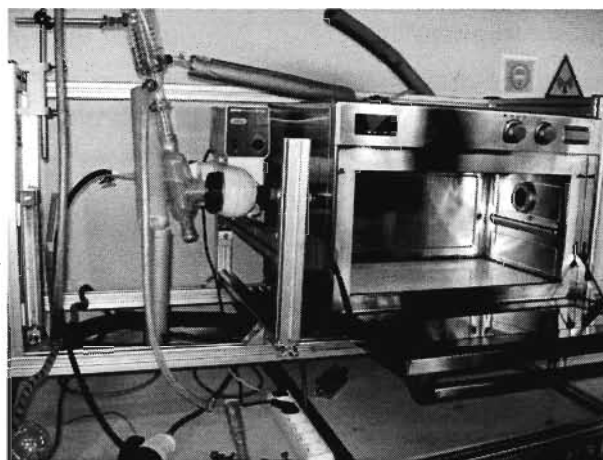


Figure 2.13 : Colloidal Microwave Processing (CMP) experimental setup.

The functionality of this method is based on the microwave supported thermal decomposition of Pd/Pt-precursors to decorate a carbon support with metals, therefore, a certain amount of powdered carbon material is heated by the microwaves in a liquid solution containing the precursor. Due to the high electrical conductivity of the carbon materials used, the microwaves are particularly absorbed by them, that results in a local overheating of the carbons surface. This effect leads to a decomposition of the precursor located in the immediate vicinity of the carbon and thus, to a very smooth, nanoscaled metal deposition on their surface. The experiments were performed in a rotary evapo-

rator, equipped with a 2,1kW commercial microwave oven, operating at a frequency of 2,45GHz, the precursors used were platinum 2,4-pentanedione ( $Pt(C_5H_7O_2)_2$ ) and palladium 2,4-pentanedione ( $Pd(C_5H_7O_2)_2$ ). Experiments were carried out at FutureCarbon GmbH with CNT-MW (purified), CNF-PL (purified) as well as high surface area activated carbon IRH40 as a carbon support. The metal content on the samples was adjusted by the mass of precursor used during the synthesis, for all samples the aim was to gain a metal density of 8wt%. The samples obtained are identified as **IRH40 (8wt% Pd)**, **CNT-MW (8wt% Pd)**, **CNF-PL (8wt% Pd)** and **CNF-PL (8wt% Pt)**.

# Chapter 3

## Sample Characterization

### 3.1 Solid state analytics

#### 3.1.1 X-ray crystallography (XRD)

X-ray diffraction is an analysis technique commonly used in materials science for the characterization of the crystalline structure of a solid material [22, 23]. The physical basis of this method is the diffraction of X-rays of a certain energy on the spatial periodical arranged lattice planes in the solid material that are representative for a certain crystalline structure. Diffraction occurs when the distance of the lattice planes is in the range of the wavelength of the X-rays, which usually is in the dimension of about  $100pm$ . In the electro-magnetic field of the incoming X-rays of a certain wavelength, the electrons in the solid material are forced to vibrate, and as a consequence, do emit X-rays themselves with the same wavelength. These re-emitted X-rays now interfere constructive and destructive depending on the crystalline structure of the atoms of the solid. By observing the solid

at different angles, constructive and destructive interference can be visualized in a graph by plotting the viewing angle versus the X-ray intensity recorded at the certain angle. By the comparison of the spectra gained with the XRD elements database, the sample can be characterized regarding its chemical compounds and elements. The condition for constructive interference can be expressed by Bragg's law :

$$n\lambda = 2d \cdot \sin(\Theta) \quad (3.1)$$

whereas  $n$  is an integer,  $\lambda$  the wavelength of the X-rays,  $d$  is the spacing between the planes in the atomic lattice, and  $\Theta$  is the angle between the incident ray and the scattering planes.

In this thesis, X-ray diffraction was used to characterize most of the samples synthesized. However, goal of the synthesis process always was to generate a monolayer that can not be detected by XRD, as a consequence peaks appearing in the XRD spectra were an indicator of thick coating. In comparison with X-ray Photoelectron Spectroscopy (XPS) described in subsection 3.1.2, XRD is a characterization technique which allows not just the analysis of the first 10nm of the samples surface, but features an insight through the whole diameter of the sample.

### **3.1.2 X-ray Photoelectron Spectroscopy (XPS)**

X-ray Photoelectron Spectroscopy (XPS) is a quantitative spectroscopic technique that allows the analysis of the empirical formula, the chemical state and the electronic state of the elements that exist on a samples surface. An electron is ejected from a core

level by an X-ray photon of the energy  $h\nu$ . The kinetic energy ( $E_K$ ) and the number of these emitted photoelectrons that escape from the top 1 to 10nm of the sample is then analyzed by an electron spectrometer [24, 25]. However, the kinetic energy of the electrons is not an intrinsic material property but is dependent on the photon energy of the X-rays employed, the binding energy ( $E_B$ ) is the parameter which identifies the electron specifically, both in terms of its element and atomic level. The relationship between the X-ray photon energy, the kinetic energy and the binding energy is :

$$E_B = h\nu - E_K - W \quad (3.2)$$

where  $W$  is the spectrometer work function. All three quantities known on the right hand side of the equation allow the determination of the binding energy.

By counting the number of electrons being ejected at a certain X-ray energy and plotting this number of electrons ejected per second versus the binding energy, one receives the XPS spectra characterizing the surface of the sample. By comparing this spectra with the XPS elements database, the samples surface can be characterized and classified. A few sample were characterized by this method within this thesis.

## 3.2 Hydrogen adsorption measurements

This section describes the two methods generally used for the determination of a samples hydrogen adsorption capacity. Both methods described have major advantages and disadvantages. The volumetric measurement setups available at the IRH and at FutureCarbon GmbH complete each other regarding the pressure range in which the samples adsorption capacity can be determined. For low pressure characterization ( $< 0,1$  MPa), the automatic measuring apparatuses at the IRH can be used (Quantachrome Autosorb<sup>®</sup> -1 and Micromeritics<sup>®</sup> ASAP 2020), whereas for high pressure measurements up to 4 MPa the self constructed Sieverts apparatus at FutureCarbon GmbH is used. All volumetric setups used, allow the determination of the adsorption capacity at temperatures down to 77 K. For measurements at room temperature and pressures up to 4 MPa the gravimetric setup at the IRH is used due to its better accuracy.

### 3.2.1 Volumetric method (Sieverts apparatus)

The basic idea of the volumetric method is to determine the hydrogen adsorption capacity of a sample via gas expansions from a reference volume to a measuring volume whereas the sample is located inside the measuring volume. The pressure change between those expansions allows the calculation of the amount of gas adsorbed on the sample [26, 27]. The following list explains the setup of such a system. Figure 3.1 prints out a typical setup for a volumetric test bed (Sieverts apparatus) and figure 3.2 shows the physical setup of such a test bed at FutureCarbon GmbH.

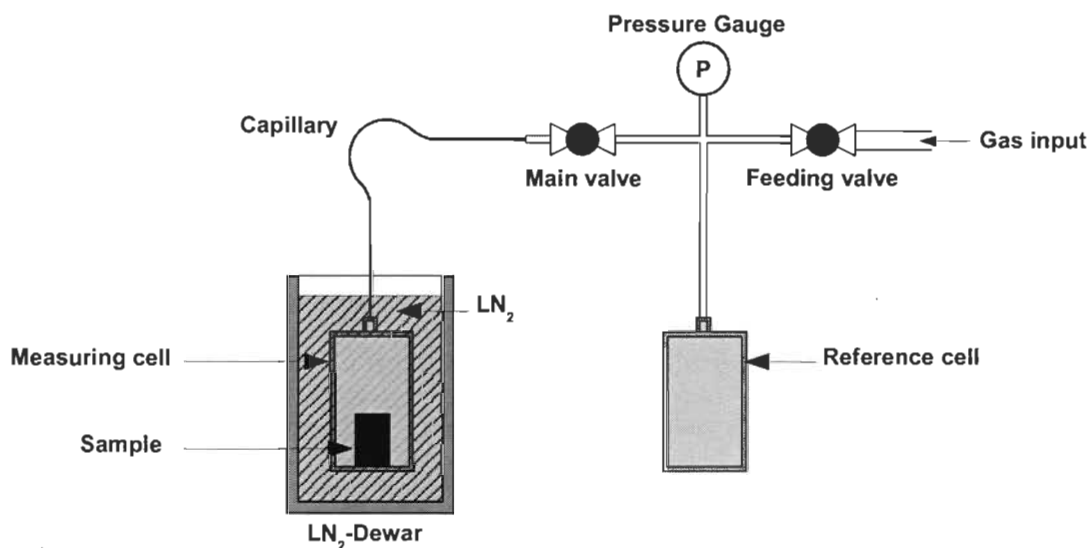


Figure 3.1 : Typical setup of a volumetric measurement system (Sieverts apparatus) showing two volumes (measuring volume and reference volume) separated by the main valve. Through gas expansion from the reference volume into the measuring volume, the hydrogen adsorption capacity of a sample located in the measuring cell can be determined through the pressure drop caused by the gas expansion.

1. The test bed consists of two volumes (measuring volume and reference volume (also reference cell)) separated by a valve (main valve). The biggest part is the measuring cell, that acts as a sample holder for a small quantity of adsorbent whose mass and density is known. To be able to test the sample adsorption capacity at temperatures other than ambient, a temperature control system could be installed. In the present case, this system is realized by a dewar that can be filled with liquid nitrogen (boiling point 77,35 K) to allow adsorption measurements at low temperatures.
2. At the beginning of every recording of an adsorption isotherm, all volumes are evacuated by a mechanical pump and the main valve is closed. A certain amount

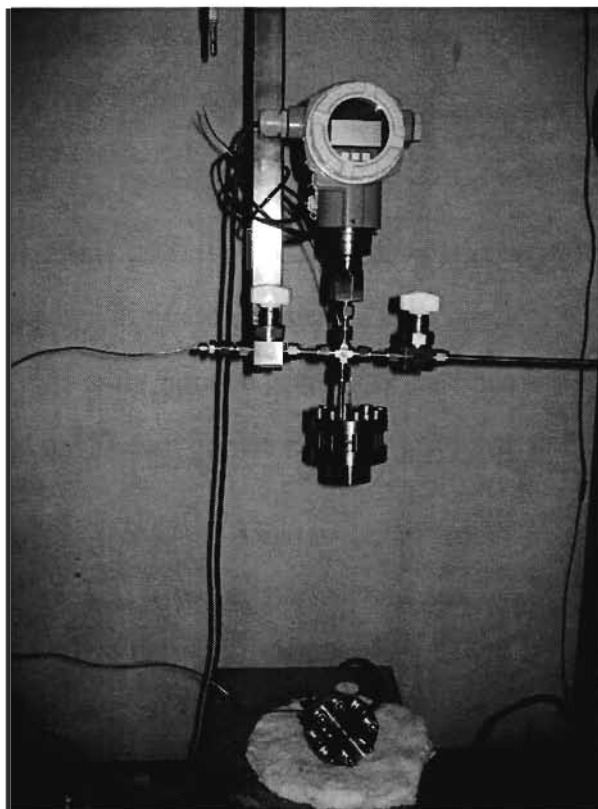


Figure 3.2 : Volumetric test bed at FutureCarbon GmbH in Bayreuth, Germany. The test bed is designed for the measurement of adsorption isotherms of samples with a mass up to 10 g at temperatures ranging from 77 K to 500 K and pressures up to 100 bar.

of gas (here hydrogen) is dosed in the reference volume by a gas feed line. This amount can be determined through the volume, the pressure and the temperature of the gas. After the feeding has occurred, the reference volume is disconnected from the feeding line by closing the feeding valve.

3. The main valve is opened and the gas in the reference volume expands in the measuring volume where a certain quantity of the gas is adsorbed on the sample (adsorbate) inside the measuring cell. The quantity adsorbed can now be calculated



through the known temperature and the volume of both cells and the pressure drop occurring during the expansion. The value calculated represents the first point of an excess isotherm.

4. For obtaining the second point of the isotherm, the main valve is closed and the reference volume is dosed with a certain amount of hydrogen by opening the feeding valve. The pressure in the reference volume after this second dosing has to be significantly higher than the pressure in the measuring volume.
5. The main valve is reopened to expand the gas from the reference volume into the measuring volume and the second point of the isotherm can be calculated as described above.
6. By this method an arbitrary amount of isotherm points can be recorded.

For the calculation of the adsorption capacity the real gas law is used :

$$p \cdot V = m \cdot R_S \cdot T \cdot z \quad (3.3)$$

with  $R_S$  as the specific gas constant of hydrogen ( $R_{S,hydrogen} = 4124 \frac{J}{kg \cdot K}$ ) and  $z$  as the compression factor which is calculated by the NIST database (NIST Reference Fluid Thermodynamic and Transport Properties Database (REFPROP) : Version 7.0). For every expansion it is assumed that the amount of gas in the reference cell before the expansion is equal to the amount of gas being in the whole system after the expansion :

$$m_{bef.exp.} = m_{aft.exp.} \quad (3.4)$$

By applying the real gas law one obtains :

$$\left( \frac{p \cdot V}{R_S \cdot T \cdot z} \right)_{bef.exp.} = \left( \frac{p \cdot V}{R_S \cdot T \cdot z} \right)_{aft.exp.} \quad (3.5)$$

The amount of gas before the expansion can be simply calculated by the pressure and the known volume of the reference cell :

$$m_{bef.exp.} = \frac{p_{bef.exp.} \cdot V_{ref.}}{R_S \cdot T_{RT} \cdot z_{bef.exp.,RT}} \quad (3.6)$$

For the calculation of the amount of hydrogen in the system after the expansion we have to take account of the different parts of the measuring volume being at different temperatures. As shown in figure 3.1, just the part of the measuring volume containing the sample (measuring cell) is at the measurement temperature ( $V_{meas.,temp.}$ ), but a small volume connecting the measuring cell with the main valve remains at room temperature ( $V_{meas.,RT}$ ). In the setup, this volume is represented by a steel capillary and a SWAGELOK fitting for the connection to the main valve. The amount of gas being present in the system after the expansion is calculated by :

$$m_{aft.exp.} = \frac{p_{aft.exp.} \cdot V_{ref.}}{R_S \cdot T_{RT} \cdot z_{aft.exp.,RT}} + \frac{p_{aft.exp.} \cdot V_{meas.,RT}}{R_S \cdot T_{RT} \cdot z_{aft.exp.,RT}} + \frac{p_{aft.exp.} \cdot V_{meas.,temp.}}{R_S \cdot T_{temp.} \cdot z_{aft.exp.,temp.}} + m_{ads.}^{exc.} \quad (3.7)$$

whereas  $m_{ads.}^{exc.}$  is the amount adsorbed on the sample in excess of the amount of gas that would be present in the volume taken by the sample without the presence of the sample. By applying the equations 3.6 and 3.7 on equation 3.4, we obtain for the excess amount

adsorbed at the pressure  $p_{aft.exp.(1)}$  :

$$m_{ads.(1)}^{exc.} = \frac{p_{bef.exp.,(1)} \cdot V_{ref.}}{R_S \cdot T_{RT} \cdot z_{bef.exp.,RT,(1)}} - \frac{p_{aft.exp.,(1)} \cdot V_{ref.}}{R_S \cdot T_{RT} \cdot z_{aft.exp.,RT,(1)}} - \frac{p_{aft.exp.,(1)} \cdot V_{meas.,RT}}{R_S \cdot T_{RT} \cdot z_{aft.exp.,RT,(1)}} - \frac{p_{aft.exp.,(1)} \cdot V_{meas.,temp.}}{R_S \cdot T_{temp.} \cdot z_{aft.exp.,temp,(1)}} \cong m_{p_{aft.exp.,(1)}}^{exc.} \quad (3.8)$$

This amount represents the first point of the excess adsorption isotherm. To gather the second point of the isotherm, another gas expansion from the reference volume into the measuring volume is performed as described on page 37. The amount of gas remaining in the measuring volume from the last preceding expansion has to be added to equation 3.8. The excess amount adsorbed for the second expansion is thus calculated by :

$$m_{ads.,(2)}^{exc.} = \frac{p_{aft.exp.,(1)} \cdot V_{meas.,RT}}{R_S \cdot T_{RT} \cdot z_{aft.exp.,RT,(1)}} + \frac{p_{aft.exp.,(1)} \cdot V_{meas.,temp.}}{R_S \cdot T_{temp.} \cdot z_{aft.exp.,temp,(1)}} + \frac{p_{bef.exp.,(2)} \cdot V_{ref.}}{R_S \cdot T_{RT} \cdot z_{bef.exp.,RT,(2)}} - \frac{p_{aft.exp.,(2)} \cdot V_{ref.}}{R_S \cdot T_{RT} \cdot z_{aft.exp.,RT,(2)}} - \frac{p_{aft.exp.,(2)} \cdot V_{meas.,RT}}{R_S \cdot T_{RT} \cdot z_{aft.exp.,RT,(2)}} - \frac{p_{aft.exp.,(2)} \cdot V_{meas.,temp.}}{R_S \cdot T_{temp.} \cdot z_{aft.exp.,temp,(2)}} \quad (3.9)$$

The calculated value represents the excess amount adsorbed in addition to the first calculated amount adsorbed ( $m_{ads.,(1)}^{exc.}$ ). Adding up both values returns the excess amount adsorbed at pressure  $p_{aft.exp.,(2)}$  which represents the second point of the isotherm :

$$m_{p_{aft.exp.,(2)}}^{exc.} = m_{ads.,(2)}^{exc.} + m_{ads.,(1)}^{exc.} \quad (3.10)$$

By continuing this procedure the desired number of isotherm points can be calculated :

$$\begin{aligned}
m_{p_{aft.exp.,(n)}}^{exc.} = & \frac{p_{aft.exp.,(n-1)} \cdot V_{meas.,RT}}{R_S \cdot T_{RT} \cdot z_{aft.exp.,RT,(n-1)}} + \frac{p_{aft.exp.,(n-1)} \cdot V_{meas.,temp.}}{R_S \cdot T_{temp.} \cdot z_{aft.exp.,temp,(n-1)}} + \\
& + \frac{p_{bef.exp.,(n)} \cdot V_{ref.}}{R_S \cdot T_{RT} \cdot z_{bef.exp.,RT,(n)}} - \frac{p_{aft.exp.,(n)} \cdot V_{ref.}}{R_S \cdot T_{RT} \cdot z_{aft.exp.,RT,(n)}} - \\
& - \frac{p_{aft.exp.,(n)} \cdot V_{meas.,RT}}{R_S \cdot T_{RT} \cdot z_{aft.exp.,RT,(n)}} - \frac{p_{aft.exp.,(n)} \cdot V_{meas.,temp.}}{R_S \cdot T_{temp.} \cdot z_{aft.exp.,temp,(n)}} + \sum_{i=1}^{n-1} m_{ads.,(i)}^{exc.} \quad (3.11)
\end{aligned}$$

For adsorption measurements at room temperature were the reference volume and the measuring volume have the same temperature, a differentiation between the two parts of the measuring volume (here : capillary with SWAGELOK fitting and measuring cell) is not necessary, consequently equation 3.11 can be simplified to :

$$\begin{aligned}
m_{p_{aft.exp.,(n)}}^{exc.} = & \frac{p_{aft.exp.,(n-1)} \cdot V_{meas.}}{R_S \cdot T_{RT} \cdot z_{aft.exp.,RT,(n-1)}} + \frac{p_{bef.exp.,(n)} \cdot V_{ref.}}{R_S \cdot T_{RT} \cdot z_{bef.exp.,RT,(n)}} - \\
& - \frac{p_{aft.exp.,(n)} \cdot V_{ref.}}{R_S \cdot T_{RT} \cdot z_{aft.exp.,RT,(n)}} - \frac{p_{aft.exp.,(n)} \cdot V_{meas.}}{R_S \cdot T_{RT} \cdot z_{aft.exp.,RT,(n)}} + \sum_{i=1}^{n-1} m_{ads.,(i)}^{exc.} \quad (3.12)
\end{aligned}$$

### 3.2.2 Common problems presented the volumetric method

This subsection describes common problems usually occurring with the use of the volumetric method. The nature of these problems depends on the setup of the Sieverts apparatus and may differ as the case arises.

#### Temperature gradient

Adsorption measurements at temperatures different from ambient require a temperature control system that allows the adjustment of the measuring cells temperature. However,

having the measuring cell and the reference cell at different temperatures leads to a temperature gradient somewhere in the system, which makes it very difficult to calculate the amount of gas being present in that part of the system. This problem can be minimized by using a connection with a very low volume between the measuring cell and the reference cell. In the present system used, this connection has been realized by a 30 *cm* steel capillary with an inside diameter of 0,15*mm*. This leads to an internal volume of about 0,0053 *cm*<sup>3</sup> that is around 4 orders of magnitude smaller than the volume of the rest of the system. By having the temperature gradient occur over such a small volume, the amount of gas being present in the capillary can be calculated by assuming an averaged temperature all over the capillary.

### Identification of the systems volume

When setting up a volumetric system from scratch, usually neither the reference volume nor the measuring volume is known, however both values are required for the adsorption measurements. The determination of both values requires the use of a well known calibration volume  $V_{cal}$  e.g. in form of a sphere or another body with simple geometry, which can be placed in the measuring volume of the Sieverts apparatus. The volumes are then determined the following way :

1. The empty system (no sample or calibration volume used) is pumped out by the use of the mechanical pump.
2. The main valve is closed and the reference volume is dosed with a certain amount of hydrogen gas. The feeding valve is closed after this dosing. The pressure gauge

shows the pressure being present now in the reference volume before the expansion.

3. By opening the main valve, the gas is expanded from the reference volume into the measuring volume. The pressure after this expansion can be read on the pressure gauge. With both pressure values (before and after the gas expansion), the proportion between the reference and the measuring volume  $\frac{V_{ref.}}{V_{meas.}}$  can be calculated :

$$\begin{aligned}
 m_{bef.exp.} &= m_{aft.exp.} \\
 \frac{p_{bef.exp.} \cdot V_{ref.}}{R_S \cdot T_{RT} \cdot z_{bef.exp.}} &= \frac{p_{aft.exp.} \cdot V_{ref.}}{R_S \cdot T_{RT} \cdot z_{aft.exp.}} + \frac{p_{aft.exp.} \cdot V_{meas.}}{R_S \cdot T_{RT} \cdot z_{aft.exp.}} \\
 \frac{V_{ref.}}{V_{meas.}} &= \frac{p_{aft.exp.}}{z_{aft.exp.} \cdot \left( \frac{p_{bef.exp.}}{z_{bef.exp.}} - \frac{p_{aft.exp.}}{z_{aft.exp.}} \right)} \quad (3.13)
 \end{aligned}$$

4. The system is opened and the calibration volume is placed inside the measuring cell.
5. The system is closed and evacuated by the mechanical pump.
6. A second expansion is performed as described before.
7. With the help of the proportion  $\frac{V_{ref.}}{V_{meas.}}$  and the known pressures before and after this expansion, the measuring volume  $V_{meas.}$  can be calculated :

$$\begin{aligned}
 m_{bef.exp.} &= m_{aft.exp.} \\
 m_{ref.} &= m_{ref.} + m_{meas.} - m_{cal.} \\
 \frac{p_{bef.exp.} \cdot V_{ref.}}{R_S \cdot T_{RT} \cdot z_{bef.exp.}} &= \frac{p_{aft.exp.} \cdot V_{ref.}}{R_S \cdot T_{RT} \cdot z_{aft.exp.}} + \frac{p_{aft.exp.} \cdot V_{meas.}}{R_S \cdot T_{RT} \cdot z_{aft.exp.}} - \frac{p_{aft.exp.} \cdot V_{cal.}}{R_S \cdot T_{RT} \cdot z_{aft.exp.}}
 \end{aligned}$$

$$V_{meas.} = \frac{V_{cal.}}{1 - \frac{V_{ref.}}{V_{meas.}} \cdot \left( \frac{p_{bef.exp.} \cdot z_{aft.exp.}}{z_{bef.exp.} \cdot p_{aft.exp.}} - 1 \right)} \quad (3.14)$$

8. The reference volume  $V_{ref.}$  can be calculated with the known proportion  $\frac{V_{ref.}}{V_{meas.}}$  and the measuring volume  $V_{meas.}$ .
9. By repeating these steps e.g. 10 times, the measurements repeatability can be checked and the final volumes can be determined by averaging the gained values.

### 3.2.3 Gravimetric method

Another well-known method for the determination of the gas uptake of a sample is the use of a magnetic suspension balance or a beam balance [26, 28, 29]. The gravimetric determination of a samples gas uptake commonly has a few advantages in comparison to the volumetric determination [27] as described in subsection 3.2.1. These are in detail :

- The mass of the sample is measured directly. As a consequence, the calculation of the amount of gas adsorbed on the sample turns out to be very simple, instead of calculating the amount adsorbed through pressures, temperatures and volumes, just buoyancy effects have to be considered.
- The volumetric method requires a fixed, known volume of all pipes and valves being installed in the system which means that every change or adaption of the components used demands a complete recalibration of the system. A gravimetric system does not show this disadvantage.

- The supersensitive balances generally used for gravimetric measurement systems usually allow smaller sample sizes than volumetric systems do. As a consequence, volumetric setups are usually more predestinated for large samples.
- One disadvantage of gravimetric systems compared to volumetric systems is their vulnerability to impurities of the sorbent.

The balance in the gravimetric system used, was a beam balance type *Cahn D410* (figure 3.3) with a sensitivity up to  $10\ \mu g$ . Figure 3.4 shows a sketch of the system and figure

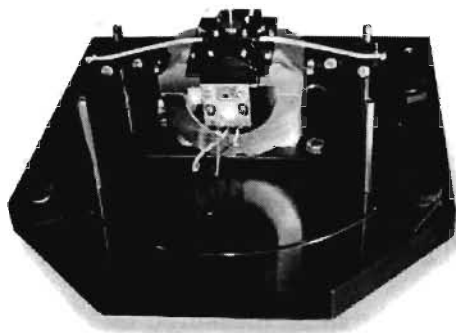


Figure 3.3 : Photo of the beam balance type *Cahn D410* used for the gravimetric experiments

3.5 an experimental setup as it was realized at the IRH and used for the measurements within this thesis. The setup used, consists of a beam balance inside a hermetically sealed stainless steel measuring chamber. A pressure sensor is connected to the chamber to allow a measurement of the static pressure inside. The gas feeding line allows to fill up the measurement chamber with the desired gas at a certain pressure. The left arm of the beam balance carries a well known reference mass whereas the right arm carries a sample holder that can be loaded with a sample by opening the measuring chamber at



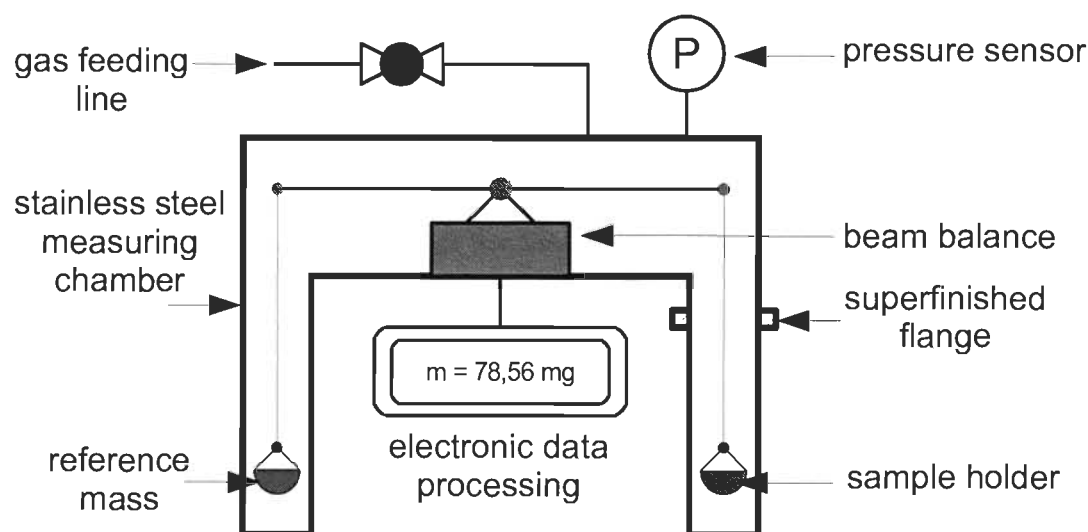


Figure 3.4 : Sketch of a gravimetric measurement system. The hydrogen adsorption at a certain pressure can be determined through the mass measured by the balance minus the buoyancy of the sample caused by the surrounding hydrogen gas.

the superfinished flange. The beam balance is connected to an electronic data processing system and a display to show the mass measured by the balance. The mass shown by the balance is made up of the samples mass present in the sample holder and two additional physical effects :

1. The first effect is the gas ab/adsorption on the sample which is dependent on the temperature and pressure the sample is exposed to, as well as the samples physical and/or chemical properties allowing more or less physical or chemical ab/adsorption. Generally, the mass of gas physisorbed or chemisorbed on the sample increases with the pressure.
2. The second effect influencing the measurement is buoyancy caused by the gas surrounding the sample. The buoyancy effect also increases with rising pressure, how-

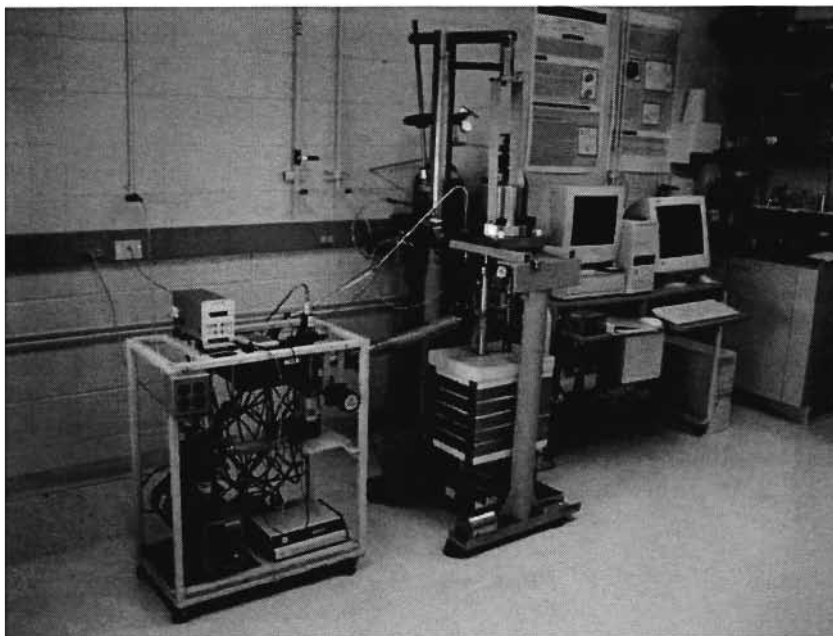


Figure 3.5 : Gravimetric setup at the IRH allowing measurements at pressures up to 100 bar.

ever, the force of the effect is vectored in the opposite to the adsorption effect.

Whereas high pressure causes a high amount of gas ab/adsorbed on the sample and thus leads to a greater mass value shown by the balance, it also results in a greater buoyancy of the sample caused by the surrounding gas, which results in a subsidence of the mass being measured. Unfortunately, when measuring the hydrogen adsorption, both effects interfere and thus cannot be measured independently by using a gas that could ab/adsorb on the sample under study. As a consequence, the buoyancy has to be measured via a different gas whose physi- or chemisorption on the sample is negligible. Therefore helium gas is used, due to its inert character it does not interact with the sample by ab/adsorption and thus can be used to investigate buoyancy effects of the

sample. The buoyancy is given by :

$$F = \rho \cdot V \cdot g \quad (3.15)$$

whereas  $\rho$  is the density of the gas,  $V$  the displaced volume and  $g$  the gravitational acceleration. Looking at the formula 3.15 the only thing that changes the buoyancy force by using different gases is the density of the gas. The densities of hydrogen and helium under normal conditions (1013,25 mbar and 273,15 K) are :

$$\begin{aligned} \rho_{Hydrogen} &= 0,08988 \frac{kg}{m^3} \\ \rho_{Helium} &= 0,17849 \frac{kg}{m^3} \end{aligned} \quad (3.16)$$

As shown in equation 3.16, the density of helium gas is about two times the density of hydrogen gas, as a consequence the buoyancy determined by helium measurements has to be divided by a factor of two to obtain the actual buoyancy caused by hydrogen gas. By subtracting the buoyancy of the mass displayed by the balance, the mass of hydrogen gas actually adsorbed on the sample surface can be calculated.

# Chapter 4

## Results

In this chapter the results obtained by XRD, XPS and hydrogen adsorption measurements are presented and discussed. Table 4.1 and 4.2 show an overview of the pretreatment procedures and the characterization methods the pristine materials and the coated samples were analyzed with.

<i>Name of sample</i>	<i>Sample pretreatment</i>	<i>Adsorption Isotherm Volum. 0 - 1bar 77K and/or 295K</i>	<i>Adsorption Isotherm Grav. 0 - 40bar 295K</i>	<i>XRD</i>
IRH40		yes (295K, 77K)	yes	-
CNT-MW (purified)	heating	-	yes	-
CNT-MW (as synth.)	under Ar at 500 °C	yes	-	-
CNF-PL (purified)	for 2h	-	yes	yes
CNF-PL (as synth.)		yes	-	yes

Table 4.1 : List of pristine materials, their pretreatments and analysis.

<i>Name of sample</i>	<i>Pristine material</i>	<i>Dopant</i>	<i>Sample mass available [mg]</i>	<i>Sample pretreatment</i>	<i>Adsorption Isotherm Volum. 0 - 1bar 77K and/or 295K</i>	<i>Adsorption Isotherm Grav. 0 - 40bar 295K</i>	<i>XRD</i>	<i>XPS</i>
TiD1	IRH40	Ti	2500		-	yes	-	-
TiD2	IRH40	Ti	1600	heating	yes (295K, 77K)	-	yes	-
TiD3	IRH40	Ti	1770	under Ar	-	yes	yes	yes
TiD4	IRH40	Ti	1600	at 500 °C	-	-	-	yes
TiD5	IRH40	Ti	1800	for 2h	-	-	yes	-
TiD6	IRH40	Ti	1800		-	yes	-	-
TiL1	CNT-MW (as synth.)	Ti	ca. 500	heating under	yes	-	yes	-
TiL2	CNF-PL (as synth.)	Ti	1078	vacuum at 300 °C	-	-	yes	-
TiL3	IRH40	Ti	1456	>12h	yes	-	-	-
IRH40 (8wt% Pd)	IRH40	Pd	1500		-	yes	-	-
CNT-MW (8wt% Pd)	CNT-MW (purified)	Pd	1000	heating under	-	yes	-	-
CNF-PL (8wt% Pd)	CNF-PL (purified)	Pd	1000	vacuum at 500 °C for 2h	-	yes	yes	-
CNF-PL (8wt% Pt)	CNF-PL (purified)	Pt	500		-	yes	-	-

Table 4.2 : List of metal doped samples, their pretreatments and analysis.

The following two sections describe the outcome of the analysis performed with the titanium and the platinum/palladium doped nano-carbons. All graphs mentioned are included in the appendix.

## 4.1 Results of nano-carbons used for doping processes

- **IRH40** (sample representing the pristine materials for experiments performed with the CVD/PVD process and others). The in-house produced high surface area activated carbon IRH40 of the IRH acts as a carbon support for most samples produced. Offering a BET-surface area of about  $2000 \text{ m}^2/\text{g}$ , its hydrogen adsorption capacity nearly reaches  $250 \text{ ml/g}$  at 1 bar and 77 K. Figures C.1, C.2, C.3 and C.4 show the adsorption isotherms for IRH40 at different temperatures and pressures. The isotherms on figure C.3 and C.4 especially show the fully reversible desorption process that proves the storage effect of hydrogen on IRH40 to be physisorption.
- **CNT-MW (purified)** (sample representing the pristine material for experiments performed with colloidal microwave processing). The multi-walled carbon nanotubes produced by FutureCarbon normally contain Co based catalysts as a holdover from their production process. These substances are removed through an adequate HCl treatment. As shown in figure C.1, their hydrogen adsorption capacity reaches  $0,8 \text{ g/kg}$  at 40 bar and a temperature of 295 K which is around 4 times lower than the capacity of IRH40 at the same conditions. This can be explained by their low

BET surface area of  $200 \text{ m}^2/\text{g}$ .

- **CNT-MW (as synth.)** (sample representing the pristine material for experiments performed with the wet chemical process). These CNT-MWs did not pass a HCl treatment and should still contain small amounts of the metal catalysts used for their production. As shown in figure A.2 no Co catalysts could be detected by XRD.
- **CNF-PL (purified)** (sample representing the pristine material for experiments performed with colloidal microwave processing). The carbon nanofibers platelet type produced by FutureCarbon normally contain Fe based catalysts as a holdover from their production process. These substances are removed through an adequate HCl treatment. As shown in figure C.1, their hydrogen adsorption capacity reaches  $0,5 \text{ g/kg}$  at 40 bar and a temperature of 295 K which is around 7 times lower than the capacity of IRH40 at the same conditions. This can be explained by their low BET surface area of  $120 \text{ m}^2/\text{g}$ .
- **CNF-PL (as synth.)** (sample representing the pristine material for experiments performed with the wet chemical process). These CNF-PLs did not pass a HCl treatment and do still contain the metal catalysts used for their production. These catalysts are not interfering with the chemicals used for the wet chemical doping approach.

## 4.2 Results of Ti decorated nano-carbons

- **TiD1** (sample representing the first set of experiments performed with the CVD/-PVD process, pristine material : IRH40). During the experiments the formation of white vapor in the Erlenmeyer flask could be observed, after the analysis of the water in the flask the occurrence of HCl could be verified due to the low pH-value (2) of the water. Most of the  $\text{TiCl}_4$  traveling through the oven is believed not to be adsorbed on the samples surface but reacted with the water under the formation of  $\text{TiO}_x$  and HCl. Hydrogen adsorption measurements as shown in figure C.2 in the appendix show a small subsidence of the samples hydrogen adsorption capacity compared to the undoped pristine material IRH40.
- **TiD2** (sample representing the second set of experiments performed with the CVD/PVD process, pristine material : IRH40). Figure C.5 and C.6 show a lower hydrogen adsorption capacity of TiD2 compared to IRH40 at 77 K and at ambient. XRD analysis prove the presence of  $\text{TiO}_2$  on the samples surface which is inactive regarding hydrogen adsorption and thus preventing the samples hydrogen adsorption to be higher than that of IRH40.
- **TiD3** (sample representing the third set of experiments performed with the CVD/-PVD process, pristine material : IRH40). XPS results in figure B.1, B.2, B.3 and B.4 demonstrate the presence of titanium as well as oxygen on the sample. XRD analysis of TiD3 in figure A.7 and A.8 reveal the formation of  $\text{TiO}_2$  as well as  $\text{TiH}_2$  on the sample. This indicates that at least a small amount of  $\text{TiO}_2$  could be reduced to Ti during the synthesis, nevertheless figure C.2 indicates a reduced adsorption



capacity compared to IRH40. The SEM image (figure 4.1) shows the metallic oxide on the surface whereas among big particles with a diameter of about 100 nm, small formations of  $TiO_2$  ranging in between 5 nm and 10 nm can be detected.

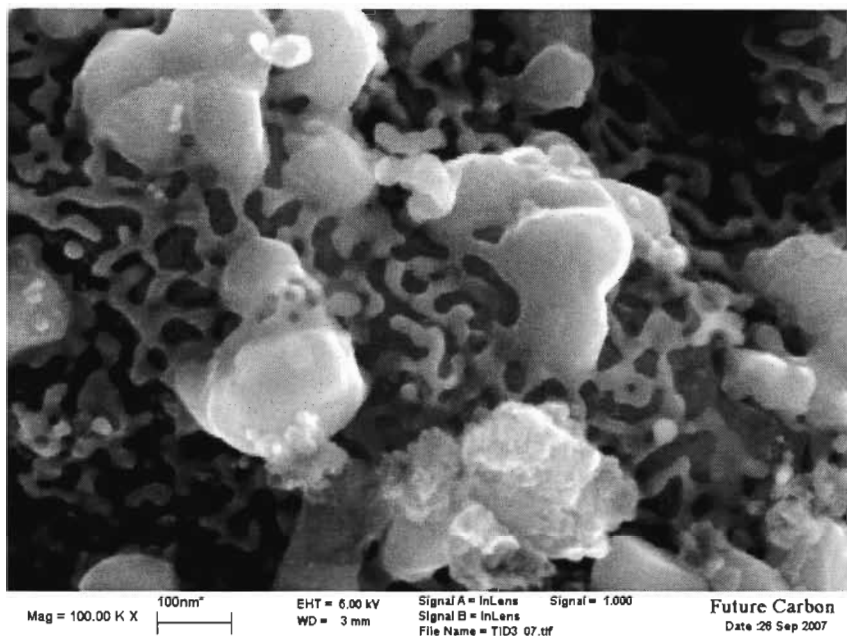


Figure 4.1 : (TiD3) Formation of  $TiO_2$  on the surface of activated carbon.

- **TiD4** (sample representing the fourth set of experiments performed with the CVD/-PVD process, pristine material : IRH40). XPS results in figure B.6, B.7 and B.8 do not show any presence of Ti on the samples surface. These results indicate that the CVD process as it was set up in this set of experiments was not effective regarding the deposition of any Ti on the samples surface.
- **TiD5** (sample representing the fifth set of experiments performed with the CVD/-PVD process, pristine material : IRH40). XRD analysis in figure A.9, A.10 and

A.11 indicate the formation of different metal compounds like NiFe and CrFe as well as  $\text{TiO}_2$  on the samples surface. The occurrence of metals can be explained by a dissolution of the metal container which contained the sample through the HCl, that was released during the synthesis. This metal contamination makes any hydrogen adsorption measurement useless. Figure 4.2 shows the formation of a large layer containing different metals on the surface of the activated carbon sample.

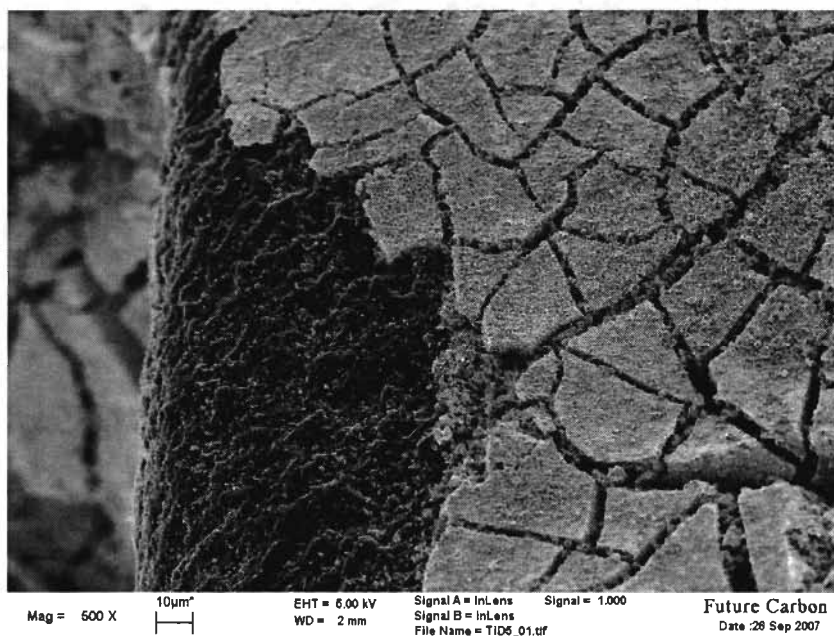


Figure 4.2 : (TiD5) Formation of different metals on the surface of the activated carbon sample.

- **TiD6** (sample representing the sixth set of experiments performed with the CVD/-PVD process, pristine material : IRH40). Adsorption measurements of TiD6 in figure C.2 indicate a decreased adsorption capacity compared to IRH40. Nevertheless, the SEM image (figure 4.3) demonstrates the formation of nano-scaled  $\text{TiO}_2$

particles on the surface of the activated carbon ranging in between 5 nm and 10 nm. In comparison with figure 4.1, an improvement of the doping process is clearly demonstrated.

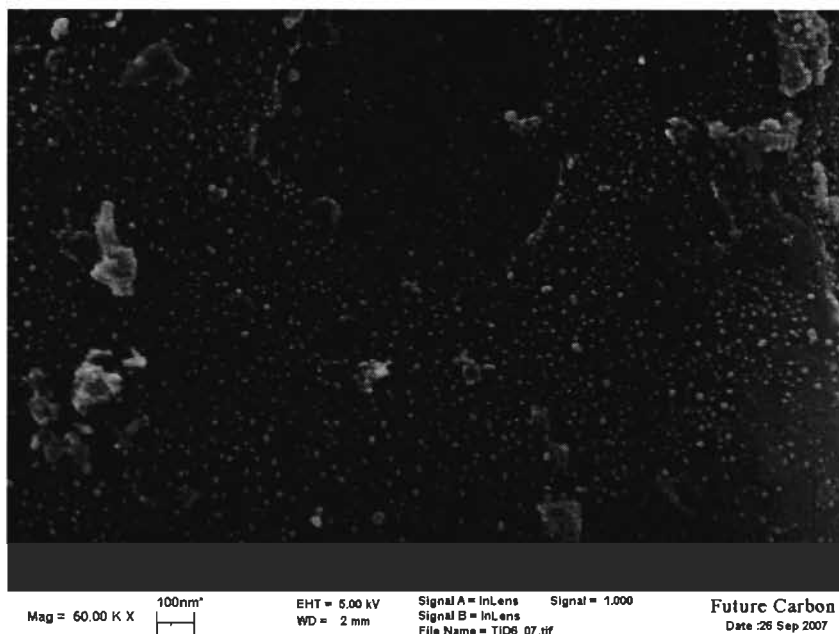


Figure 4.3 : (TiD6) Formation of nano-scaled  $TiO_2$  on the surface of the activated carbon sample.

- **TiL1** (sample representing the first set of experiments performed with the wet chemical process, pristine material : CNT-MW (as synth.)). XRD analysis of TiL1 in figure A.12, A.13, A.14 and A.15 show the formation of  $TiO_2$ ,  $TiC_x$  as well as pure Ti on the sample, thus a chemical link between the Ti and the C support could be demonstrated. The hydrogen adsorption isotherms indicate a decreased adsorption capacity as shown in figure C.7. Although the doping process was a success, the oxidation of Ti could not be prevented completely even by handling

the sample in a glove box. Figure 4.4 is showing a SEM image of TiL1 where the formation of  $TiO_2$  on the surface of the nanotubes can be clearly observed.

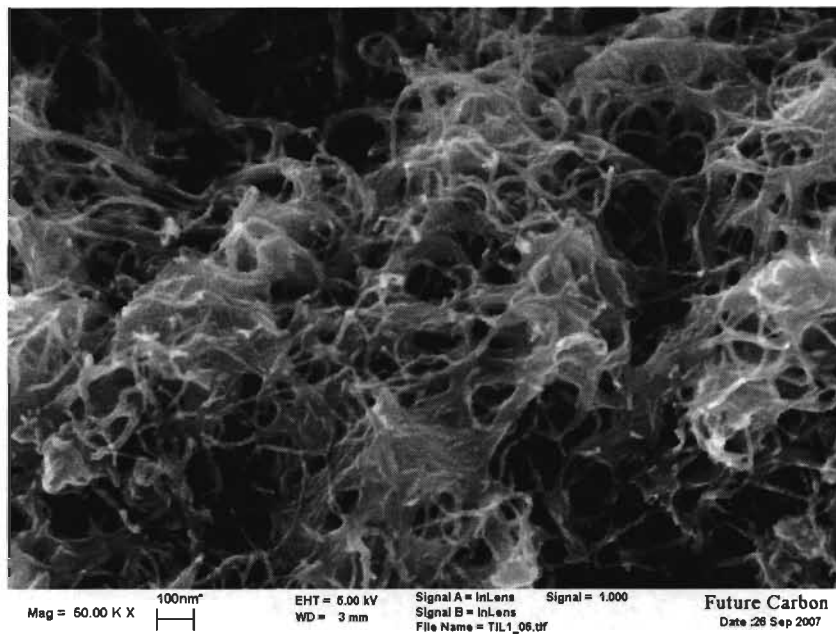


Figure 4.4 : (TiL1) Formation of  $TiO_2$  on the surface of multi-walled nanotubes.

- **TiL2** (sample representing the second set of experiments performed with the wet chemical process, pristine material : CNF-PL (as synth.)). XRD analysis of TiL2 in figure A.16, A.17 and A.18 do not show any significant amount of Ti on the sample. However, small quantities of  $TiO_2$  could be detected that indicates that all Ti deposited on the sample has been oxidized.
- **TiL3** (sample representing the third set of experiments performed with the wet chemical process, pristine material : IRH40). The samples hydrogen adsorption capacity in figure C.8 is about 70% of the capacity of IRH40. The desorption

characterisation in the same graph indicate a fully reversible adsorption isotherm that identifies the adsorption effect to be physisorption. Figure 4.5 is showing a SEM image of TiL3 featuring small amounts of  $TiO_2$  on the surface of the activated carbon.

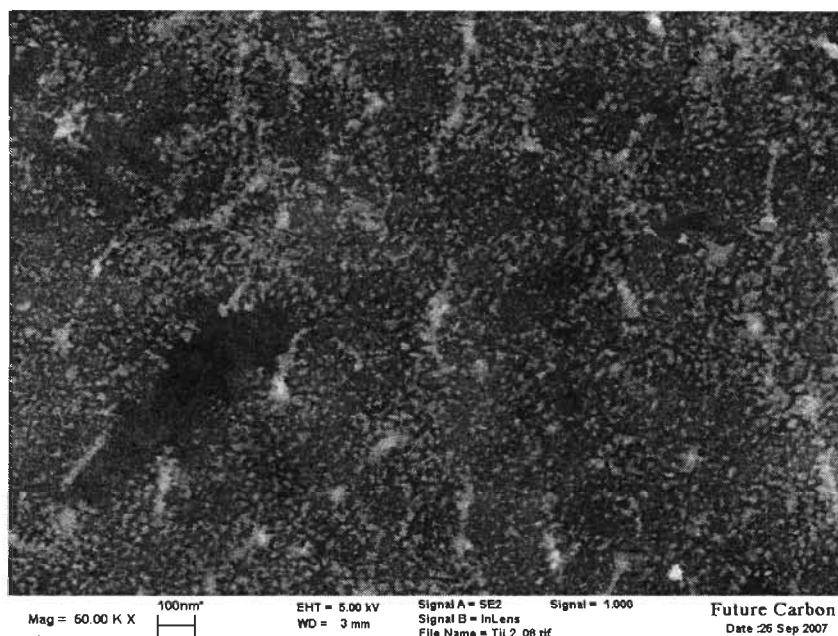


Figure 4.5 : (TiL3) Formation of  $TiO_2$  on the surface of activated carbon particles. An SE-detector was used for the imaging process to highlight the metal content.

### 4.3 Results of Pd/Pt decorated nano-carbons

- **IRH40 (8wt% Pd)** (sample decorated with Pd by Colloidal Microwave Processing (CMP), pristine material : IRH40). Figure C.1 shows the adsorption isotherm of the sample recorded at a temperature of 295 K that indicates a lower hydrogen adsorption capacity than IRH40 at pressures greater than 1 MPa. However, at

low pressures up to 1 MPa the adsorption capacity exceeds the one of IRH40 a little bit. Both isotherms intersect at a pressure of 1 MPa. The small bend of the isotherm can be explained by the formation of palladium-hydride that already occurs at very low pressures. This advantage in storage capacity decreases with increasing pressure and turns into a disadvantage at pressures greater than 1 bar where the palladium is saturated with hydrogen and more or less inactive for further hydrogen storage. The adsorption process can be fully explained by physisorption on the surface of the carbon and chemisorption on the palladium.

- **CNT-MW (8wt% Pd)** (sample decorated with Pd by Colloidal Microwave Processing (CMP), pristine material : CNT-MW (purified)). Figure C.1 shows the adsorption isotherm of the sample recorded at a temperature of 295 K that indicates an increased hydrogen adsorption capacity in the whole pressure range up to 4 MPa. The isotherm also indicates a small bend at a pressure of 0,1 MPa which attests the formation of palladium hydride. Nevertheless, the slope of the isotherm is slightly lower compared to the isotherm of the pristine material. The point of intersection is believed to be at high pressures of about 10 MPa. The adsorption process can be fully explained by physisorption on the surface of the carbon and chemisorption on the palladium.
- **CNF-PL (8wt% Pd)** (sample decorated with Pd by Colloidal Microwave Processing (CMP), pristine material : CNF-PL (purified)) Figure C.1 shows the adsorption isotherm of the sample recorded at a temperature of 295 K that also indicates an increased adsorption capacity in the whole pressure range recorded. The slope of

the isotherm is clearly lower compared to the isotherm of the pristine material, the point of intersection should be located around 6 MPa. The adsorption process can be fully explained by physisorption on the surface of the carbon and chemisorption on the palladium. Figure A.1 shows an X-ray diffractogram of the sample identifying the palladium on the samples surface

- **CNF-PL (8wt% Pt)** (sample decorated with Pt by Colloidal Microwave Processing (CMP), pristine material : CNF-PL (purified)). Figure C.1 shows the adsorption isotherm of the sample recorded at a temperature of 295 K that generally indicates the same behaviour as the isotherm of the palladium coated sample. The only difference is the bend of the isotherm which is occurring at 0,1 MPa due to the different formation process of platinum hydride. All adsorption processes can be explained by physisorption and chemisorption.

## Chapter 5

# Adsorption measurements at temperatures from 30 K to 77 K

As already stated in the summery, an additional part of the thesis was to modify an existing volumetric measurement system in order to allow the recording of adsorption isotherms at temperatures between 30 K and 77 K. In this temperature range, liquid nitrogen is no longer suitable as a cooling agent, as a consequence liquid helium has to be used. The work performed in this field will be published as a scientific article in an renowned journal, the following pages show a draft of this article explaining the work done so far and the results gained.



# $H_2$ adsorption on high surface area activated carbon at cryogenic temperatures from 30 K to 77 K

Julian Michelsen<sup>†</sup>, Richard Chahine<sup>†</sup>, Daniel Cossement<sup>†</sup>

<sup>†</sup> Institut de recherche sur l'hydrogène  
Université du Québec à Trois-Rivières  
3351 des Forges, PO Box 500  
Trois-Rivières (Qc) G9A 5H7  
Canada

## Abstract

Measurements regarding the hydrogen storage capacity of activated carbon are usually done from room temperature down to the liquid nitrogen boiling point (77,35 K at 1013 hPa) and at typical pressures up to a few MPa. However, temperatures in an activated carbon based hydrogen storage system can decrease well below 77 K due to desorption kinetics when emptying a filled storage system quickly. In this work we investigate the adsorption isotherms of AX-21 in a temperature range from 77 K down to 30 K at pressures up to 6 MPa. The measurements were realized using a Sieverts apparatus, which has been extended with a helium cooling system in order to reach temperatures below the boiling point of liquid nitrogen.

## 1 Introduction

High surface area activated carbon is one possible candidate for a storage medium in a hydrogen powered vehicle or any other hydrogen powered machine. For highly activated carbons like AX-21, the adsorption capacity can reach up to 5,4wt% at a temperature of 77 K and a pressure of 3,5 MPa [1]. However while emptying a tank, the storage medium will cool down due to the energy demanding desorption process. A lower temperature in the system causes a slower desorption process, thus a constant removal of hydrogen can not be guaranteed without a proper heat management which can keep the system temperature at an appropriate flow level. For the design of such heat management system it is necessary to understand the adsorption behaviour of the storage medium at temperatures below the normal operating level. In this work

we will show the experimental results of hydrogen excess adsorption on high surface area activated carbon at temperatures below 77 K. Furthermore we will illustrate the final storage capacity of AX-21, in comparison with a high pressure storage vessel for the same volume.

All measurements shown in this work have been performed with the high surface area activated carbon type AX-21. Table 1 shows some relevant physical properties of AX-21.

<i>AX-21 activated carbon</i>		
$S [\frac{m^2}{g}]$	$d_b [\frac{g}{cm^3}]$	$V_{mp} [\frac{m^3}{g}]$
2278	0,28	1,06

Table 1: Physical properties of AX-21. S: BET-surface area.  $D_b$ : bulk density.  $V_{mp}$ : micropore volume.

## 2 Methods

The experiments have been performed using a Sieverts apparatus as shown and explained in figure 1.

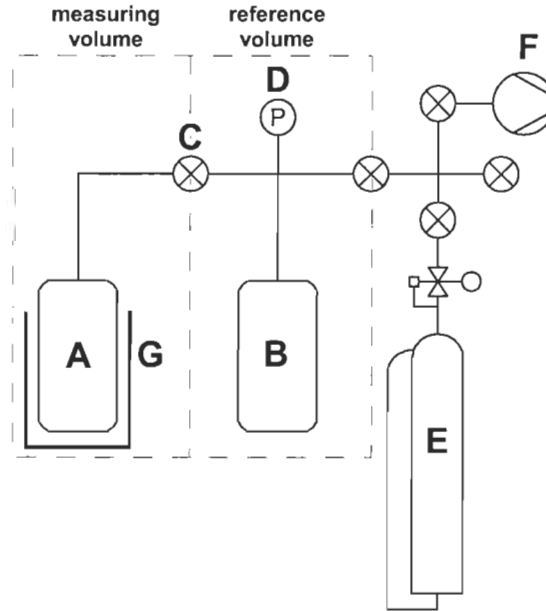


Figure 1: Sketch of the experimental setup A: measuring cell, B: reference cell, C: main valve, D: pressure gauge, E: gas supply with pressure regulator, F: vacuum pump, G: cooling system.

For determining the gas adsorption capacity of a sample located inside the measuring cell, the following procedure [2], [3] is applied:

- Reference cell and measuring cell are evacuated through a vacuum pump. The measuring cell is heated by an external heating system to degas the activated carbon sample and to remove possible impurities e.g. water in the system.
- The "dead space volume" caused by the sample occupying a small space in the measuring cell is determined through He gas expansion at room temperature (He adsorption is negligible).
- All valves are closed after a second evacuation process.
- The reference cell is filled with a certain amount of hydrogen gas. This amount can be determined by the known volume of the reference cell and the gas pressure.
- The main valve is opened and the gas expands into the measuring cell whereas a certain amount is adsorbed on the sample located inside the measuring cell.
- After a certain time the pressure and the temperature equilibrate and the amount of gas adsorbed can be calculated through the pressure difference in the system before and after opening the main valve and the known volumes of the cells (reference volume and measuring volume).
- By repeating this procedure at different pressures at a constant temperature one gains the data necessary for the calculation of a characteristic excess-adsorption isotherm.

For the calculation of these isotherms, the ideal gas law extended by the compression factor  $z$ , is used.

$$p \cdot V = n \cdot R \cdot T \cdot z \quad (1)$$

The basic approach used for determining the quantity adsorbed, is to set the total number of hydrogen molecules present in the reference cell of the system before the expansion (before opening of the main valve), equal to the number of molecules in the complete system after the opening of the main valve.

$$n_{bef.exp.} = n_{aft.exp.} \quad (2)$$

By opening the main valve, the system volume is increased ( $V_{ref.}$  is the volume of the reference cell;  $V_{meas.}$  is the volume of the measuring cell).

$$\begin{aligned} V_{bef.exp.} &= V_{ref.} \\ V_{aft.exp.} &= V_{ref.} + V_{meas.} \end{aligned} \quad (3)$$

It must also be pointed out that not the whole measuring volume is cooled by the cooling system but a small part of it remains at room temperature. For the calculation one has to distinguish between the reference volume ( $V_{ref.}$ ), the small part of the measuring volume ( $V_{meas.,room}$ ) which stays at room temperature and the part of the measuring volume which is cooled by the cooling system ( $V_{meas.,cool}$ ).

$$\begin{aligned}
n_{meas.,room} &= \frac{p_{aft.exp.} \cdot V_{meas.,room}}{R \cdot T_{room} \cdot z_{aft.exp.,room}} \\
n_{meas.,cool} &= \frac{p_{aft.exp.} \cdot V_{meas.,cool}}{R \cdot T_{cool} \cdot z_{aft.exp.,cool}} \\
n_{ref.} &= \frac{p_{aft.exp.} \cdot V_{ref.}}{R \cdot T_{room} \cdot z_{aft.exp.,room}}
\end{aligned} \tag{4}$$

After determining the number of hydrogen molecules in each part of the system, the amount adsorbed can be calculated with the following equations:

$$\begin{aligned}
n_{bef.exp.} &= \frac{p_{bef.exp.} \cdot V_{ref.}}{R \cdot T_{room} \cdot z_{bef.exp.,room}} \\
n_{aft.exp.} &= n_{meas.,room} + n_{meas.,cool} + n_{ref.} + n_{adsorbed} \\
n_{adsorbed} &= n_{bef.exp.} + n_{meas.,cool} - n_{meas.,room} - n_{ref.}
\end{aligned} \tag{5}$$

The number of molecules obtained by this calculation is the so called excess adsorption, which is the amount of gas adsorbed in excess to the bulk gas which would normally occupy the volume of the adsorbent at a certain temperature and pressure [4].

The function of the cooling system (part G in figure 1) is to keep the measuring cell at a constant temperature. To achieve isotherms at 77 K, liquid nitrogen can be used as a coolant. A remaining problem is to handle the temperature gradient occurring between the measuring cell and the reference cell. To approach this problem we used a long polyetheretherketone (PEEK™) capillary with an extremely low volume (0,05 cm on 2 m length) as a connection line between the measuring cell and the main valve. As a consequence the temperature gradient is occurring over the capillary the volume of which is so low, that it can be neglected in the calculation. However, for achieving isotherms at different fixed temperatures below 77 K it is necessary to modify the cooling system whereas the following targets have been aimed:

- Possibility to adjust the temperature of the measuring cell in 1 K steps with an accuracy of 0,1 K.
- Avoidance of any temperature gradient over the measuring cell itself ( $\Delta T$  smaller than 0,1 K).
- Low consumption of liquid helium coolant.

- Small and accurate system to perform tests with a low amount of activated carbon (1 g).

In the final version of the setup, the stainless steel measuring cell was surrounded by a cylindrical copper mantle to guarantee an even temperature distribution. The good thermal heat conductivity of copper increases even more at very low temperatures. For performing experiments at low temperatures, this copper rod was then directly inserted into a liquid helium Dewar whereas it had no contact to liquid helium but was just cooled by the helium vapor present in the upper part of the Dewar. For measuring the temperature gradient we used two platinum RTDs installed at the bottom and the top of the measuring cell. A small low power (max. 4 W) heating system made out of Teflon insulated constantan wire was installed at the very bottom of the copper coat to balance the temperature gradient caused by the heat flux coming from the top. In the final experiments it was possible to keep the temperature gradient over the measuring cell less than 30 mK. The whole volume of the measuring cell was filled with 1 g AX-21 powder. The hydrogen feeding line contained a small amount of cotton to avoid any intrusion of the activated carbon powder in the rest of the system. The accuracy of the pressure reading was any time better than  $\pm 100$  Pa. Figure 2 shows photos of the setup and figure 3 shows a sketch of the complete setup of the cooling device.

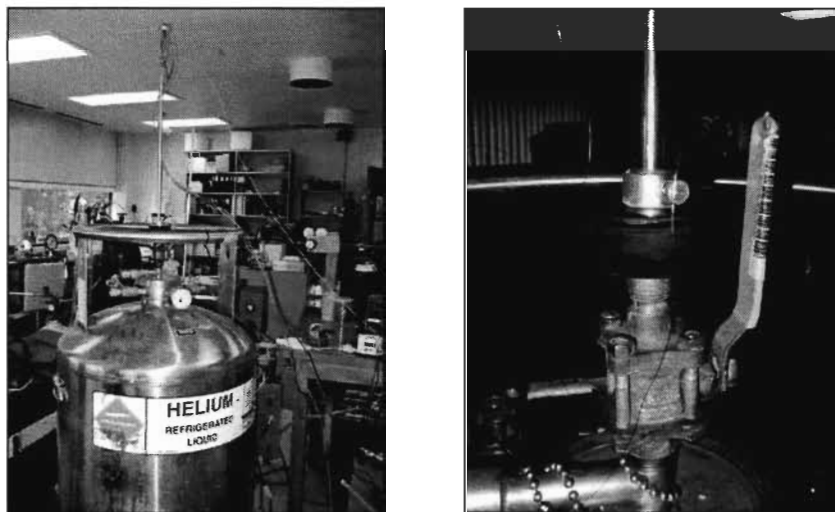


Figure 2: Photos of the measuring device including the helium cooling system.

The temperature of the measuring cell was adjusted by changing the immersion level of the setup in the helium Dewar. By pulling it more out the temperature was increased, by pushing it more in the temperature was decreased. A change of the immersion level of 1mm caused a temperature change of approximately 1 K inside the measuring cell. Without using the heating system to avoid the temperature gradient, we measured up to 15 K difference between

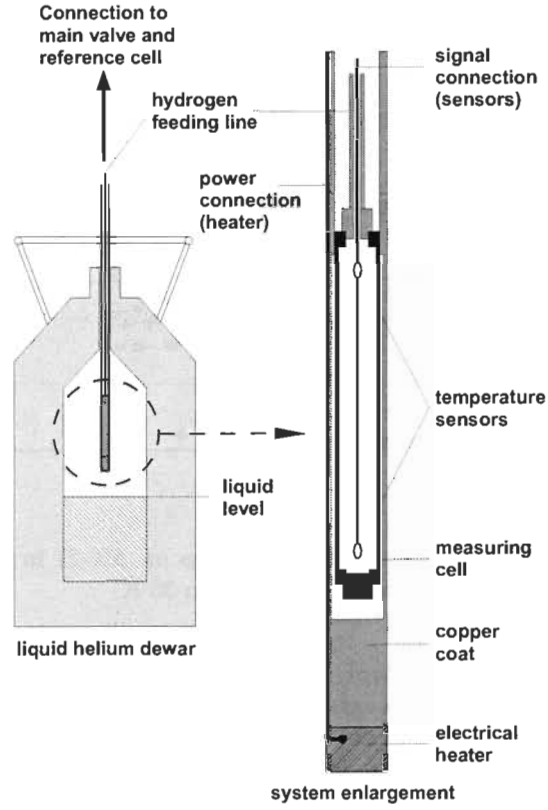


Figure 3: Drawing of the helium cooling system. The left side of the sketch shows the measuring cell inside the copper rod immersed in the helium Dewar. The right side is an enlargement of the copper rod containing the measuring cell including temperature sensors and heating system.

the top and the bottom of the measuring cell.

Before the record of every isotherm the AX-21 was heated out for approximately 3 hours at 100°C. inside the measuring cell by using an external heating element and the mechanical vacuum pump.

### 3 Results and discussion

The whole system was calibrated by recording isotherms at room temperature and at 77 K. The gained data was then compared with existing one to guarantee the functionality of the setup. After this verification we recorded isotherms from 60 K down to 30 K as shown in figure 4.

The recording time of one isotherm with 15 to 20 points varied between 8

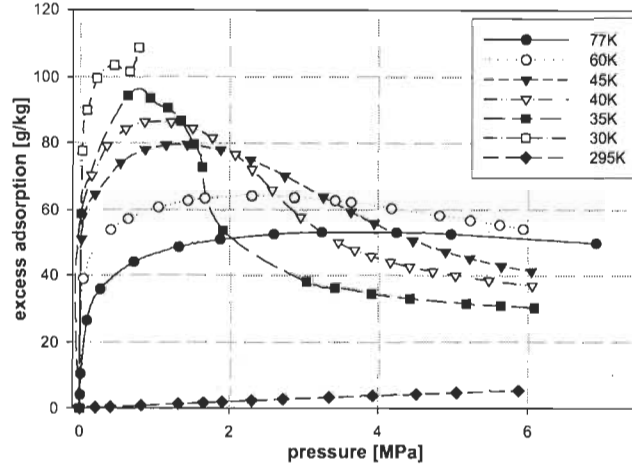


Figure 4: Hydrogen excess adsorption isotherms on AX-21 in g hydrogen per kilogram of activated carbon from 77 K down to 30 K.

and 10 hours which means approximately 30 min per measured point. It was necessary to readjust the temperature by varying the power of the heater and the immersion level of the copper rod for every single point because the absolute temperature and the temperature gradient varied depending on the pressure in the system. The helium consumption was less than 100 ml liquid Helium per isotherm.

The specifications of the PEEK<sup>TM</sup> tubing mentioned a maximum pressure of 6000 psi ( $\approx 40$  MPa) when it contains liquids like acids or solvents. Meanwhile we observed a low permeability of  $H_2$  through the walls, which is not detectable with a leak detector. Such  $H_2$  loss is very low and does not affect the final results due to the amount of AX-21 sample (1 g) used for the tests.

As apparent in Figure 4, all isotherms at 77 K and below show a maximum. At this maximum the partial density of the hydrogen molecules (number of molecules) over the pressure is the same for the adsorbed phase as well for the gas phase.

$$\left. \frac{\partial n}{\partial p} \right|_{\text{adsorbed phase}} = \left. \frac{\partial n}{\partial p} \right|_{\text{gas phase}} \quad (6)$$

Beyond this point, any increase in pressure causes a faster increase of the density in the gas phase than in the density of the adsorbed phase. This causes the decrease of any isotherm at higher pressures. The only exception is the isotherm at 30 K where the hydrogen liquefies at around 0,9 MPa.

To complete the data gained for AX-21 up to room temperature, we included former work done by P.Bénard and R. Chahine who performed excess adsorption measurements on AX-21 from 77 K to 295 K, shown in figure 5.

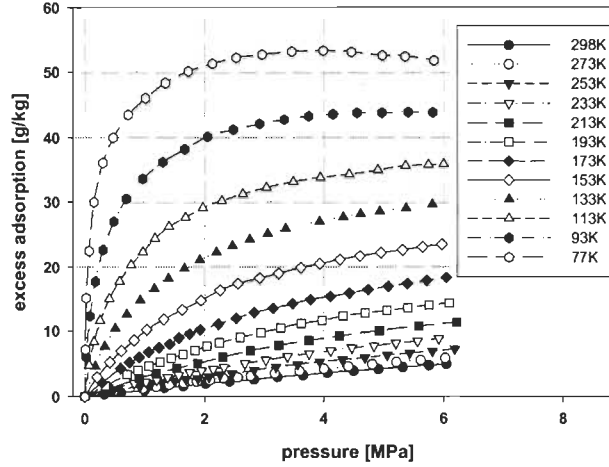


Figure 5: Hydrogen excess adsorption isotherms on AX-21 in g hydrogen per kilogram of activated carbon from 296 K down to 77 K.

In figure 6 we focused on the behavior of AX-21 at 30 K up to pressures of 6 MPa.

The excess adsorption shows the amount of hydrogen actually adsorbed on the surface area of the activated carbon. However to calculate the final storage capacity of an activated carbon based cryogenic adsorption system, one has to take account of the gaseous hydrogen being present in the volume of the meso- and macropores of the activated carbon. By adding both, one obtains the total amount of hydrogen stored in the tank system. We also added to the graph the amount of hydrogen which would be stored in this tank system at 30 K in the absence of activated carbon.

Especially at low pressures around 1 MPa the activated carbon based storage system shows about 4 times greater storage capacity than a pressure vessel with the same volume (at 30 K). The advantage of the adsorbent shrinks with higher pressures and disappears completely at pressures around 5 MPa.



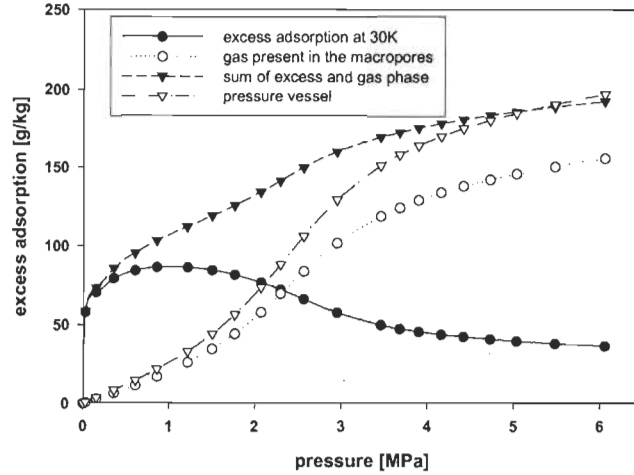


Figure 6: Comparison between an AX-21 filled activated carbon storage system and a compressed hydrogen storage system (at 30 K). The graph shows the excess adsorption, the hydrogen gas present in the meso- and macropores of the activated carbon, the sum of both, which is the total amount of hydrogen gas stored in the activated carbon based storage system, as well as the amount of gas stored in a pressure vessel with the same volume as the activated carbon based storage system.

## References

- [1] Bénard, P.; Chahine, R. Determination of the Adsorption Isotherms of Hydrogen on Activated Carbons above the Critical Temperature of the Adsorbate over Wide Temperature and Pressure Ranges: *Langmuir* 2001, 17, 1950-1955
- [2] Belmabkhout, Y.; Frère, M.; DeWeireld, G. High-pressure adsorption measurements. A comparative study of the volumetric and gravimetric methods: *Meas. Sci. Technol.* 15 (2004) 848858
- [3] Keller, J.; Robens, E.; von Hohenesche, C.d.F. Thermogravimetric and Sorption Measurement Techniques/Instruments:
- [4] Myers, A.L. Adsorption in Microporous Materials: Analytical Equations for Type I Isotherms at High Pressure: Department of Chemical and Biomolecular Engineering University of Pennsylvania, Philadelphia PA 19104 USA

# Chapter 6

## Conclusion

The procedures and techniques used for the metal doping of the nano-carbon materials were basically working. Both methods used for the synthesis of titanium doped materials (CVD/PVD and wet chemical method) turned out to be suitable for depositing titanium on the surface of the samples, however, the processes were linked with difficulties :

1. The CVD/PVD process just allowed a poor control of the amount of titanium being deposited and thus, over the thickness of the titanium layer on the samples surface. XRD measurements show that the thickness of that layer sometimes reached more than 100 molecule diameters which is way too much for proving the increased hydrogen storage effect as it was predicted by [2] and [3].
2. The greatest problem concerning the titanium coating technologies turned out to be the formation of solid  $\text{TiO}_2$  during or after the synthesis. In the CVD/PVD  $\text{TiO}_2$  was produced intentionally to obtain a solid phase on the surface of the sample, however, the reduction of that substance was hardly possible without destroying

the molecular structure of the sample. As a consequence just a fraction of the  $\text{TiO}_2$  could be turned into pure titanium. Additionally, pure titanium immediately oxidizes in an ambient atmosphere, so the samples had to be prepared for analysis inside a glove-box. Even inside the glove-box, which was filled with argon gas and usually showed an oxygen concentration of maximum 300 ppm, the titanium did oxidize after a few days.

None of the hydrogen adsorption measurements of the samples decorated with titanium did show an increased adsorption capacity which can be explained by the formation of  $\text{TiO}_2$  that occurred intentionally during the synthesis or as soon as the sample was exposed to small quantities of oxygen. The presence of  $\text{TiO}_2$  could be proven by XRD as well as XPS analysis for most of the samples. Due to the inactivity of  $\text{TiO}_2$  regarding hydrogen adsorption the coating acted as a ballast, the remaining adsorption capacity can be fully explained by physisorption on the samples surface. A storage effect as described by [2, 3, 4] could not be generated.

Decorating nano-carbons with noble metals like palladium and platinum by Colloidal Microwave Processing allowed a better control of the amount of metal deposited on the samples surface. Hydrogen adsorption measurements of samples decorated with palladium or platinum showed an increasing of their adsorption capacity after the doping process. However, two important points have to be considered :

1. The adsorption isotherms of the metal doped materials usually shows a bend at low pressures around 1 bar up to which the adsorption capacity rises very fast. This behavior can be explained by the formation of metal hydrides (palladium/platinum

hydride) which already get saturated at low pressures. At pressures greater 1bar, the additional adsorption is caused by physisorption on the remaining surface of the sample.

2. The slope of the adsorption isotherms of the metal decorated materials is, at pressures greater 1bar, lower in comparison with the undoped pristine materials. Depending on the doping and the pristine material the adsorption isotherms of both, the doped material and same material undoped, intersect at a certain pressure. At this pressure the adsorption capacity of the undoped pristine material gets higher than the capacity of the doped one.

The adsorption effects measured can be fully explained by simple chemi- and physisorption. A spillover effect as it was mentioned by [13, 14] could not be measured.

Future work in this field should aim at adapting the methods developed for the doping process in order to gain a better control of the metal layer deposited on the samples surface. In case of the titanium doping, efforts have to be made to prevent an oxidation of the sample by preventing any contact with oxygen.

# Appendix A

## XRD results

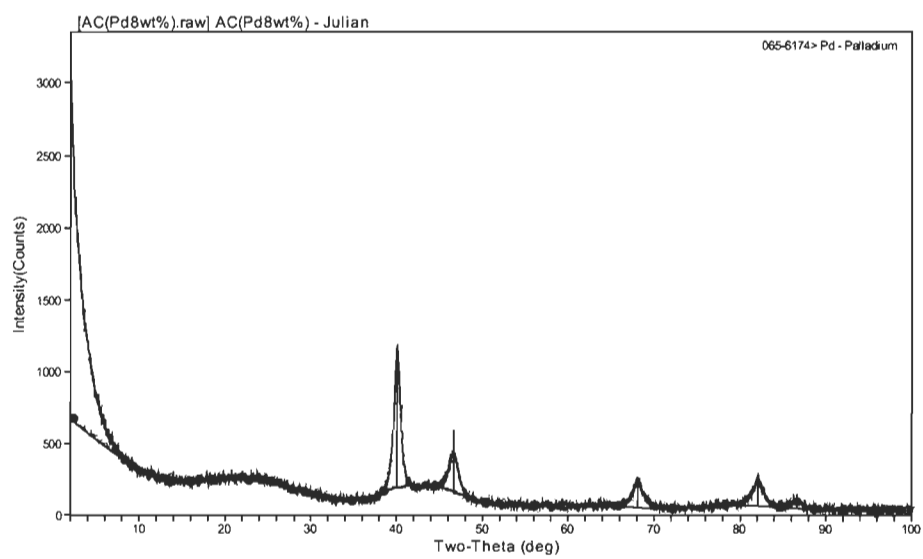


Figure A.1 : XRD spectrum of activated carbon IRH40 doped with 8wt% *Pd* showing the peaks related to *Pd*.

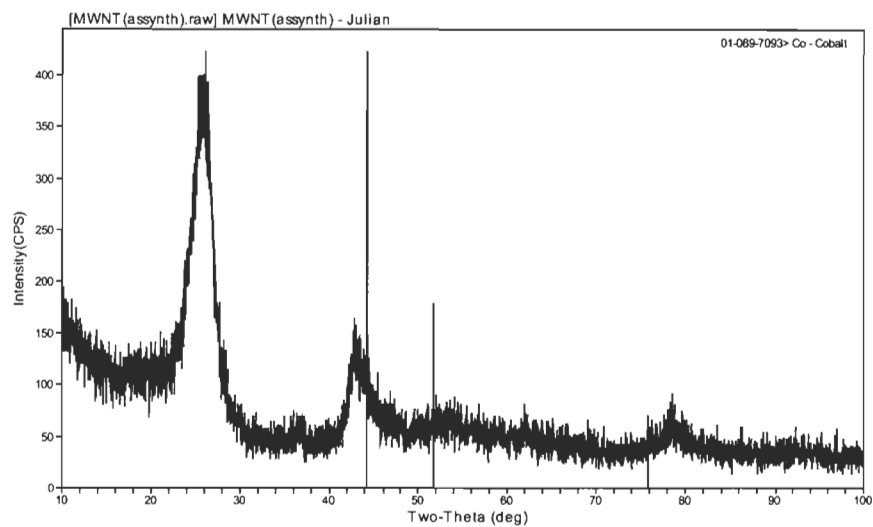


Figure A.2 : XRD spectrum of carbon nanotubes CNT-MW 'as synthesized' showing the peaks related to  $Co$ .

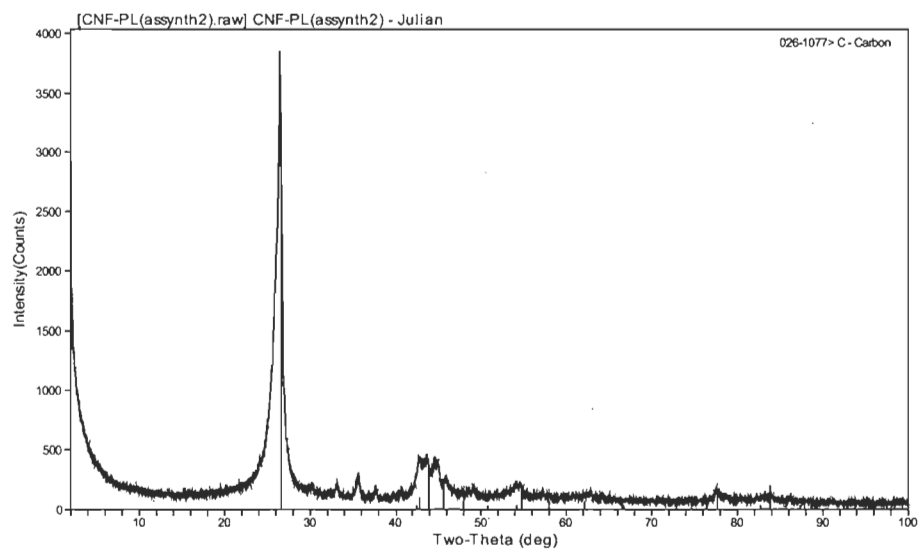


Figure A.3 : XRD spectrum of carbon nanofibers CNF-PL 'as synthesized' showing the peaks related to  $C$ .

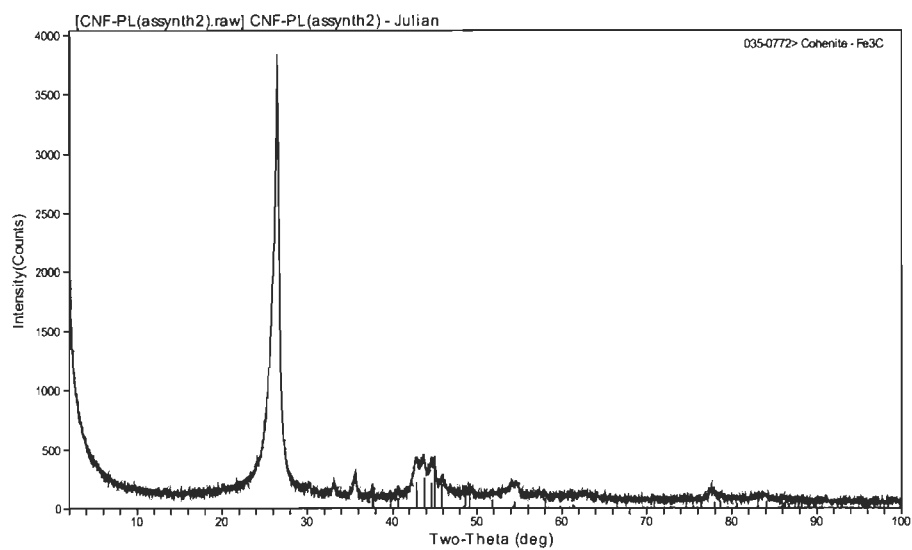


Figure A.4 : XRD spectrum of carbon nanofibers CNF-PL 'as synthesized' showing the peaks related to  $Fe_3C$ .

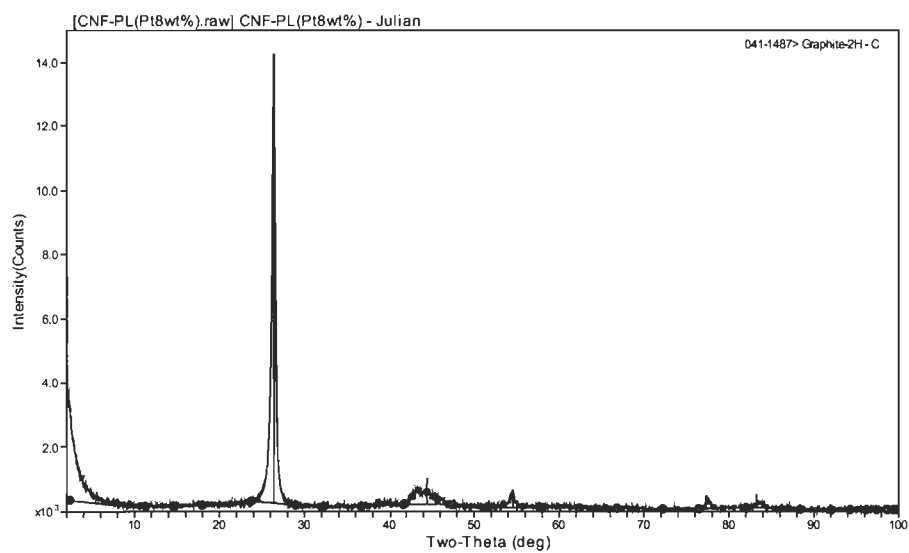


Figure A.5 : XRD spectrum of carbon nanofibers CNF-PL doped with 8wt%  $Pd$  showing the peaks related to  $C$ .



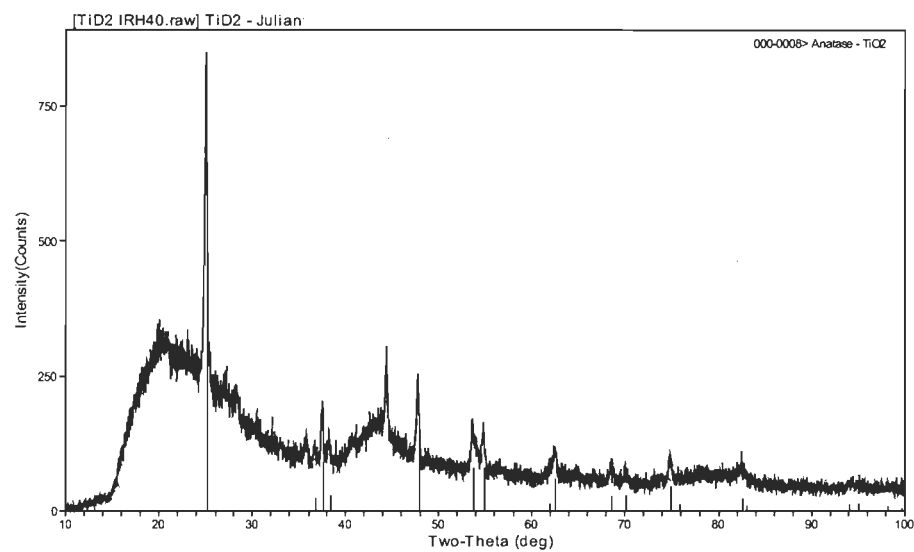


Figure A.6 : XRD spectrum of TiD2 showing the peaks related to  $TiO_2$ .

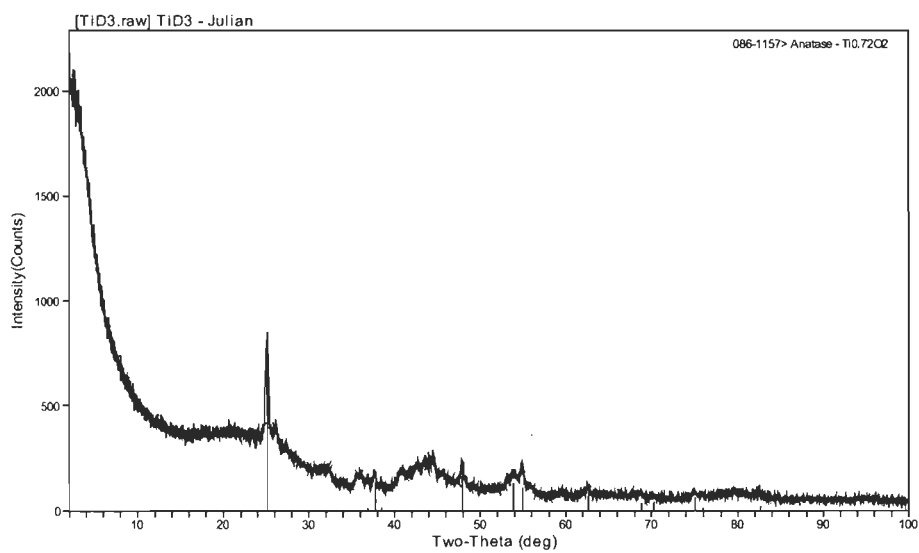


Figure A.7 : XRD spectrum of TiD3 showing the peaks related to  $TiO_2$ .

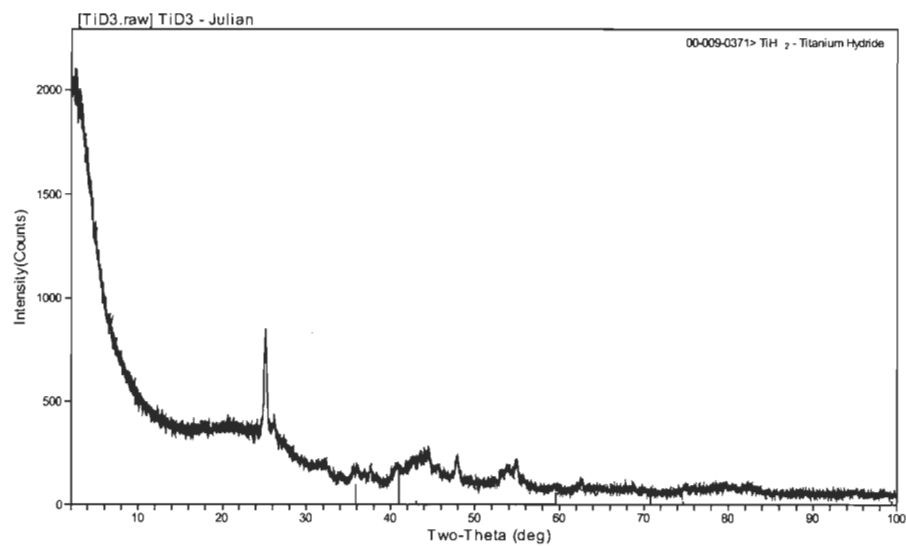


Figure A.8 : XRD spectrum of TiD3 showing the peaks related to  $TiH_2$ .

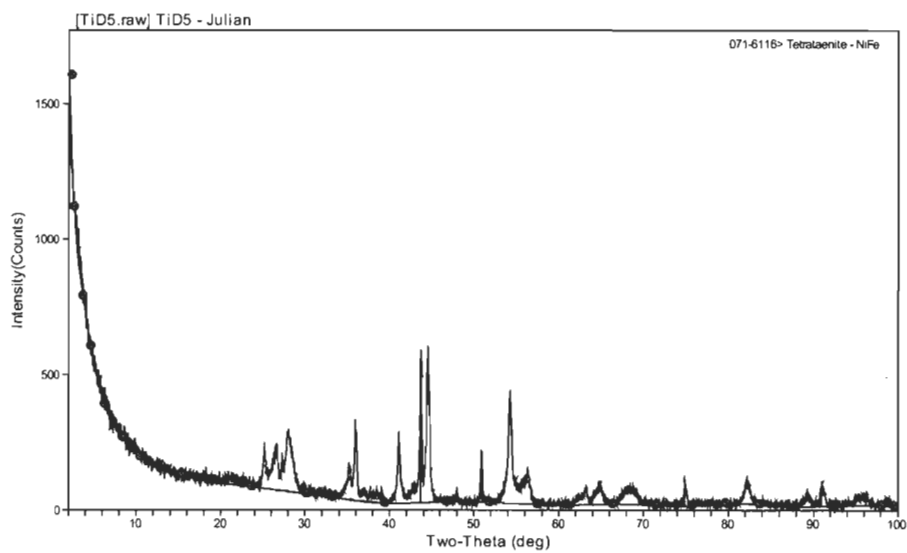


Figure A.9 : XRD spectrum of TiD5 showing the peaks related to  $NiFe$ .

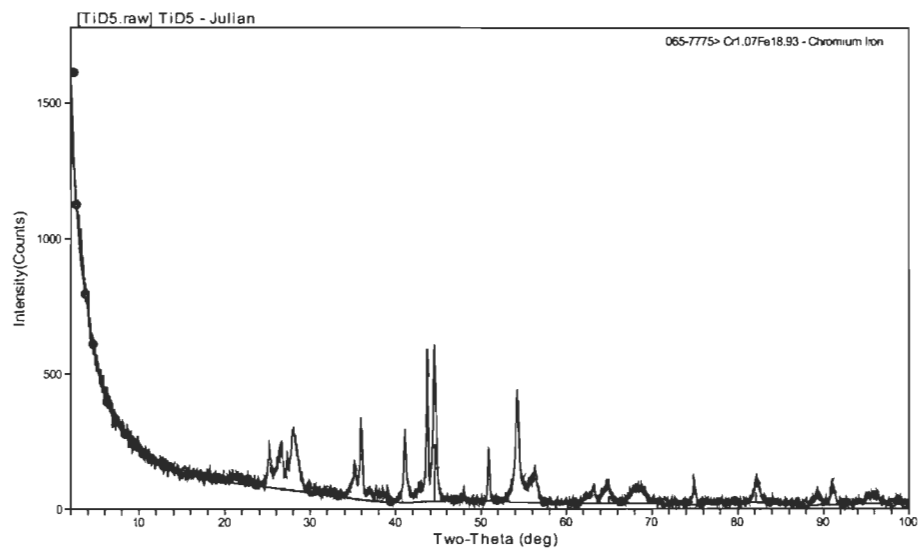


Figure A.10 : XRD spectrum of TiD5 showing the peaks related to  $CrFe$ .

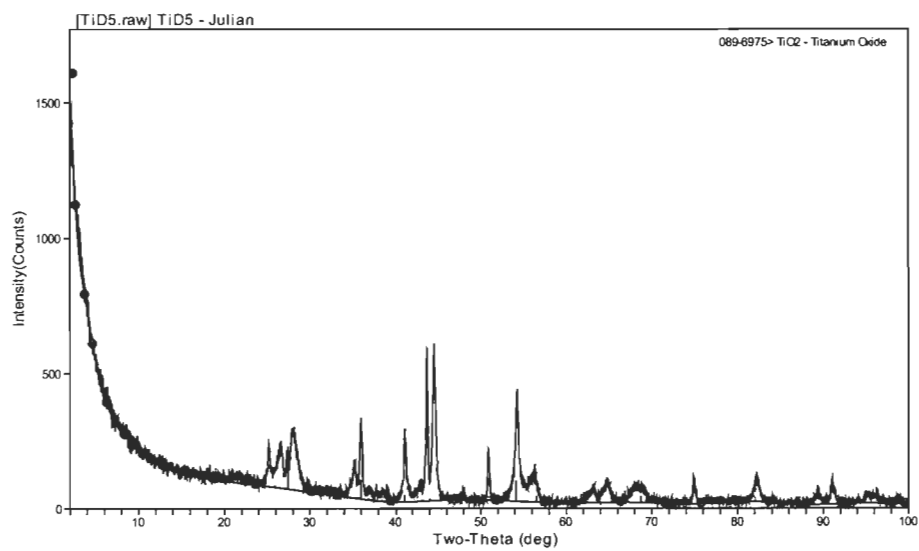


Figure A.11 : XRD spectrum of TiD5 showing the peaks related to  $TiO_2$ .

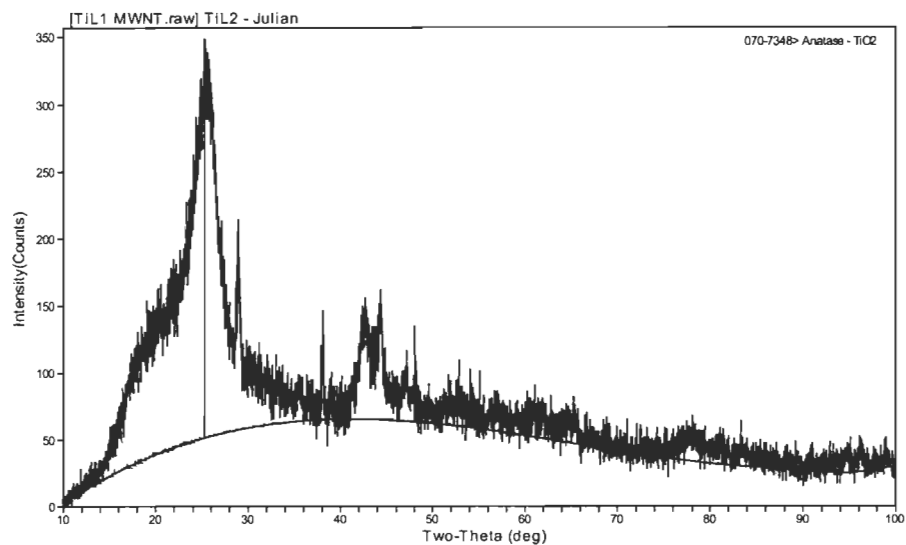


Figure A.12 : XRD spectrum of TiL1 showing the peaks related to  $TiO_2$ .

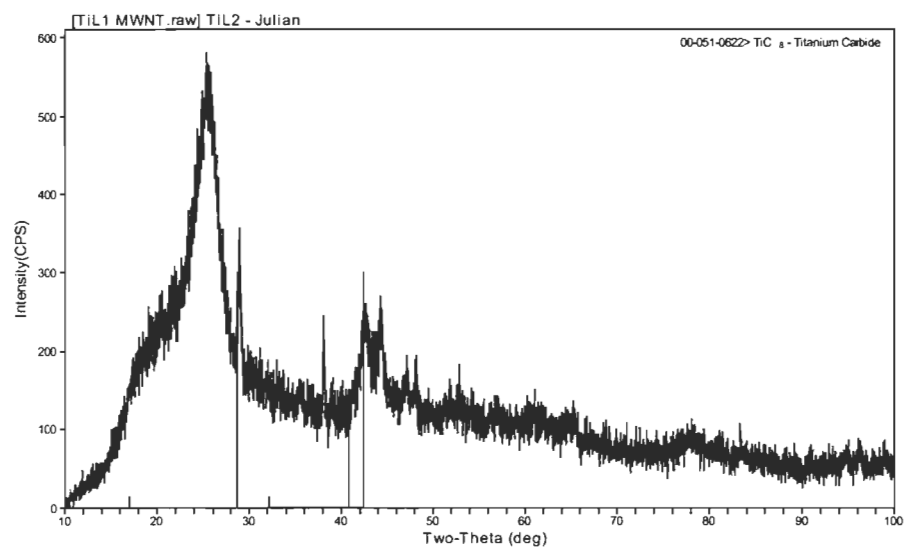


Figure A.13 : XRD spectrum of TiL1 showing the peaks related to  $TiC_8$ .

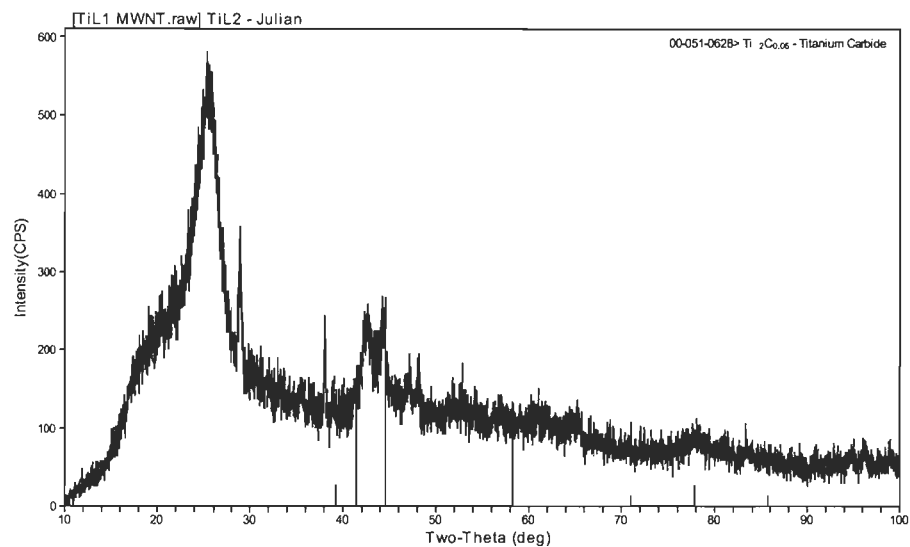


Figure A.14 : XRD spectrum of TiL1 showing the peaks related to  $TiC$ .

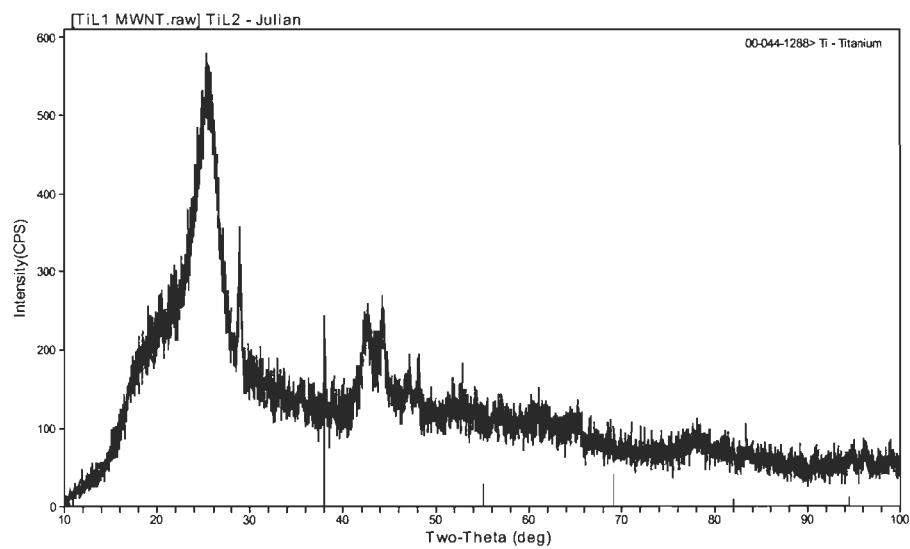


Figure A.15 : XRD spectrum of TiL1 showing the peaks related to  $Ti$ .

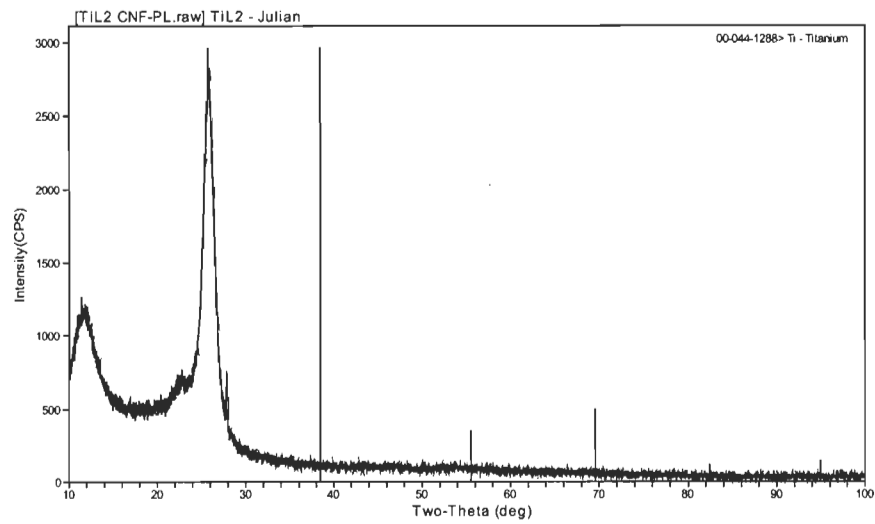


Figure A.16 : XRD spectrum of TiL2 showing the peaks related to  $Ti$ .

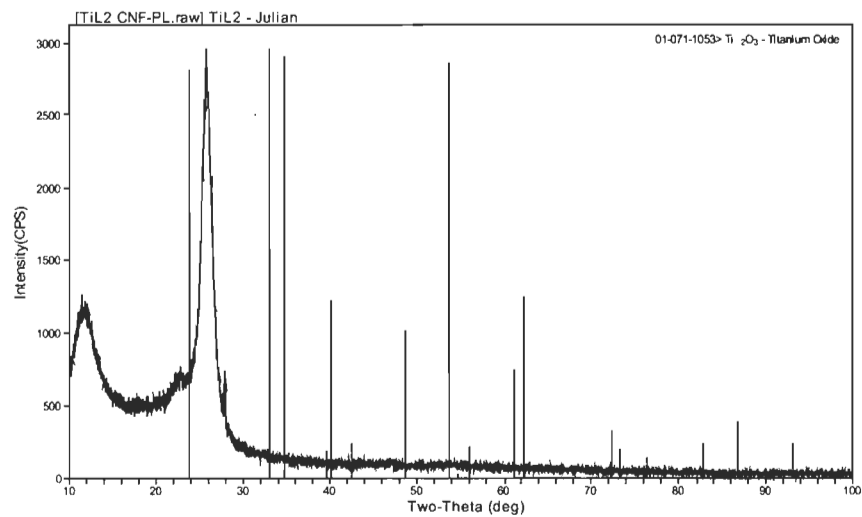


Figure A.17 : XRD spectrum of TiL2 showing the peaks related to  $Ti_2O_3$ .

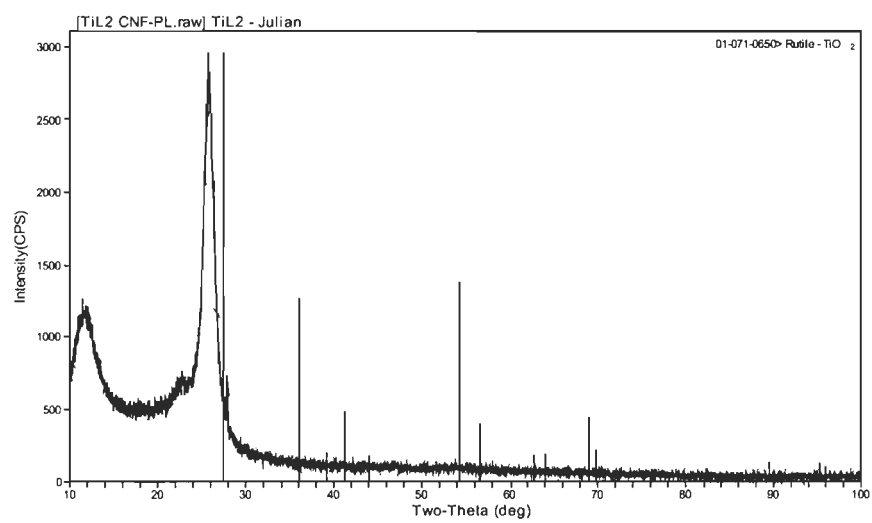


Figure A.18 : XRD spectrum of TiL2 showing the peaks related to  $TiO_2$ .

## Appendix B

### XPS results



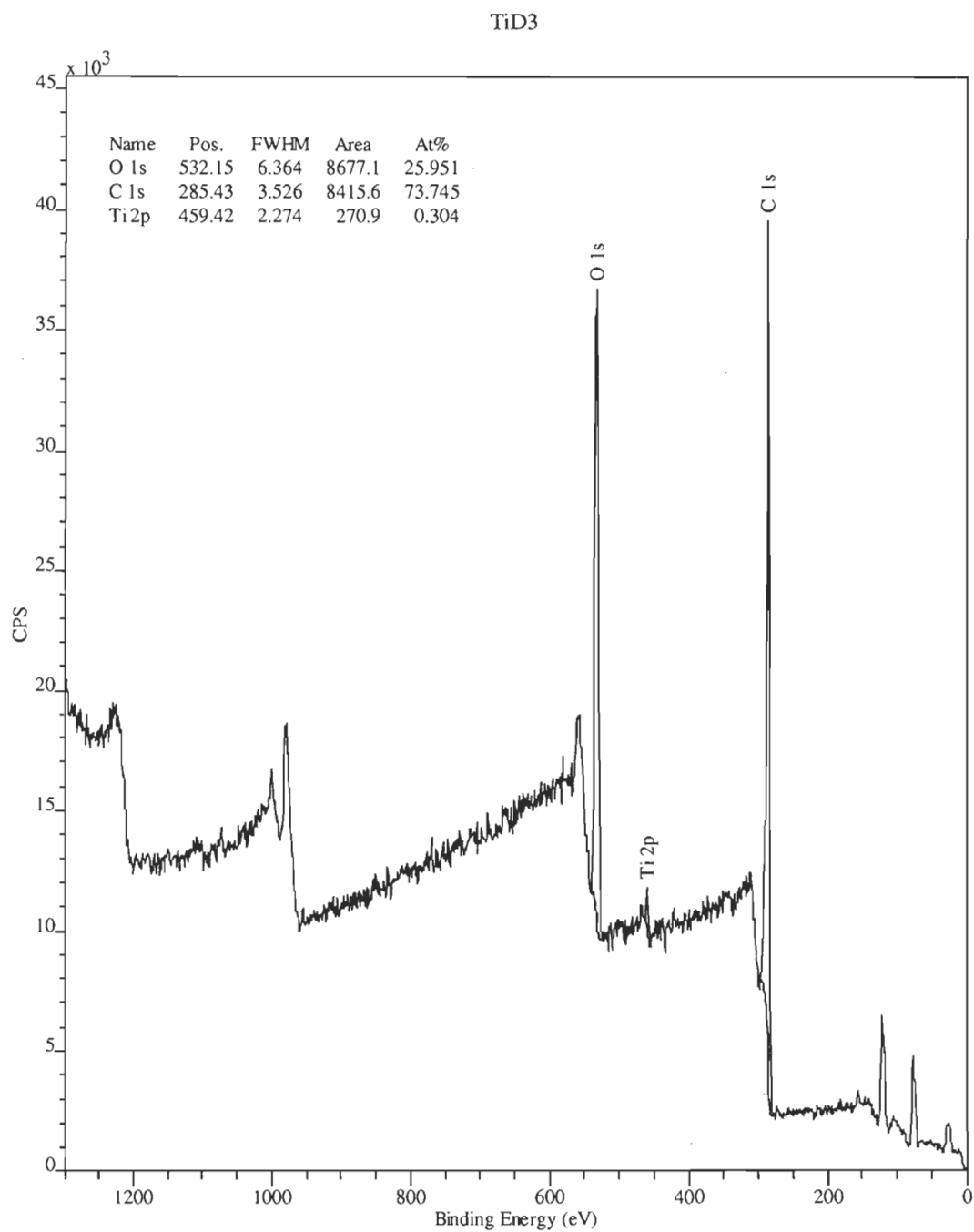


Figure B.1 : XPS spectrum of TiD3 showing 3 emission lines for titanium, oxygen and carbon.

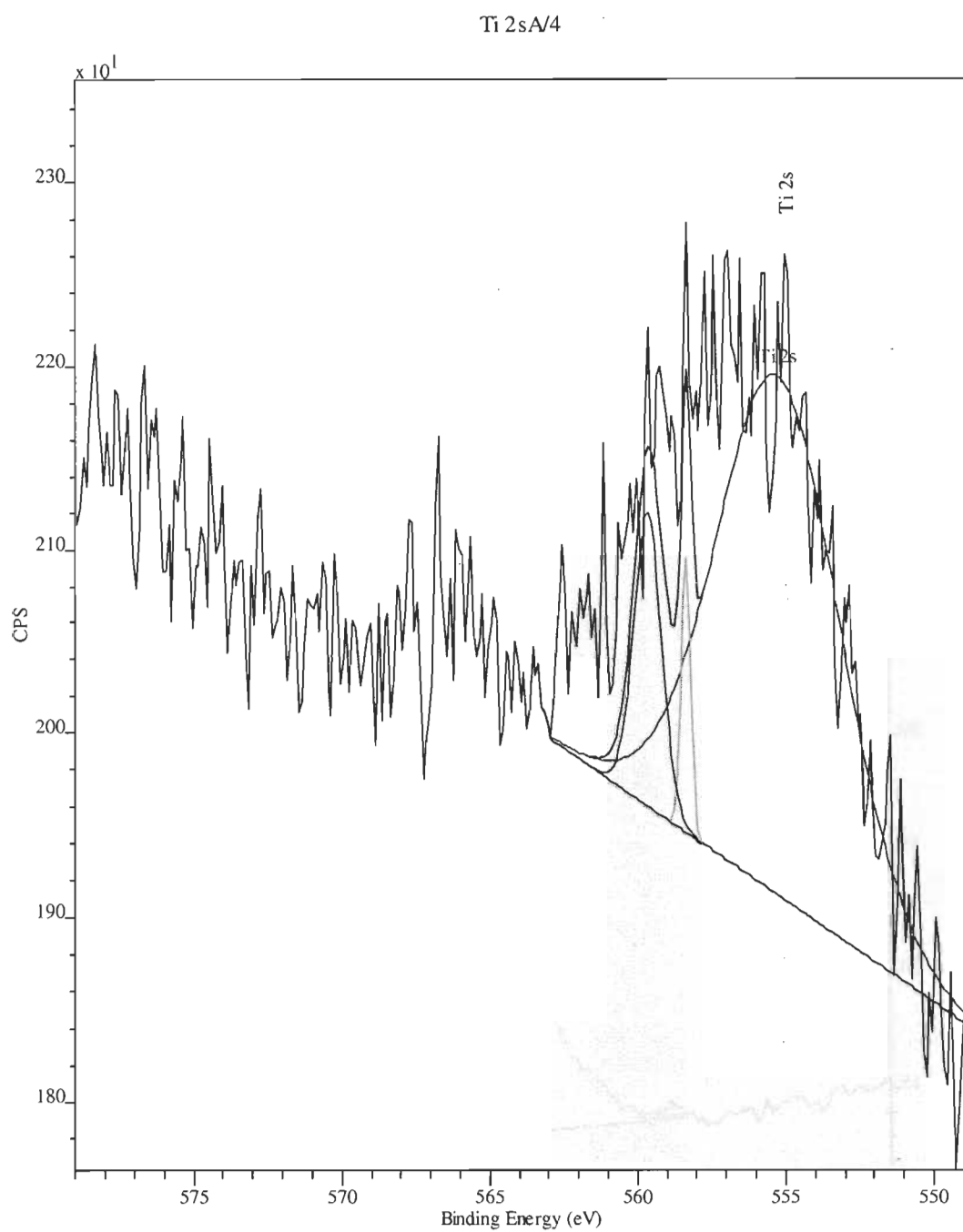


Figure B.2 : XPS spectrum of TiD<sub>3</sub> with focus on emission line Ti 2s.

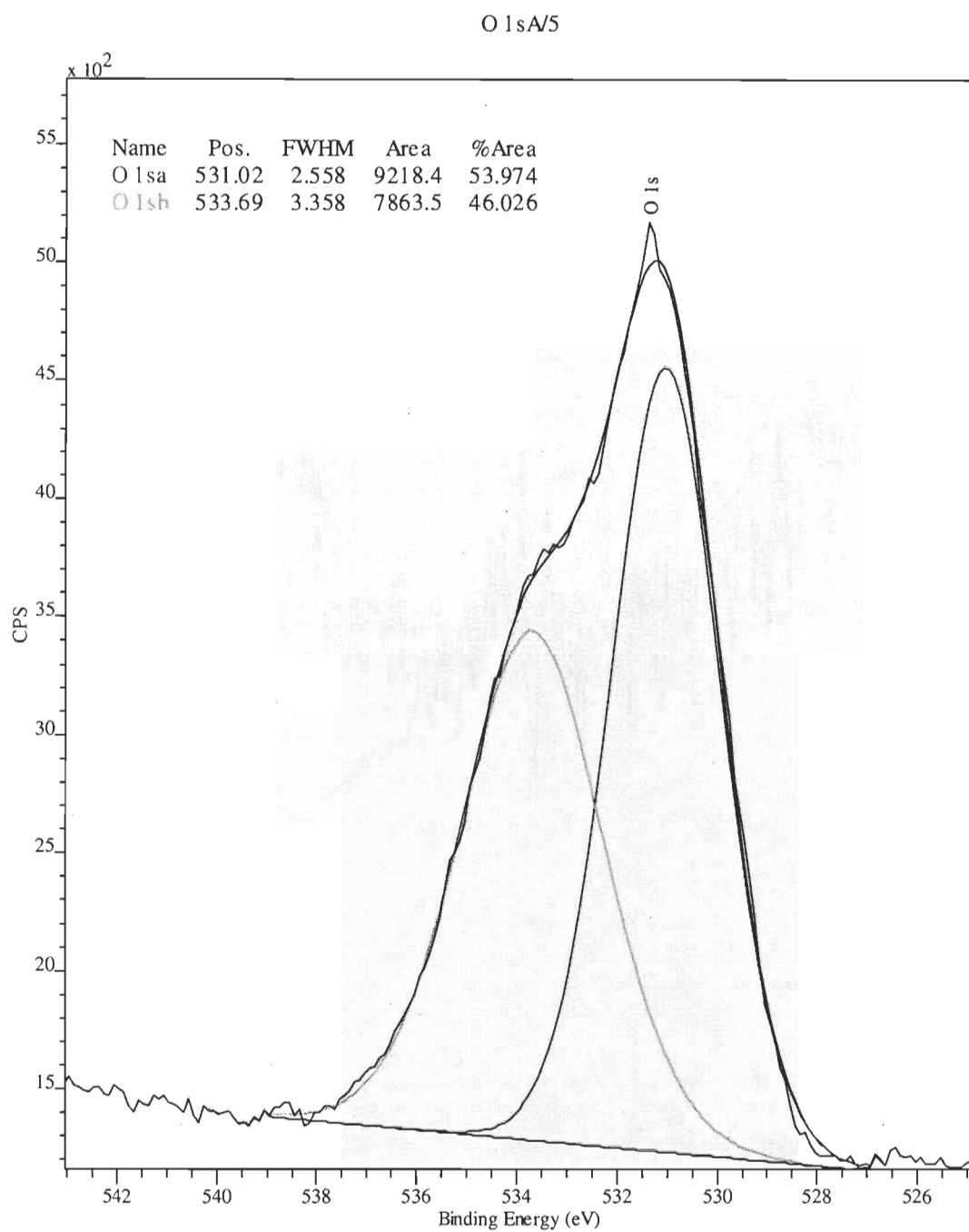


Figure B.3 : XPS spectrum of TiD3 with focus on emission line O 1s.

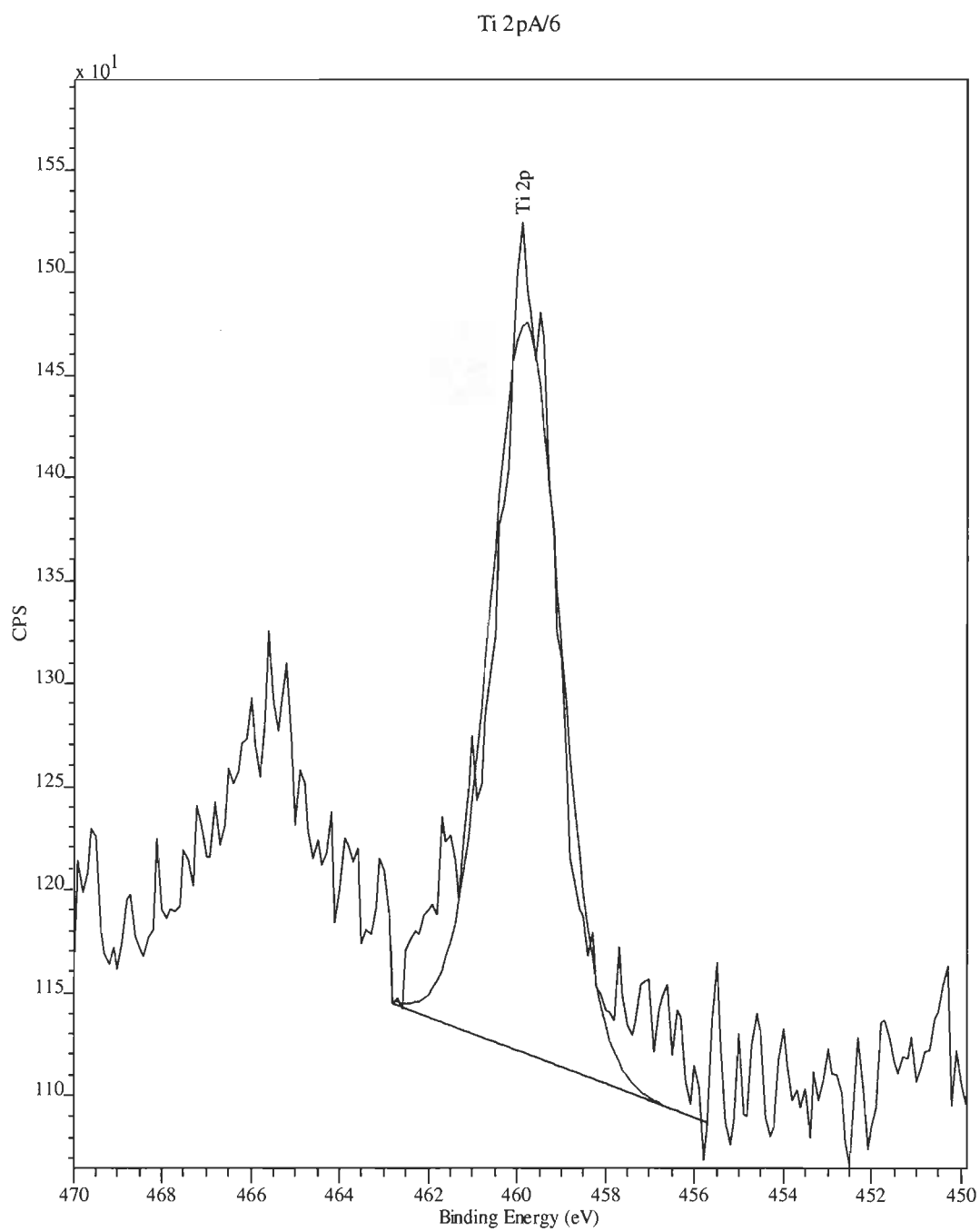


Figure B.4 : XPS spectrum of TiD<sub>3</sub> with focus on emission line Ti 2p.

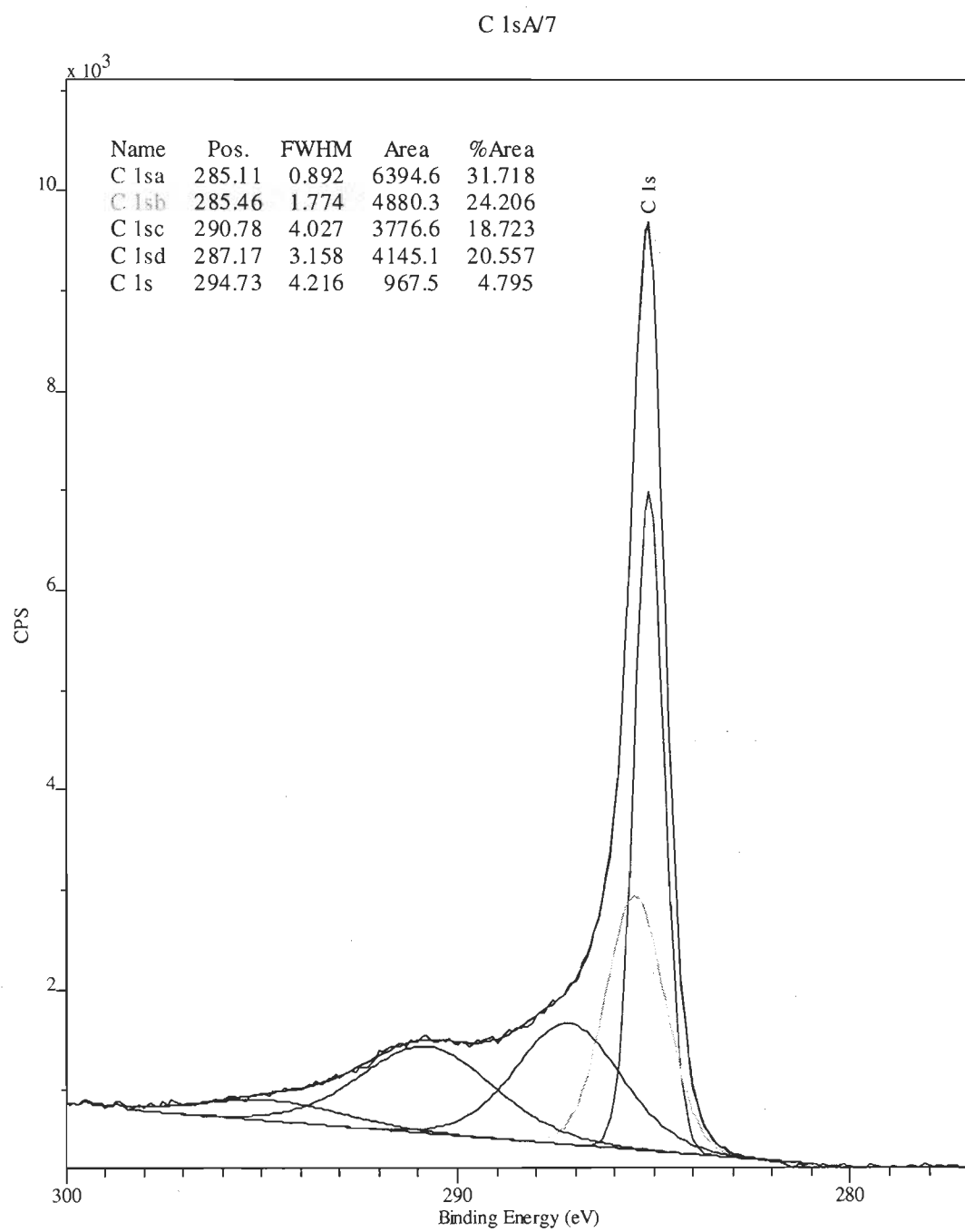


Figure B.5 : XPS spectrum of TiD3 with focus on emission line C 1s.

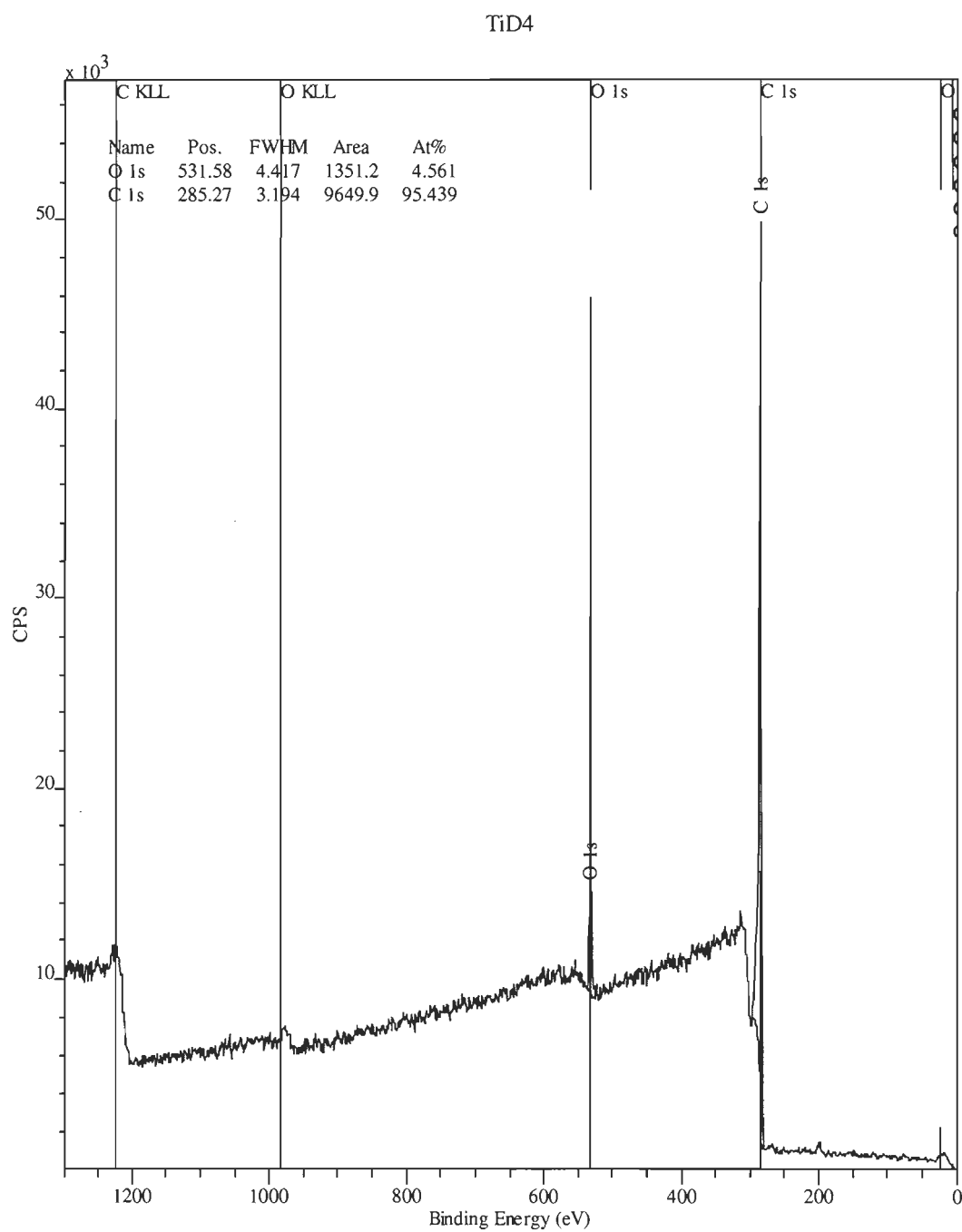


Figure B.6 : XPS spectrum of TiD4 showing 2 emission lines for oxygen and carbon.

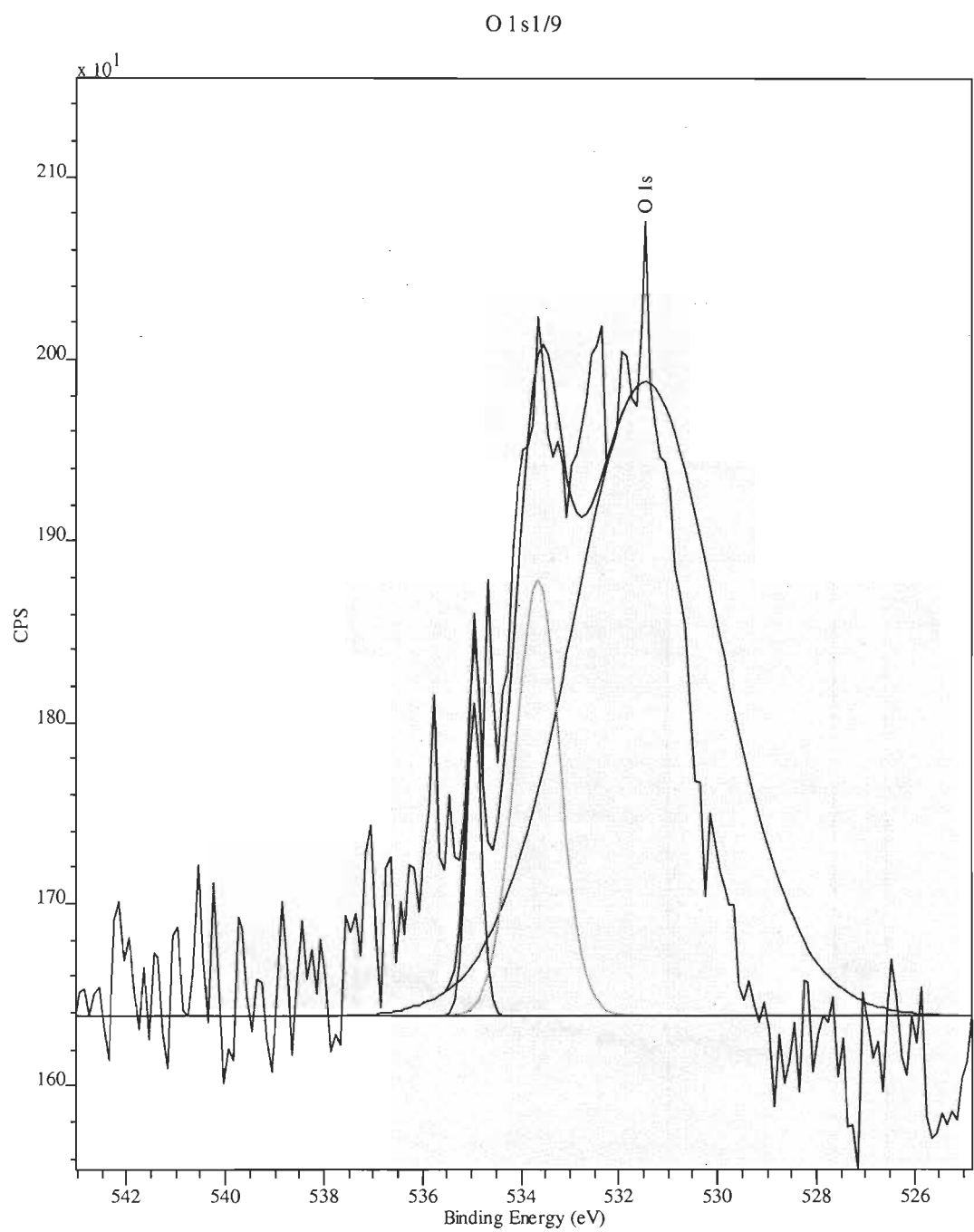


Figure B.7 : XPS spectrum of TiD4 with focus on emission line O 1s.

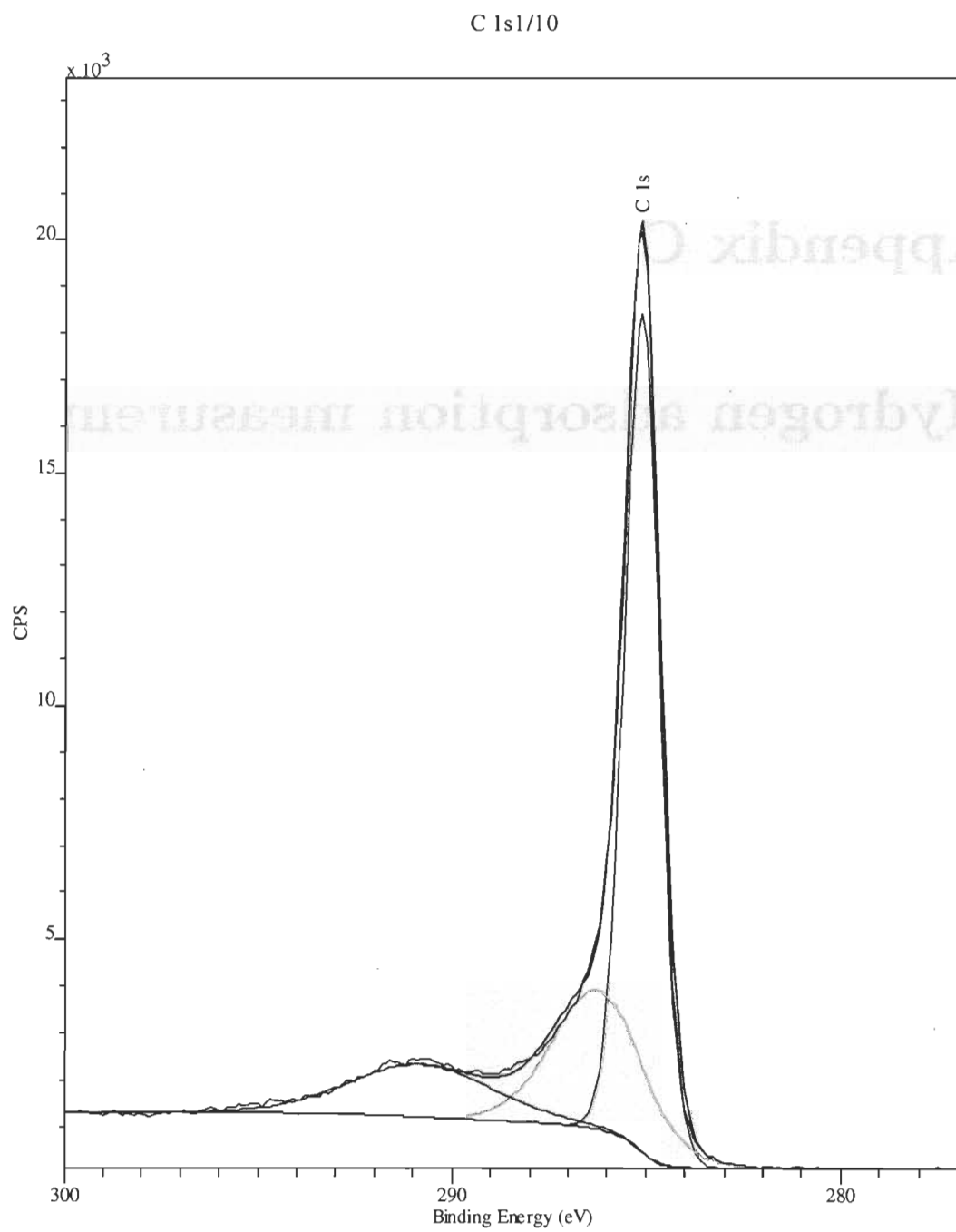


Figure B.8 : XPS spectrum of TiD4 with focus on emission line C 1s.



## Appendix C

### Hydrogen adsorption measurements

## Hydrogen Adsorption on Pd/Pt-doped Materials at 295K

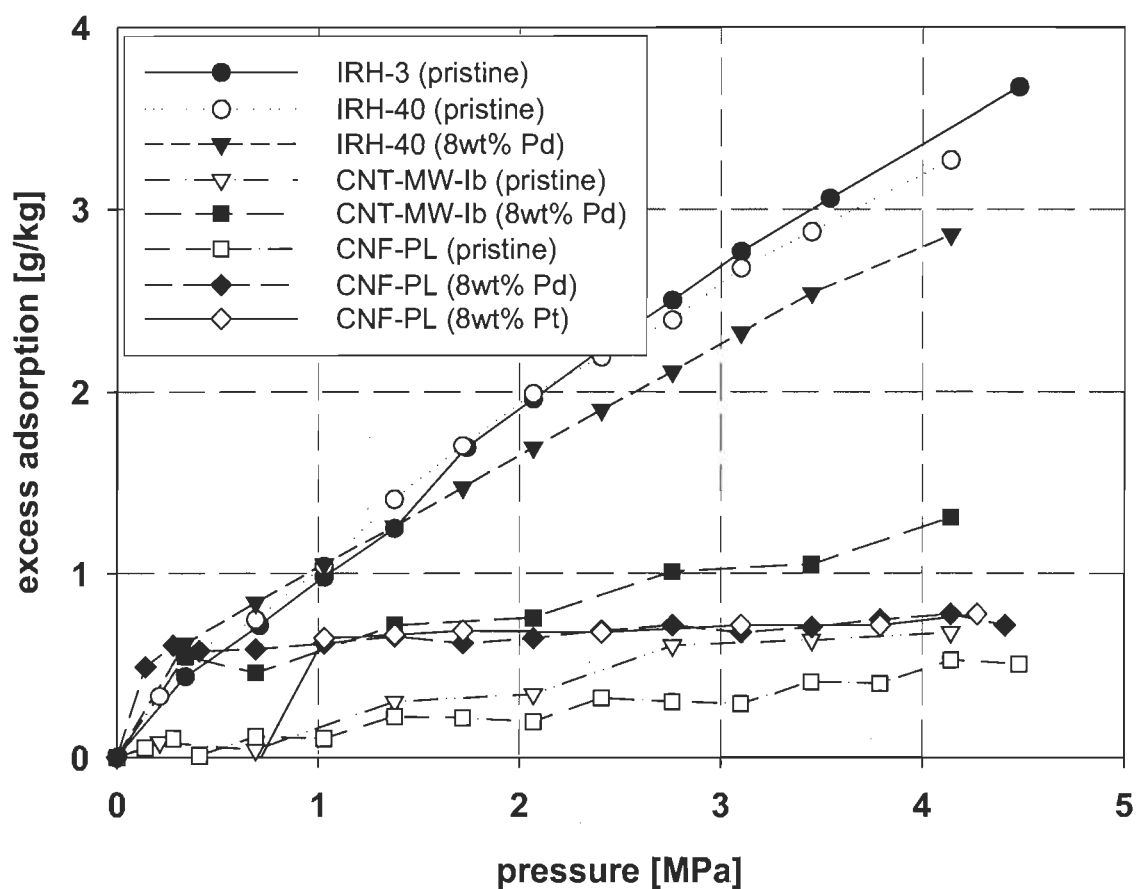


Figure C.1 : Hydrogen adsorption measurements performed with the gravimetric measurement system at a temperature of 295 K and pressures up to 4 MPa. Samples shown are Pd and Pt covered carbon materials in comparison with their undoped pristine materials.

## Hydrogen Adsorption on Ti-doped Materials at 295K

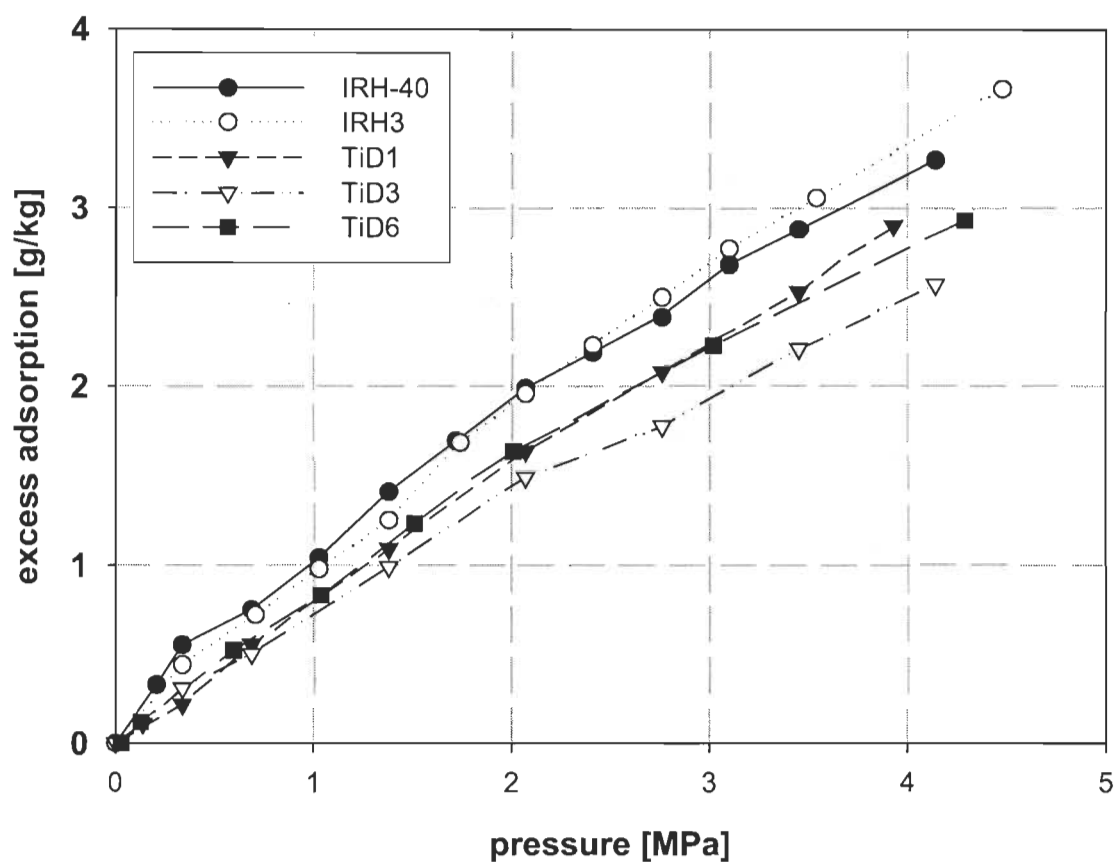


Figure C.2 : Hydrogen adsorption measurements performed with the gravimetric measurement system at a temperature of 295 K and pressures up to 4 MPa. Samples shown are Ti covered carbon materials in comparison with their undoped pristine materials.

### Hydrogen Adsorption on IRH 40 at 77K

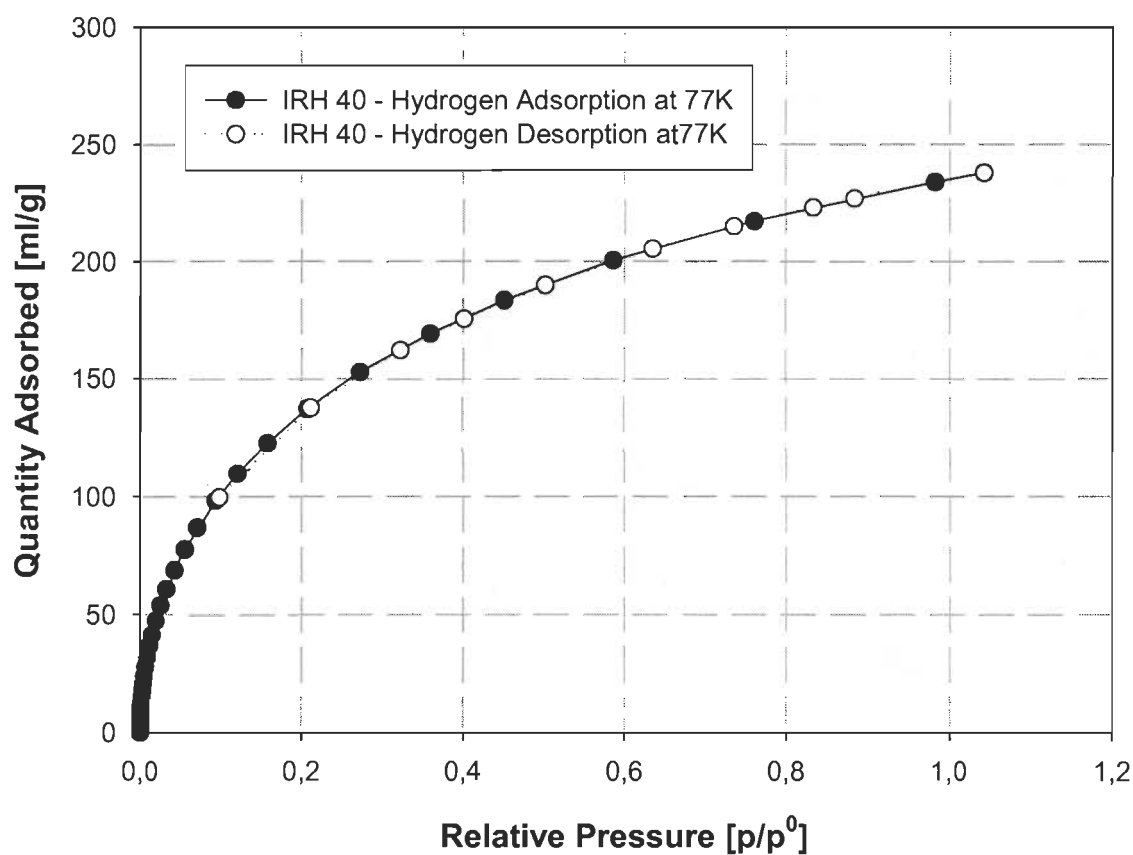


Figure C.3 : Hydrogen adsorption measurements performed with the volumetric measurement system at a temperature of 77 K and pressures up to 1 bar. Sample shown is the activated carbon IRH40.

### Hydrogen Adsorption on IRH 40 at 295K

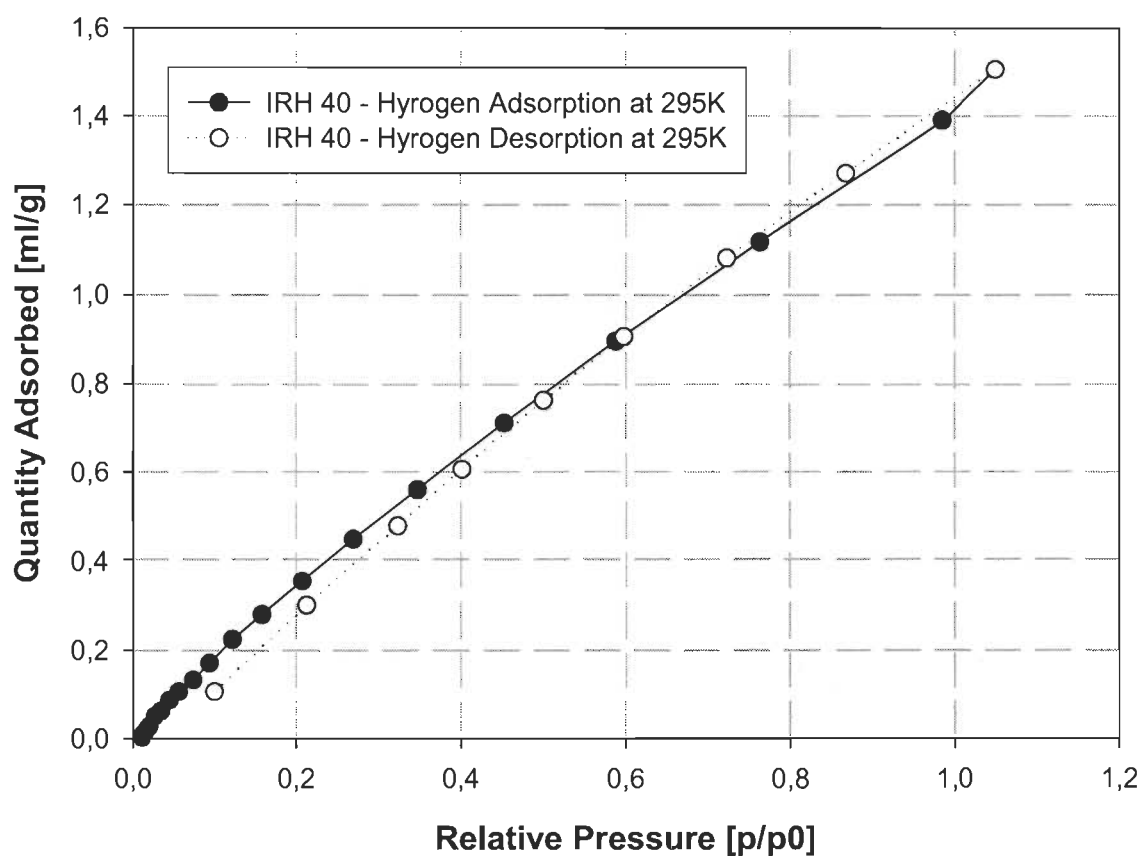


Figure C.4 : Hydrogen adsorption measurements performed with the volumetric measurement system at a temperature of 295 K and pressures up to 1 bar. Sample shown is the activated carbon IRH40.

### Hydrogen adsorption on TiD2 at 77K

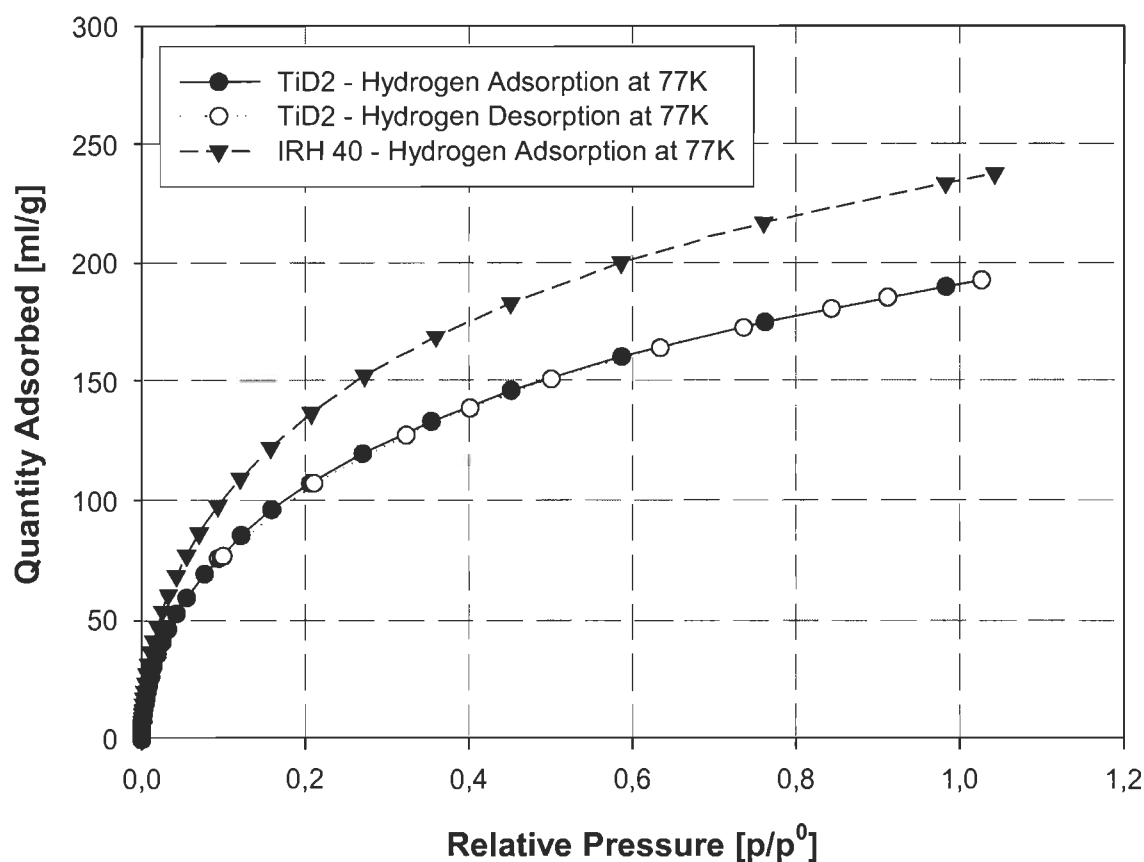


Figure C.5 : Hydrogen adsorption measurements performed with the volumetric measurement system at a temperature of 77 K and pressures up to 1 bar. Sample shown is the Ti covered sample TiD2 in comparison with its pristine material IRH40.

## Hydrogen Adsorption on TiD2 at 295K

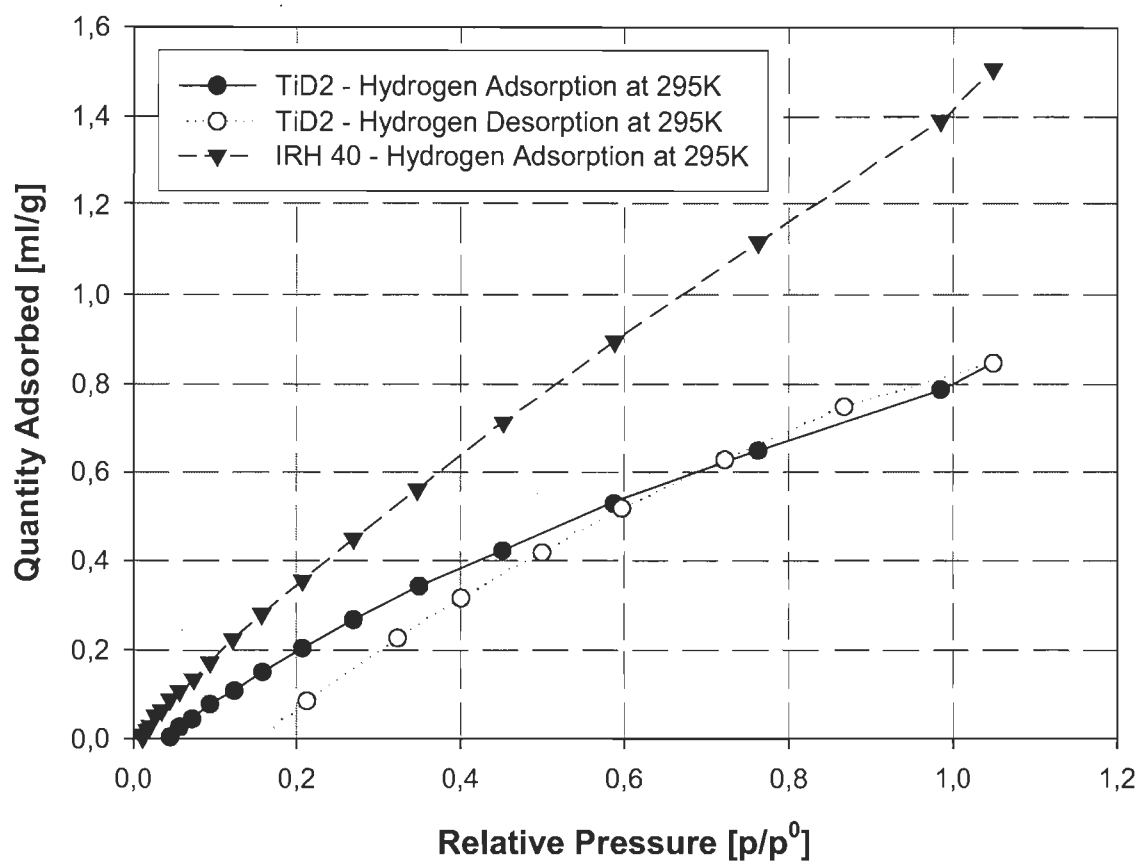


Figure C.6 : Hydrogen adsorption measurements performed with the volumetric measurement system at a temperature of 295 K and pressures up to 1 bar. Sample shown is the Ti covered sample TiD2 in comparison with its pristine material IRH40.

### Hydrogen Adsorption on TiL1 at 77K

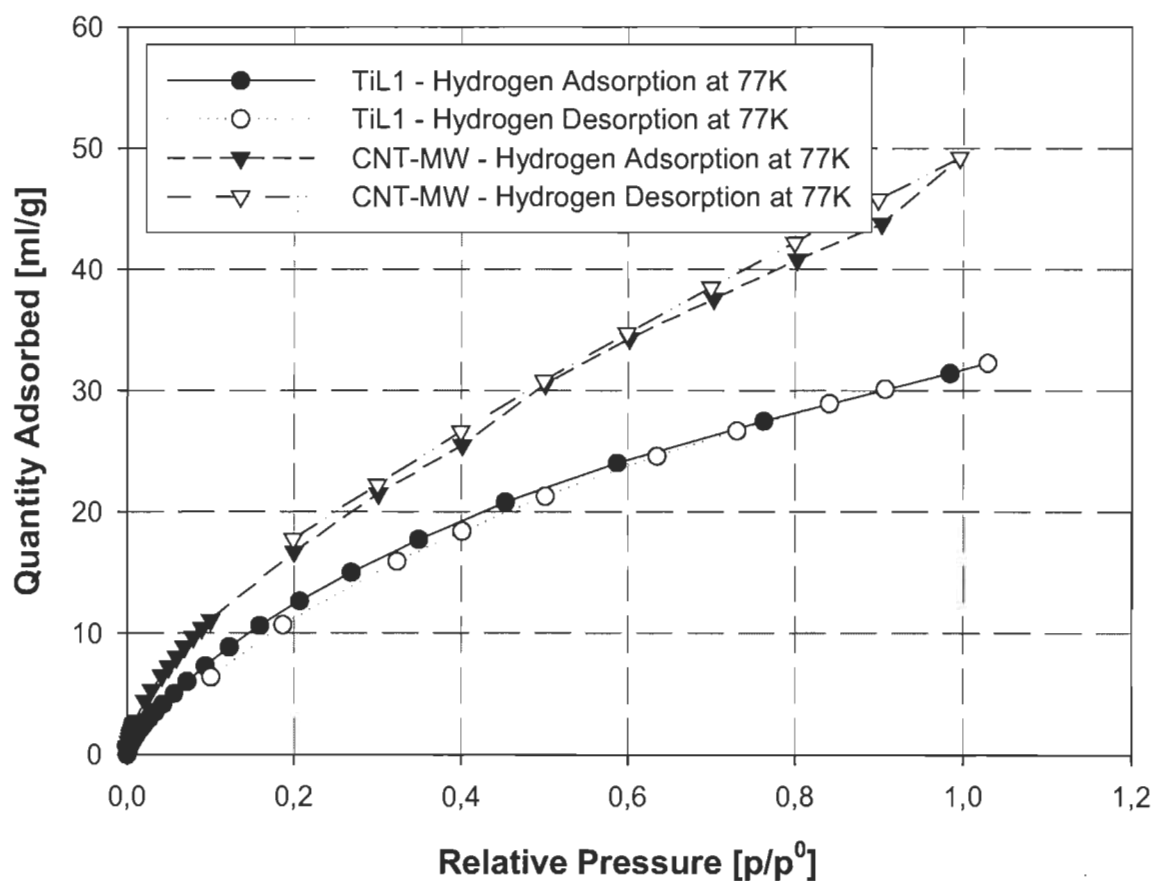


Figure C.7 : Hydrogen adsorption measurements performed with the volumetric measurement system at a temperature of 77 K and pressures up to 1 bar. Sample shown is the Ti covered sample TiL1 in comparison with its pristine material CNT-MW.



### Hydrogen Adsorption on TiL3 at 77K

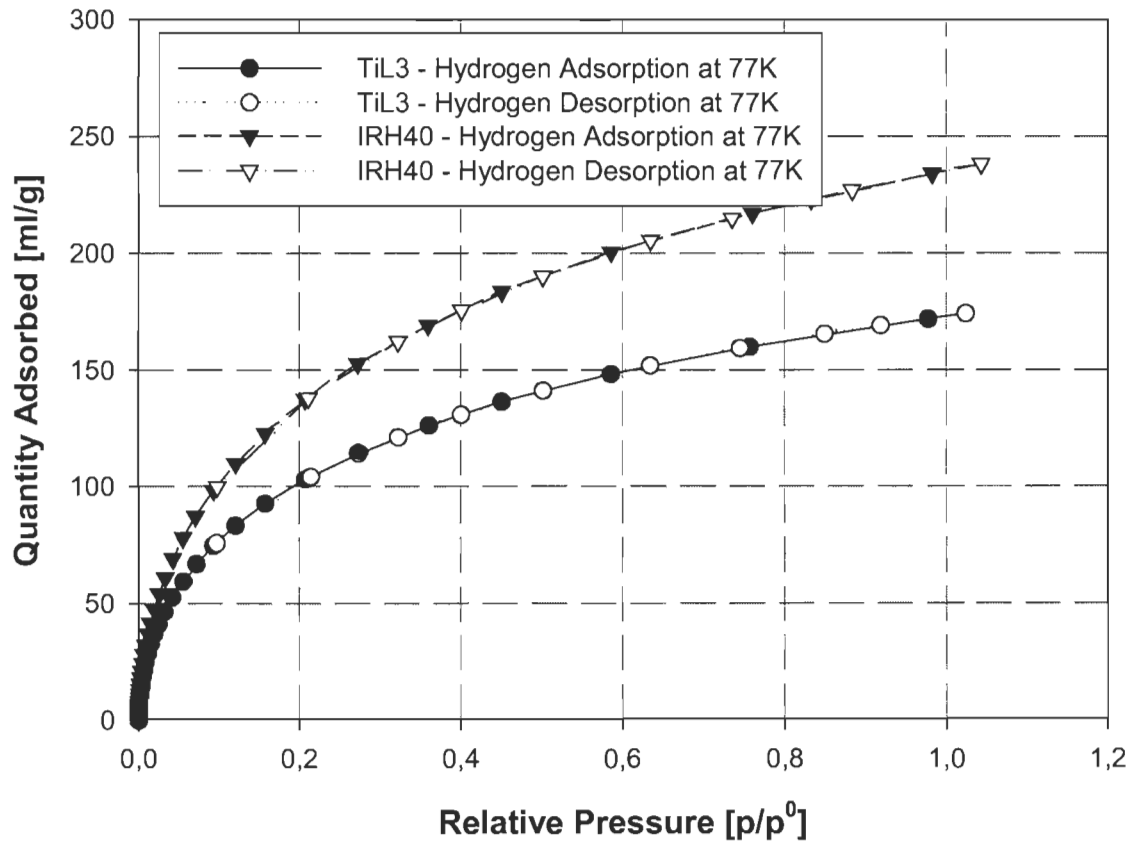


Figure C.8 : Hydrogen adsorption measurements performed with the volumetric measurement system at a temperature of 77 K and pressures up to 1 bar. Sample shown is the Ti covered sample TiL3 in comparison with its pristine material IRH40.

# Bibliography

- [1] PANELLA, B. HIRSCHER, M. ROTH, S. 2005. Hydrogen adsorption in different carbon nanostructures. Stuttgart : Carbon, vol. 33
- [2] YILDIRIM, T. and CIRACI, S. 2005. Titanium-Decorated Carbon Nanotubes as a Potential High-Capacity Hydrogen Storage Medium. Maryland : Physical Review Letters, vol. 94
- [3] DAG, S. OZTURK, Y. CIRACI, S. and YILDIRIM, T. 2005. Adsorption and dissociation of hydrogen molecules on bare and functionalized carbon nanotubes. Ankara : Physical Review B, vol. 72
- [4] YILDIRIM, T. ÍÑIGUEZ, J. and CIRACI, S. 2005. Molecular and dissociative adsorption of multiple hydrogens on transition metal decorated  $C_{60}$ . Gaithersburg : Physical Review B, vol. 72
- [5] DAG, S. DURGUN, E. and CIRACI, S. 2004. High-conducting magnetic nanowires obtained from uniform titanium-covered carbon nanotubes. Ankara : Physical Review B, vol. 69

- [6] DAG, S. CIRACI, S. 2005. Coverage and strain dependent magnetization of titanium-coated carbon nanotubes. Ankara : Physical Review B, vol. 71
- [7] ZHAO, Y. KIM, Y.-H. DILLON, A.C. HEBEN, M.J. and ZHANG, S.B. 2005. Hydrogen Storage in Novel Organometallic Buckyballs. Colorado : Physical Review Letters, vol. 94
- [8] KIM, Y.-H. ZHAO, Y. WILLIAMSON, A. HEBEN, M.J. and ZHANG, S.B. 2005. Non-dissociative adsorption of hydrogen molecules in light-element doped fullerenes. Colorado : Physical Review Letters, vol. 96
- [9] GALLEGO, N.C. CONTESCU, C.I. BAKER, F.S. BASOVA, Y.V. EDIE, D.D. 2006. Mechanism of Metal-Assisted Hydrogen Storage in Nanostructured Carbons. Arlington : Annual Merit Review Meeting
- [10] NOBUHARA, K. NAKANISHI, H. KASAI, H. OKIJI, A. 2000. Behaviour of H atom in adsorption states on metal surfaces - localization and delocalization. Osaka : Surface Science 493 271-277
- [11] LACHAWIEC, A.J. GONGSHIN, Q. and YANG, R.T. 2005. Hydrogen Storage in Nanostructured Carbons my Spillover: Bridge-Building Enhancement. Michigan : Langmuir, vol. 21
- [12] LI, L.YANG, R.T. 2005. Significantly Enhanced Hydrogen Storage in Metal-Organic Frameworks via Spillover. Michigan : JACS Communications

- [13] LUEKING, A.D. YANG, R.T. 2002. Hydrogen Spillover from a metal Oxide Catalyst onto Carbon Nanotubes - Implications for Hydrogen Storage. Michigan : Journal of Catalysis 206, 165-168
- [14] LUEKING, A.D. YANG, R.T. 2004. Hydrogen Spillover to enhance hydrogen storage - study of the effect of carbon physicochemical properties. 2004. Pennsylvania : Applied Catalysis A: General 265 259-268
- [15] ZHANG, Y. NATHAN, W.F. CHEN, R.J. and DAI, H. 2000 Metal coating on suspended carbon nanotubes and its implication to metal-tube interaction. Stanford : Chemical Physics Letters 331 35-41
- [16] ZHANG, Y. DAI, H. 2000. Formation of metal nanowires on suspended single-walled carbon nanotubes. Applied Physics Letters, vol. 77
- [17] ZHANG, Y. ZHANG, Q. LI, Y. WANG, N. ZHU, J. 2000. Coating of carbon nanotubes with tungsten by physical vapor deposition. Beijing : Solid State Communications, vol. 115 51-55
- [18] FAN, W. GAO, L. SUN, J. 2006. Tin Oxide Nanoparticle-Functionalized Multi-Walled Carbon Nanotubes by the Vapor Phase Method. Shanghai : JACS, vol. 89 26712673
- [19] SCHUBERT, T. WILLERT-PORADA, M. 2006. Microwave Assisted Synthesis of Catalyst Materials for PEM Fuel Cells. Bayreuth : Advances in Microwave and Radio Frequency Processing, Part IX

- [20] ROUQUEROL, F. ROUQUEROL, K. SING, K. 1999. Adsorption by powders and porous solids London: Academic Press
- [21] WOOD, G.O. 1992. Activated carbon adsorption capacities for vapors. Los Alamos : Carbon 30 593-599
- [22] KLUG, H.P. ALEXANDER L.E. 1974. X-Ray Diffraction Procedures: For Polycrystalline and Amorphous Materials. John Wiley & Sons Ltd ISBN 0-471-49369-4
- [23] ALLMANN, R. KERN, A. 2002. Röntgenpulverdiffraktometrie: Rechnergestützte Auswertung, Phasenanalyse und Strukturbestimmung. Springer-Verlag GmbH ISBN 3-540-43967-6
- [24] WATTS, J.F. WOLSTENHOLME, J. 2003. An Introduction to Surface Analysis by XPS and AES. John Wiley & Sons Ltd ISBN 0-470-84712-3
- [25] HÜFNER, S. 2003. Photoelectron Spectroscopy Principles and Applications. 3<sup>rd</sup> Edition Springer-Verlag Berlin Heidelberg New York ISBN 3-540-41802-4
- [26] BELMABKHOUT, Y. FRÈRE, M. WEIRALD, G.D. 2004. A comparative study of the volumetric and gravimetric methods. Mons : Meas. Sci. Technol. 15 848-858
- [27] ANSÓN, A. BENHAM, M. JAGIELLO, J. CALLEJAS, M.A. BENITO, A.M. MASER, W.K. ZÜTTEL, A. SUDAN, P. MARTÍNEZ, M.T. 2004. Hydrogen adsorption on a single-walled carbon nanotube material: a comparative study of three different adsorption techniques. Zaragoza : Nanotechnology 15 1503-1508

- [28] LAN, A. MUKASYAN, A. 2005. Hydrogen Storage Capacity Characterization of Carbon Nanotubes by a Microgravimetical Approach. Indiana : J. Phys. Chem. B 109
- [29] KELLER, J.U. ROBENS, E. HOHENSCHKE, C.d.F. Thermogravimetric and Sorption Measurement Techniques/Instruments. Siegen

